The occurrence and timing of gold mineralization at the Red Pine Mine, western Tobacco Root Mountains, southwestern Montana
by Teresa May Kinley

A thesis submitted in partial fulfillment of the requirements for the degree of Master of Science in Earth Sciences
Montana State University

Abstract:
The Red Pine mine is located in Archean metasediments in the Sheridan mining district of the western Tobacco Root Mountains. The mine is developed in a fissure vein that occurs in marble and along the contact between marble and quartzofeldspathic gneiss.

The present study broadens the knowledge of gold mineralization in the range. It describes ore and gangue minerals and establishes their paragenetic sequence. The study also interprets the conditions and timing of ore emplacement and the sources of ore metals and fluids.

Two principal periods of mineralization and a minor period of secondary alteration are evident in the deposit. Moreover, textures show that multiple episodes of fracturing and brecciation accompanied the mineralization. Gold is present primarily in the first period of mineralization as discrete grains in fractures in pyrite or on the borders of brecciated pyrite. It is also found as minute inclusions and open-space fillings within pyrite. Gold is also associated with milky quartz, bismuthinite, and, less commonly, with carbonate, chalcopyrite, and tetrahedrite.

Period I mineralization, recognized by milky quartz, contains pyrite, bismuthinite, chalcopyrite, sphalerite, and silver-bearing tetrahedrite. Trace amounts of pyrrhotite have been noted with pyrite and chalcopyrite. A major episode of brecciation separates Period 1 from Period 2. Gangue mineralization predominates in Period 2 with the deposition of graphite, white mica, dark gray microcrystalline quartz, calcite, and minor amounts of pyrite and chalcedony. Some gold is found along fractures in milky quartz that are filled with graphite and mica. Gold is also attached to graphite in these fractures. Goethite, djurleite, malachite, and minor covellite occur ' as sulfide alteration products.

Interpretations of timing and pressure-temperature conditions of ore emplacement are made from mineralogy, textures, paragenetic sequence, and geologic relations observed at the mine. A mesothermal to hypothermal temperature (200° to 500° C) of deposition at pressures no greater than 2 kilobars is indicated by field relations and sulfide paragenesis. Ore deposition is interpreted as hydrothermal and as related to the Tobacco Root batholith or an associated igneous body. This relationship suggests a Late Cretaceous to early Tertiary age for the deposit.

THE OCCURRENCE AND TIMING OF GOLD MINERALIZATION AT THE RED PINE MINE, WESTERN TOBACCO ROOT MOUNTAINS, SOUTHWESTERN MONTANA

by

Teresa May Kinley

A thesis submitted in partial fulfillment
of the requirements for the degree

of

Master of Science

in

Earth Sciences

MONTANA STATE UNIVERSITY
Bozeman, Montana

March 1987

APPROVAL

of a thesis submitted by

Teresa May Kinley

This thesis has been read by each member of the thesis committee and has been found to be satisfactory regarding content, English usage, format, citations, bibliographic style, and consistency, and is ready for submission to the College of Graduate Studies.

March 24 1987
Date

David W. Mogk
Chairperson, Graduate Committee

Approved for the Major Department

24 March 87
Date

Stephen G. Custer
Head, Major Department

Approved for the College of Graduate Studies

March 30, 1987
Date

Henry L. Parsons
Graduate Dean

STATEMENT OF PERMISSION TO USE

In presenting this thesis in partial fulfillment of the requirements for a master's degree at Montana State University, I agree that the Library shall make it available to borrowers under rules of the Library. Brief quotations from this thesis are allowable without special permission, provided that accurate acknowledgment of source is made.

Permission for extensive quotation from or reproduction of this thesis may be granted by my major professor, or in his absence, by the Director of Libraries when, in the opinion of either, the proposed use of the material is for scholarly purposes. Any copying or use of the material in this thesis for financial gain shall not be allowed without my written permission.

ACKNOWLEDGMENTS

Great appreciation is extended to the many people who have given generous encouragement, guidance, and/or financial support or who have shared their skills, knowledge, and/or insight, throughout this project. The author especially acknowledges the contributions of the late Dr. Robert A. Chadwick and the late Dr. Donald L. Smith. Dr. Chadwick, who advised this project and my graduate career until September 1985, provided encouragement and guidance and shared his knowledge of geology and underground mapping. Dr. Smith gave encouragement at the beginning of my graduate career. Special thanks go to Dr. David Mogk for sharing his knowledge of geology and scientific writing and for taking on additional advising responsibilities. Thanks are also extended to Dr. John Childs and Dr. David Lageson for constructive comments on the text and for help in their areas of expertise. Special thanks are offered to John Magnus of Shermont Mining Company for providing access to the Red Pine mine and helpful answers to numerous questions. Great appreciation is extended to Lester Zeihen, Dr. Vernon Griffiths, Dr. Henry McClernan, and Dr. Graham Wilson for their interest in this project and help in various analyses. Financial assistance has been gratefully received through a grant from the Montana Bureau of Mines and Geology, through a graduate teaching assistantship and work study at Montana State University, from John Magnus, and from Marshall and Thelma Kinley.

TABLE OF CONTENTS

TABLE OF CONTENTS--Continued

TABLE OF CONTENTS--Continued

LIST OF TABLES

LIST OF FIGURES

LIST OF FIGURES--Continued

LIST OF FIGURES--Continued

LIST OF FIGURES--Continued

LIST OF PLATES

ABSTRACT

The Red Pine mine is located in Archean metasediments in the Sheridan mining district of the western Tobacco Root Mountains. The mine is developed in a fissure vein that occurs in marble and along the contact between marble and quartzofeldspathic gneiss.

The present study broadens the knowledge of gold mineralization in the range. It describes ore and gangue minerals and establishes their paragenetic sequence. The study also interprets the conditions and timing of ore emplacement and the sources of ore metals and fluids.

Two principal periods of mineralization and a minor period of secondary alteration are evident in the deposit. Moreover, textures show that multiple episodes of fracturing and brecciation accompanied the mineralization. Gold is present primarily in the first period of mineralization as discrete grains in fractures in pyrite or on the borders of brecciated pyrite. It is also found as minute inclusions and open-space fillings within pyrite. Gold is also associated with milky quartz, bismuthinite, and, less commonly, with carbonate, chalcopyrite, and tetrahedrite.

Period 1 mineralization, recognized by milky quartz, contains pyrite, bismuthinite, chalcopyrite, sphalerite, and silver-bearing tetrahedrite. Trace amounts of pyrrhotite have been noted with pyrite and chalcopyrite. A major episode of brecciation separates Period 1 from Period 2. Gangue mineralization predominates in Period 2 with the deposition of graphite, white mica, dark gray microcrystalline quartz, calcite, and minor amounts of pyrite and chalcedony. Some gold is found along fractures in milky quartz that are filled with graphite and mica. Gold is also attached to graphite in these fractures. Goethite, djurleite, malachite, and minor covellite occur as sulfide alteration products.

Interpretations of timing and pressure-temperature conditions of ore emplacement are made from mineralogy, textures, paragenetic sequence, and geologic relations observed at the mine. A mesothermal to hypothermal temperature (200° to 500° C) of deposition at pressures no greater than 2 kilobars is indicated by field relations and sulfide paragenesis. Ore deposition is interpreted as hydrothermal and as related to the Tobacco Root batholith or an associated igneous body. This relationship suggests a Late Cretaceous to early Tertiary age for the deposit.

INTRODUCTION

Purpose of Study

The nature of gold mineralization in the Tobacco Root Mountains is inadequately understood because few detailed studies of mineralization have been made in the range. As a result, the timing and physical conditions of gold mineralization remain unknown.

This project includes a detailed metallogenic and petrologic study of vein mineralization at the Red Pine mine in the western Tobacco Root Mountains. The mine is developed in a fissure vein that contains quartz and auriferous pyrite. Mineralization is localized in Archean metamorphic rocks. The accessibility of the mine and the numerous underground exposures of the vein make this site ideal for study.

Primary purposes of this research project are:

1. to identify and describe ore and gangue minerals, and to determine their paragenetic sequence;
2. to interpret conditions and timing of ore emplacement, and to interpret possible sources of metals and ore fluids.

Results of this study broaden the existing knowledge of the mineralogy of veins containing auriferous pyrite in the Tobacco Root Mountains, and contribute to understanding the conditions and processes of ore emplacement and timing and source of gold

mineralization in the range. These results will be useful in the interpretation of and the exploration for gold mineralization in the Tobacco Root Mountains and in similar regions.

To accomplish its two-fold purpose, the study addresses the following:

1. regional lithologic and structural setting;
2. geologic mapping of the underground workings and surface outcrops around the mine;
3. lithologic and structural setting of the mine area;
4. paragenetic sequence and description of ore and gangue minerals.

Additional information on methods of study is given in Appendix A.

Location, Access, and Development

The Red Pine mine, a part of the Sheridan mining district, is found on the western flank of the Tobacco Root Mountains in southwestern Montana (Tansley and others, 1933; Lorain, 1937; Burger, 1966). The mine lies along Indian Creek in the Beaverhead National Forest, 13.7 kilometers northeast of Sheridan, Montana, in Madison County (Fig. 1). Specifically, it is located in the NW 1/4 of Section 3 in R4W, T4S and in the SW 1/4 of Section 34 in R4W, T3S on the Waterloo 15' topographic quadrangle by the U.S. Geological Survey. An unimproved mountain road provides access to the mine site from the Mill Creek road which intersects U.S. Highway 287 at Sheridan.

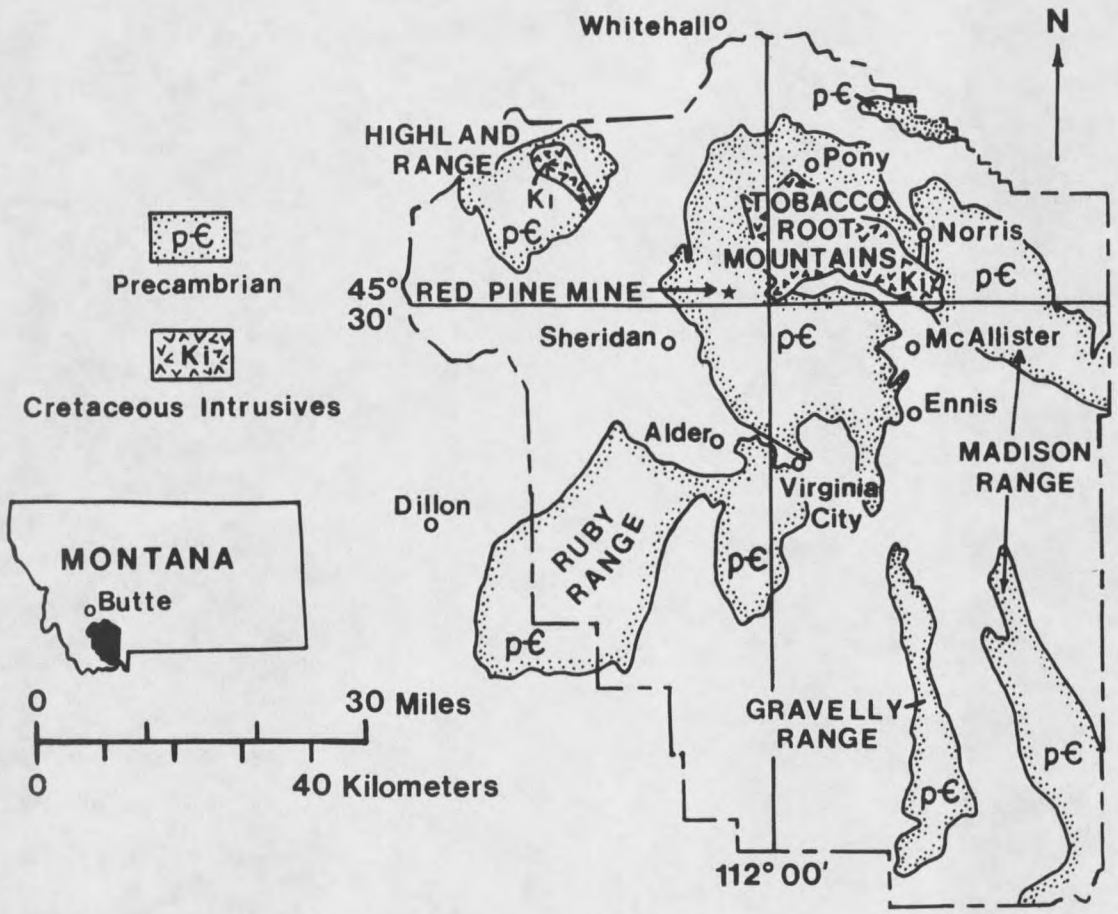

Figure 1. Location map of the Red Pine mine (modified from Vitaliano and others, 1979).

Previous owners or lessees developed the mine on two levels, an upper level at an elevation of 2446 meters and a lower level at approximately 2298 meters. Appendix B presents a synopsis of mining history at the Red Pine mine.

Property Ownership and Status

Shermont Mining Company, Sheridan, Montana, owns the Red Pine property that consists of eighteen unpatented federal claims for mining a lode deposit. Mine operator, John Magnus, of Sheridan, is the principal contact for mine access and information on mining activity in the area.

Previous Studies

Many previous petrologic, structural, and regional geologic studies have established the geologic framework of the Tobacco Root Mountains. The following synopsis identifies literature on mineral deposits in the region.

In the first reconnaissance study, Winchell (1914) reported on mining districts in the Dillon quadrangle and adjacent areas of southwestern Montana. Tansley and others (1933) conducted a reconnaissance survey of the areal geology and ore deposits in the Tobacco Root Mountains. Lorain (1937) described general settings of mines, types of ore minerals, and processing practices associated with mining of gold lodes in the Tobacco Root Mountains. Levandowski (1956) also studied mineral deposits from the southern portion of the Sheridan mining district southward to Alder, Montana. Johns (1961)

summarized the principal deposits and delineated a general paragenetic sequence for mineralization in the southern Tidal Wave district, northwest of the Sheridan district. Burger (1966), in a structural study of the Sheridan district, suggested structural controls of mineralization. He also briefly described many of the mines in the district and the ore mineralogy of the Occidental and Red Pine mines. James (1981) described the distribution and economic potential of the bedded Precambrian iron deposits of the Tobacco Root Mountains occurring in the Copper Mountain region, east of Sheridan, Montana. Cole (1983) interpreted the age of ore emplacement in the Virginia City mining district as latest Cretaceous to early Tertiary (70-60 Ma.). He also proposed an epithermal precious-metal model for the district and described the mineralogy of the U.S. Grant vein system. Ruppel (1985) suggested that Middle Cambrian carbonate rocks were sources for gold mineralization in southwestern Montana since some gold-bearing ore deposits in the Tidal Wave district are hosted in or near Meagher Limestone. Ruppel (1985) proposed that the gold had accumulated in carbonate algal reefs. Then, during the dewatering of the Park Shale, the gold was remobilized into shallow fractures in the Archean metamorphic rocks by siliceous and saline solutions (Ruppel, 1985).

REGIONAL GEOLOGIC SETTING

Lithology

The Tobacco Root Mountain Range is a domal structure in the Rocky Mountain foreland that was uplifted during the Laramide orogeny (Cordua, 1973; Vitaliano and others, 1979; Schmidt and Hendrix, 1981; Schmidt and Garihan, 1983). Archean metamorphic rocks and Cretaceous Tobacco Root batholithic or related igneous rocks predominate in the range. Proterozoic, Paleozoic, and Mesozoic sedimentary rocks and Cenozoic volcanics are present around the perimeter of the range (Vitaliano and others, 1979). The relationships and characteristics of these rocks are described in the following summary.

Archean rocks that have undergone upper-amphibolite- to granulite-facies metamorphism comprise the core of the Tobacco Root Mountains (Burger, 1966; Cordua, 1973; Vitaliano and others, 1979). Vitaliano and others (1979) have defined two distinctive lithologic associations in the Archean rocks of the range. These are quartzofeldspathic gneisses and amphibolite in the eastern portion of the range, and marbles, sillimanite schists, quartzites, iron formation, amphibolite, and a variety of quartzofeldspathic gneisses in the western half of the range.

Late Precambrian metabasic intrusives, pegmatites (deformed and undeformed), and unmetamorphosed diabase dikes have subsequently intruded the Archean rocks of the Tobacco Root Mountains (Wooden and

others, 1978; Vitaliano and others, 1979; James and Hedge, 1980). Where these intrusive bodies contact the metamorphic rocks, retrograde greenschist-facies minerals are commonly found.

Paleozoic rocks unconformably overlie Precambrian rocks on the northwestern border of the range. This northwestern Paleozoic section is composed of an estimated 80 percent carbonates and 20 percent sandstone and mudstone (Samuelson and Schmidt, 1981). Paleozoic clastic deposits on the southern and eastern edges also unconformably overlie Archean rocks (Vitaliano and others, 1979). The orientation of Paleozoic rocks in the western Tobacco Root Mountains reflects the major arch of the range (Samuelson and Schmidt, 1981). Paleozoic rocks are unconformably overlain by Mesozoic rocks (Tansley and others, 1933).

The Tobacco Root batholith and associated satellitic plutonic bodies of Late Cretaceous age intrude the Archean and Phanerozoic rocks (Vitaliano and others, 1979). Sharp and discordant contacts define near vertical surfaces between the batholith and the wall rocks (Smith, 1970). The batholith, approximately 310 square kilometers in area, was emplaced in the central to east-central portion of the mountain range (Vitaliano and others, 1979) at depths of 3 to 8 kilometers (Smith, 1970). Contact metamorphism around the batholith resulted in the development of hornfels-facies minerals (Hess, 1967; Smith, 1970).

Diorite, tonalite, granodiorite, quartz monzonite, and granite compose the batholith and show a gradational zoning pattern in their occurrence (Smith, 1970). From diorite in bordering satellitic

bodies, the rocks grade into more silicic compositions at the center of the batholith (Smith, 1970).

Tertiary volcanic rocks overlie Archean rocks on the southern and eastern borders of the range. These rocks comprise a series of lava flows and pyroclastic and volcanoclastic sedimentary units ranging in composition from basalt to rhyolite (Vitaliano and others, 1979).

Geochronology

Radiometric age determinations for rocks of the Tobacco Root region have established the timing of thermal and tectonic events. These determinations are important for limiting the possible timing of mineralization. Table 1 presents the geochronologic data available for this region. These data suggest that Archean, Proterozoic, Cretaceous, or Tertiary periods could be plausible times for ore deposition.

Structure

The Tobacco Root Mountains have been influenced by structures produced during Precambrian and Late Cretaceous to Eocene times. The Precambrian structure of the range is dominated by open and upright isoclinal folds in the metamorphic rocks, and northwest- and northeast-trending faults (Burger, 1969; Cordua, 1973; Vitaliano and others, 1979). The Late Cretaceous to Eocene Laramide structures include drag folds along northwest-trending faults described by Vitaliano and others (1979) as transcurrent. Other Laramide structures are reactivated Precambrian faults that strike to the

northwest (Samuelson and Schmidt, 1981; Schmidt and Hendrix, 1981; Schmidt and Garihan, 1983) and to the northeast (Vitaliano and others, 1979). The following discussion outlines characteristics of folds and faults in the Tobacco Root Mountains with emphasis on the southern half of the range.

Table 1. Geochronologic framework of the Tobacco Root Mountains.

Rock Type or Body	Date and Method	References
Quartzofeldspathic gneiss	2.76 +/- 0.115 Ga. average Rb/Sr whole rock isochron	James and Hedge (1980)
Quartzofeldspathic gneiss	2.667 +/- 0.066 Ga. Rb/Sr whole rock	Mueller and Cordua (1976)
Pegmatite	1.6 Ga. Muscovite K/Ar	Gilletti (1966)
Diabase dikes	1.45 Ga. Rb/Sr whole rock	Wooden and others (1978)
Diabase dikes	1.13-1.12 Ga. Rb/Sr whole rock	Wooden and others (1978)
Tobacco Root batholith	125-118 Ma. Hornblende K/Ar	Vitaliano and others (1980)
Tobacco Root batholith	75 Ma. Biotite K/Ar	Gilletti (1966)
Tobacco Root batholith	77-72 Ma. Biotite K/Ar	Vitaliano and others (1980)
Virginia City basaltic andesite	51 Ma. K/Ar whole rock	Marvin and Dobson (1979)
Virginia City basalt	34 Ma. not given	Vitaliano and others (1979)

Folds

The Mill Gulch antiform, an open fold in the Precambrian rocks, is a prominent structure in the southern portion of the range (Cordua, 1973; Vitaliano and others, 1979) (Fig. 2). In the northern part of the range, the batholith modifies the appearance of the antiform (Vitaliano and others, 1979).

Upright to overturned isoclinal folds border the Mill Gulch antiform on the west (Fig. 2) and east (Cordua, 1973). The western folds constitute the major folds in the Sheridan mining district (Burger, 1966). These folds trend N 10° W, plunge 25° N, and are overturned to the east (Burger, 1967; Cordua, 1973) (Fig. 2 and Pl. 1). They are delineated by thin beds of impure dolomitic marble (Burger, 1967).

Vitaliano and others (1979) and James (1981) recognize a later, Precambrian deformation event where recumbent "subisoclinal" folds are refolded into northeast-trending open folds. These open folds, such as the Noble Peak antiform (Pl. 1), are common in the northern Tobacco Root Mountains (Vitaliano and others, 1979).

Cordua (1973) notes the occurrence of a variety of smaller-scale folds in the rocks of the southern Tobacco Root Mountains, in addition to the major isoclinal folds. These include similar, isoclinal, convolute, ptygmatic, and intrafolial folds (Cordua, 1973).

Laramide deformation folded both Archean and Phanerozoic rocks. In the northern and northwestern Tobacco Root Mountains, drag folds along major northwest-trending faults provide evidence of this deformation (Vitaliano and others, 1979; Schmidt and Garihan, 1983).

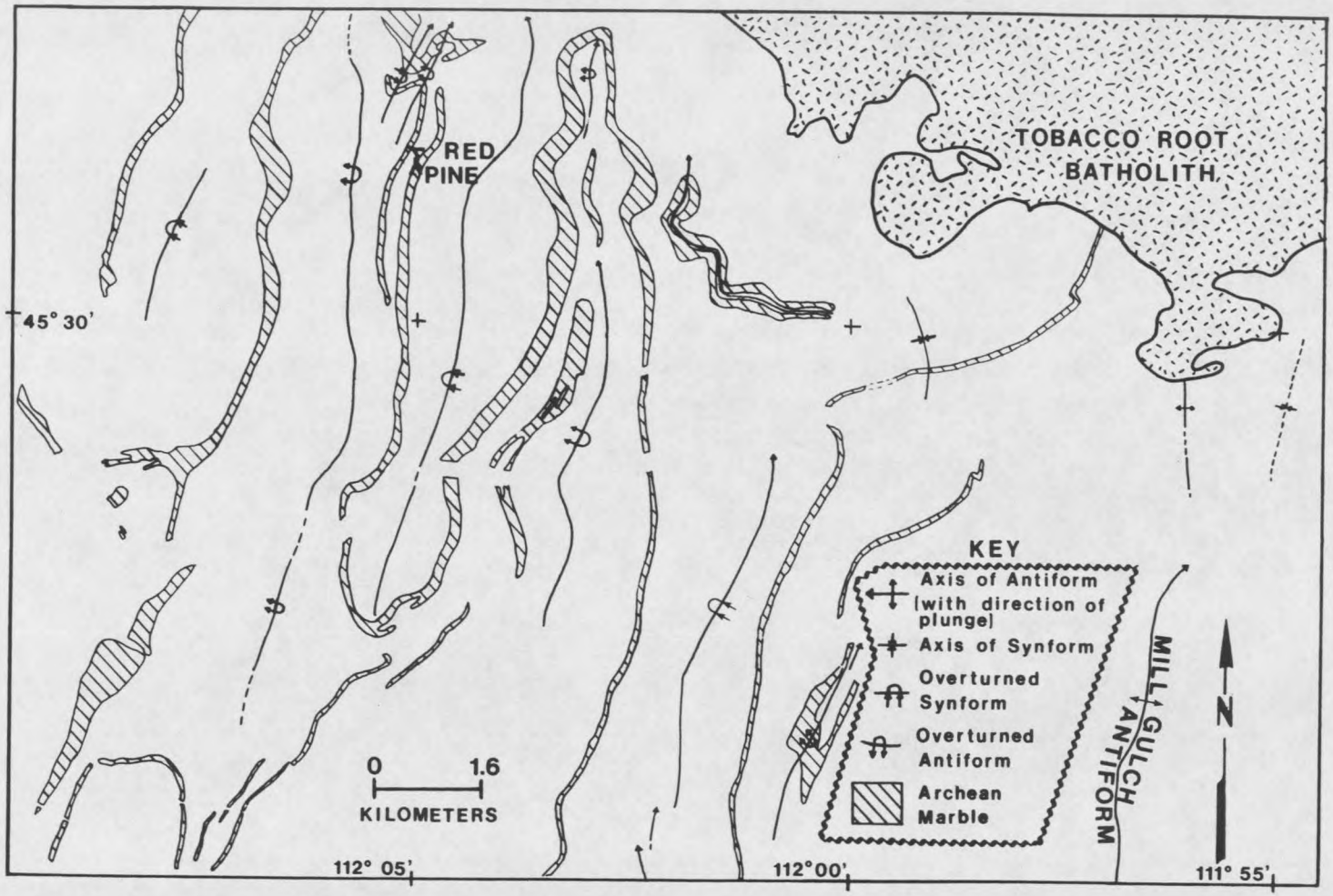

Figure 2. Sketch map of upright isoclinal folds defined by marble, west and northwest of the southern portion of the Mill Gulch antiform, southwestern Tobacco Root Mountains (modified from Vitaliano and others, 1979).

Additional evidence of Laramide folding has not as yet been recognized within the Archean rocks (Vitaliano and others, 1979).

Faults

Along with folds, major northwest-trending faults and less-prominent northeast-trending faults influence the geologic structure of the Tobacco Root Mountains. Vitaliano and others (1979) interpret both sets as high-angle faults. Some faults show evidence of strike-slip and/or dip-slip movement. Schmidt and Garihan (1983) note left-reverse movement on northwest-trending faults. Minor faults with diverse orientations also occur throughout the range (Vitaliano and others, 1979).

The predominant west-northwest orientation of faults in the range parallels the regional fault pattern in southwestern Montana (Cordua, 1973; Schmidt and Hendrix, 1981) (Fig. 3). These regional faults are thought to be reactivated Precambrian structures (Schmidt and Hendrix, 1981). Schmidt and Hendrix (1981) suggest two lines of evidence to support this. Firstly, there is a significant difference in the separation of Archean rocks in comparison with the offset of Paleozoic rocks along the same fault. For example, the Mammoth fault offsets an Archean marble unit about 3.5 kilometers in a right-lateral sense and the Cambrian-Precambrian unconformity less than 200 meters in a left-lateral sense (Schmidt and Hendrix, 1981). Secondly, the northwest-trending faults appear to have controlled the emplacement of Late Precambrian diabase dikes within or parallel to the fault zones. Schmidt and Garihan (1983) include faults striking from N 20° W to

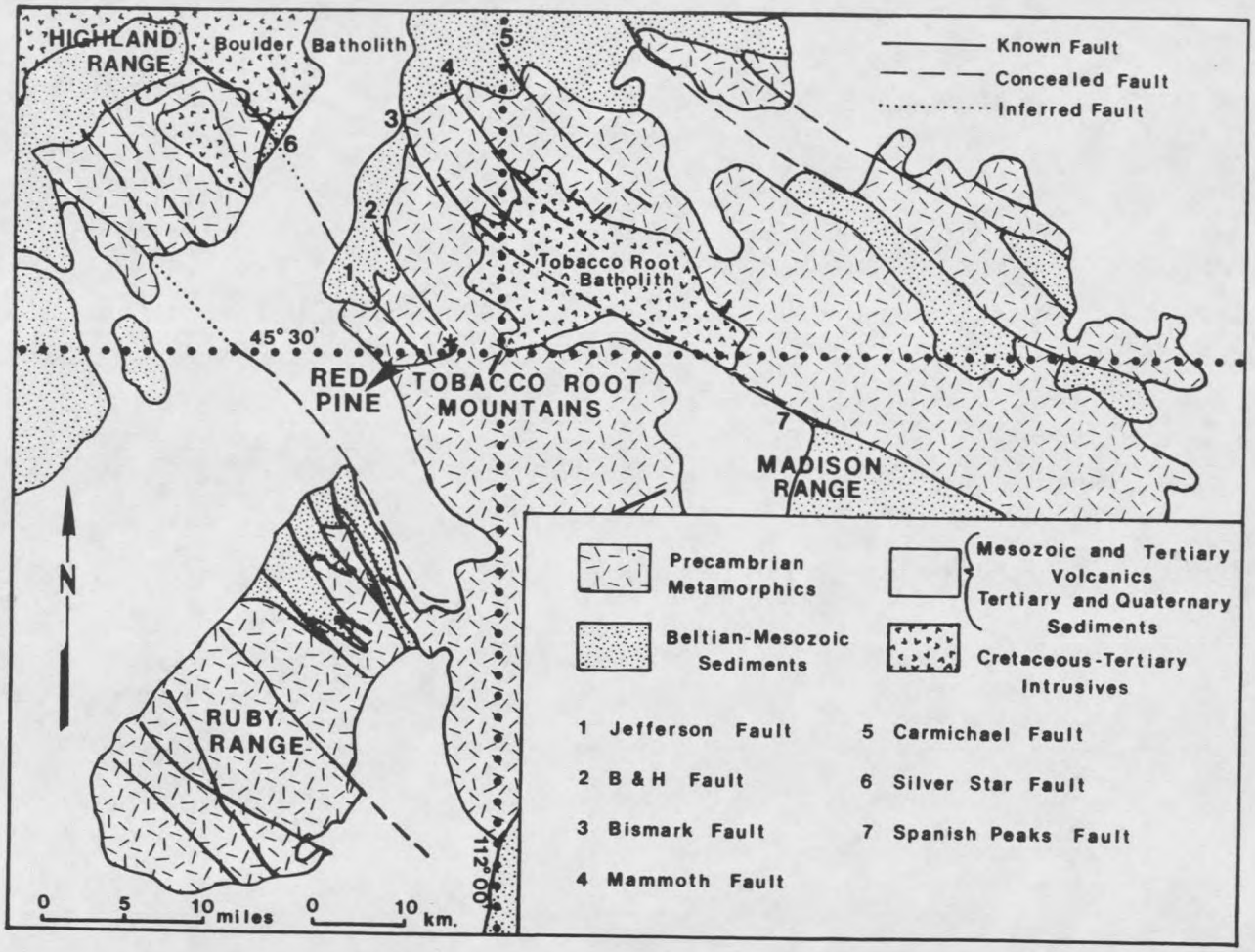

Figure 3. Map of regional geology and faults in southwestern Montana (modified from Schmidt and Hendrix, 1981). Northeast faults added from Vitaliano and others, (1979).

N 70° W with an average of N 50° W in this set. In addition, the northwest-trending faults passing through the Precambrian core of the Tobacco Root Mountains are thought to have controlled the emplacement of the Tobacco Root batholith (Smith, 1970; Vitaliano and others, 1979).

Laramide reactivation on the northwest-trending Precambrian faults offset the Tobacco Root batholith along the Bismark, Mammoth, and Carmichael faults and several smaller faults (Schmidt and Garihan, 1983). Laramide movements along the northwest-trending faults also resulted in offset of some Proterozoic diabase dikes (Schmidt and Garihan, 1983).

Laramide reactivation is also thought to have affected northeast-trending faults in the region that are believed to be of Precambrian age (Vitaliano and others, 1979). Offset of northwest-trending faults and the border to the Tobacco Root batholith by these northeast-trending faults supports this interpretation (Vitaliano and others, 1979). However, Ruppel (1982) notes that a Precambrian origin for these faults is not clear because only movements resulting from Laramide deformation have been identified.

Geologic structures affect mineralization in the range. Reid (1957) recognized control of ore deposits by both northeast- and northwest-trending faults in the northern Tobacco Root Mountains. For example, several mines are found along the northwest-trending Bismark and Mammoth faults. Burger (1966) proposed that ore deposits parallel regional fracture systems in the Sheridan mining district in the southwestern portion of the range. Many veins occur approximately

parallel to a regional system that is oriented N 30° E, 40° NW (Burger, 1966). The average orientation of the longest portion of the Red Pine vein approximates this trend.

Zoning of Metals

A regional zoning of ratios of silver to gold and ratios of copper to silver has been noted by Lorain (1937) and Cole (1983) in mining districts around the Tobacco Root batholith. Ratios of silver to gold are low in the Pony district, close to the batholith, while ratios of copper to silver are high (Cole, 1983). Farther away, in the Virginia City district, ratios of silver to gold are high while ratios of copper to silver are low (Cole, 1983). The ratios have intermediate values at moderate distances from the batholith (Cole, 1983).

The preceding summary of regional geology provides background information for the following presentation of the geology at the Red Pine mine.

GEOLOGIC SETTING OF THE RED PINE MINE

Lithology

At the Red Pine mine, the Archean country rocks can be divided into three distinctive lithologies: quartzofeldspathic gneiss, marble plus calc-silicate gneiss, and metabasite (Fig. 4). Minor rock types that are visible only in the underground workings include quartz-chlorite rock and iron formation (Pl. 2). Unmetamorphosed pegmatites of granitic and quartz-rich composition are found in the quartzofeldspathic gneiss and near the Red Pine vein, respectively (Fig. 4 and Pl. 2). The description of these rock types presented in the following subsections will aid in deciphering their relationship to Red Pine mineralization.

Gneiss

The quartzofeldspathic gneiss, the predominant type of rock at the mine, occurs as cliff-forming surface outcrops that are light to medium gray in color. Where exposed, the gneiss shows sharp contacts with adjacent rocks and well developed joints and foliation. It also has medium and coarse textures with sizes of grains ranging from 0.5 to 2 millimeters and 2 millimeters to 3 centimeters, respectively.

The primary gneissic foliation is defined by compositional layering, the alignment of ferromagnesian minerals, and locally by the alignment and elongation of quartz ribbons. The orientation of

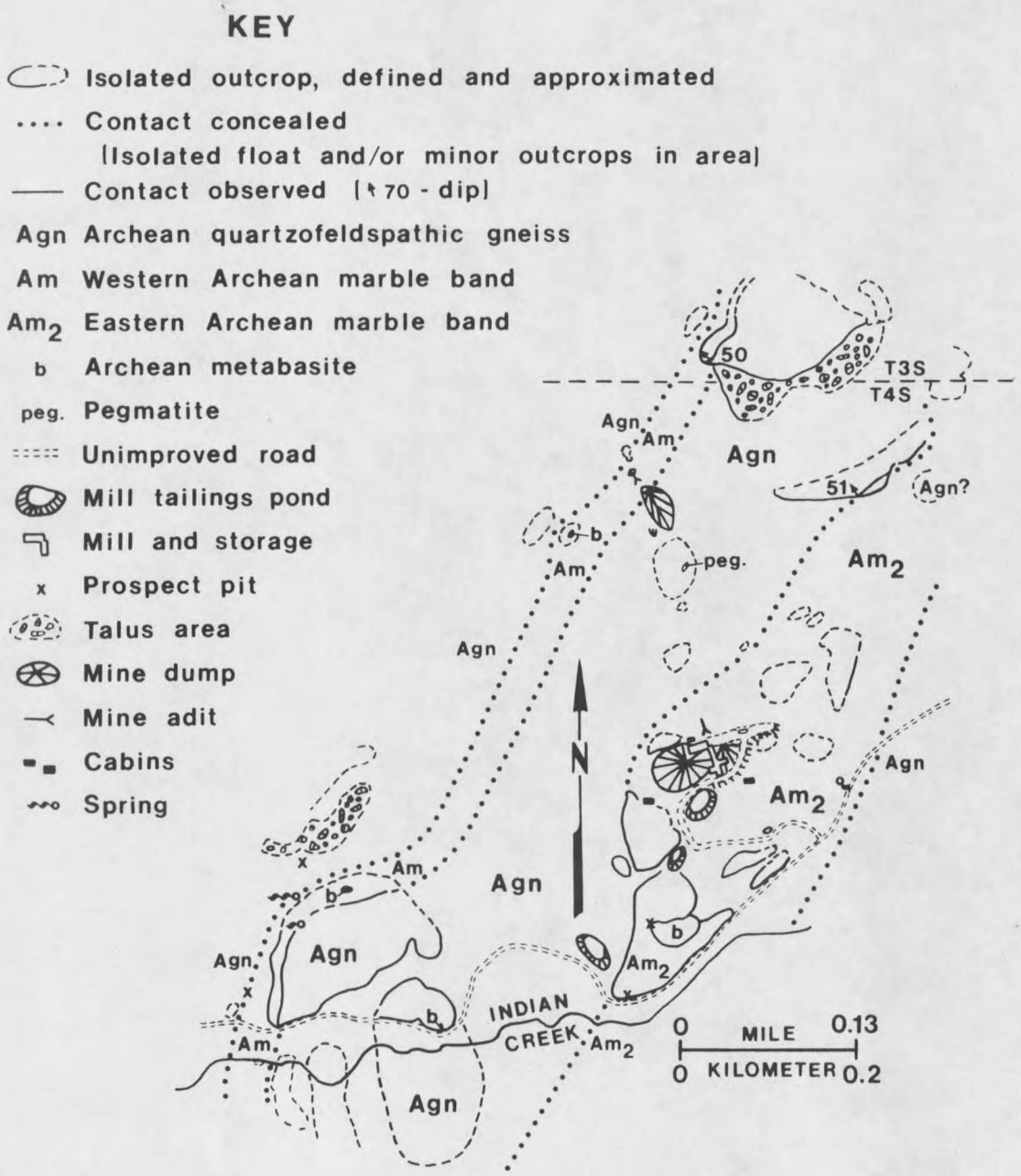

Figure 4. Outcrop and geologic map of the Red Pine mine area.

biotite shows a second, weakly developed foliation in some thin sections. Foliation strikes to the north-northeast and cuts the contacts of gneiss and marble (Fig. 5). In a few localities, foliation parallels contacts of gneiss and marble (Fig. 5 and Pls. 2 and 3).

The mineralogy of the quartzofeldspathic gneiss is relatively uniform, with plagioclase and quartz forming the bulk of the rock. Additional minerals include microcline, biotite, hornblende, and garnet. In more mafic-rich varieties of the gneiss, diopside and hypersthene are also present. Accessory minerals include zircon, apatite, tourmaline, rutile, and unidentified opaques. Cordierite occurs in some garnet-rich gneiss as an accessory mineral in rare instances. Table 2 summarizes the estimated abundances of minerals composing the quartzofeldspathic gneiss.

The texture of the quartzofeldspathic gneiss varies from granoblastic to blastomylonitic (Spry, 1969; Best, 1982). However, ragged textures exist along grain boundaries where retrograde or hydrothermal alteration has occurred.

Textures and mineral associations of the gneiss indicate crystallization under upper-amphibolite- to granulite-facies metamorphic conditions (Turner, 1981; Best, 1982, Hyndman, 1985). Specifically, these conditions are indicated by the presence of orthopyroxene and clinopyroxene in the assemblage. Furthermore, the presence of antiperthite and perthite denotes a high temperature of crystallization possible under high-grade metamorphic conditions (Best, 1982).

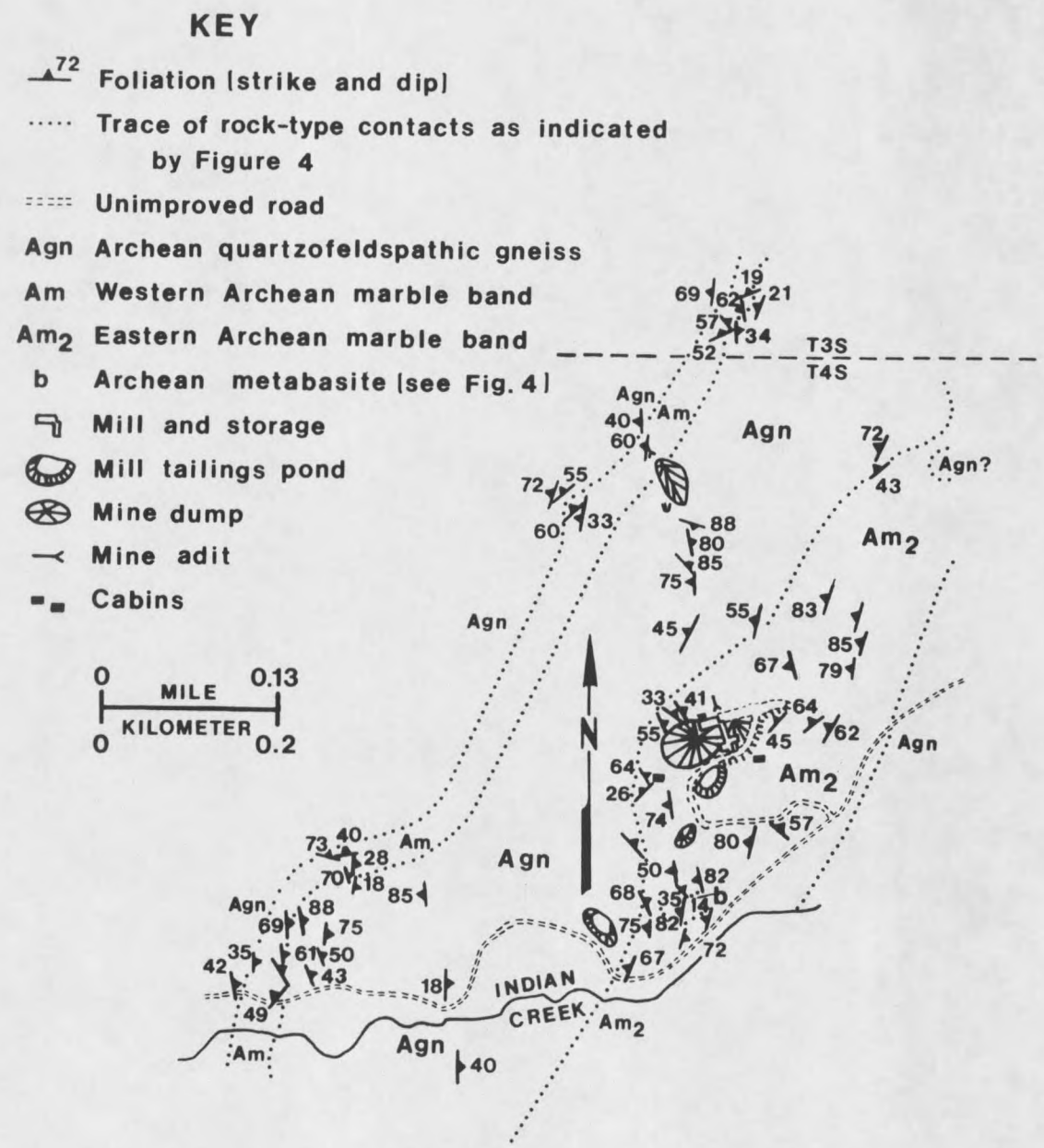

Figure 5. Surface map of strike and dip of foliation in metamorphic rocks at the Red Pine mine.

Table 2. Relative abundances of minerals in quartzofeldspathic gneiss.

Thin Section Sample Sites Keyed to Plates 2 and 3 and Appendix C

Sample Sites	A	B	C	D	E	F
MINERALS						
plagioclase	X	X	M	X	X	X
antiperthite	O	O	T	O	O	O
quartz	X	X	X-	X	X	X
microcline	X-	X	X	O	X+	O
biotite	M	O	X-	X	O	X
hornblende	M	M	X-	O	O	X
garnet	T	X	X-	X	O	M
diopside	O	O	X	O	O	O
hypersthene	O	O	X-	O	O	O
cordierite	O	O	O	T	O	O
zircon	T	T	T	T	T	T
tourmaline	O	T	T	O	O	T
rutile	O	O	O	T	O	O
apatite	T	T	T	O	T	O
opaques	T	T	T	T	O	T
chlorite	R	O	R	O	O	R
carbonate	R	O	O	O	O	R
sericite	R	R	O	O	O	R
epidote	R	O	O	O	O	O

X = Major constituent > 10 % estimated
X+ = Major constituent > 50 % estimated
M = Notable constituent 4-5 % estimated
X- = Important constituent >5 % to 10% estimated
T = Trace amounts </= 3 %
R = Retrograde mineral
O = Not observed

Marble and Calc-silicate Gneiss

Two nearly parallel bands of marble strike to the north-northeast across the Red Pine mine area (Fig. 4 and Pl. 1). These two layers are here designated as the eastern and western marble bands, respectively.

Marble, second to gneiss in abundance at the mine, occurs in outcrops that form cliffs or slopes. The outcrops are light gray to buff in color. The cliff-forming outcrops are more resistant, silica-rich bodies and/or are outcrops supported by quartzofeldspathic gneiss. Some siliceous sections of marble grade into calc-silicate gneiss. Marble outcrops also contain quartz and calc-silicate lenses, layers, or boudins that typically parallel the foliation.

The marble has rough, granular to sugary textures due to the weathering of carbonate grains and/or to the presence of relatively resistant silicate minerals. Grains have an average size ranging from 0.5 millimeter to 1.3 centimeters.

Expressions of foliation and minor folds in marble outcrops are also enhanced by weathering. The alignment of mica and the compositional layering of mineral impurities define the folds and the foliation.

The mineralogy of the marble and calc-silicate gneiss is quite complex. Calcite and diopside are most abundant in the marble. However, variable amounts of dolomite, quartz, tremolite, plagioclase, phlogopite, biotite, microcline, scapolite, dolomite, and garnet are also present. Olivine, if present, has altered to serpentine. Common accessory minerals include sphene, graphite, tourmaline, zircon,

apatite, pyrite, chalcopyrite, and unidentified opaques. Table 3 shows the estimated abundances of these minerals as determined in fourteen thin sections.

The marble and calc-silicate gneiss are granoblastic (Spry, 1969). The minerals and textures present indicate metamorphism to the upper-amphibolite or granulite facies (Turner, 1981; Best, 1982; Hyndman, 1985). Reaction textures point to subsequent incomplete retrogression to amphibolite-facies minerals (Spry, 1969; Hyndman, 1985). Moreover, greenschist-facies minerals overprint both the granulite- and amphibolite-grade events. Evidence for a greenschist event is found in the presence of quartz, carbonate, and chlorite veinlets that cut and replace minerals of higher grade. The presence of talc, serpentine, and chlorite provides additional evidence of a retrograde greenschist event (Hyndman, 1985).

Metabasite

Lenticular and pod-like bodies of metabasite occur in quartzofeldspathic gneiss and marble (Fig. 4 and Pl. 3). Sharp contacts exist between the metabasite and marble or quartzofeldspathic gneiss. Metabasite occurs in blocky outcrops that contain well developed joint sets. The outcrops of metabasite are gray to black or greenish black in color. Metabasite is a moderately foliated, fine-grained rock with grains ranging in size from <0.5 to 1.5 millimeters.

Variable amounts of hornblende, plagioclase, diopside, garnet, biotite, quartz, and hypersthene-enstatite compose the metabasite bodies. Common accessory minerals include apatite, zircon,

Table 3. Relative abundances of minerals in marble and calc-silicate gneiss.

Thin Section Sample Sites Keyed to Plates 2 and 3 and Appendix C

Sample Sites	G	H	I	J	K	L	M	N	O	P	Q	R	S	TC
MINERALS														
calcite	R	R	SR	X	X	X	X+	R	R	X	X	R	X	X
diopside	X+	X	O	X-	O	T	X	X	X+	X	O	X-	X	X-
dolomite	O	O	O	T	T	X	X-	O	O	X-	T	O	T	O
tremolite	R	R	T	O	O	R	O	R	R	O	X	TR	XR	O
phlogopite	X	X	T	O	X	T	O	T	M	O	O	O	O	O
microcline perthite	X	X	X+ T	X	O	O	O	O	T	X	O	O	O	X-
scapolite	O	O	O	X	O	O	O	X	O	X	O	O	O	X-
plagioclase	O	O	O	X-	T	O	M	X	X-	O	O	O	O	O
antiperthite	O	O	O	T	O	O	O	T	O	O	O	O	O	O
garnet	O	O	O	M	O	O	X-	X-	O	T	O	O	O	T
graphite	T	X-	X-	O	X-	O	O	O	X	T	M	T	O	T
spinel	O	O	O	O	X-	O	O	O	O	O	O	O	O	O
quartz	O	X	X	M	T	O	T	X	R	O	O	X+	O	T
sphene	T	M	T	T	O	O	T	X-	T	T	T	O	O	T
apatite	O	T	T	T	T	O	O	T	T	O	O	T	O	O
zircon	O	T	T	O	T	O	O	T	T	T	O	T	O	O
tourmaline	O	T	M	O	T	O	O	O	T	T	O	T	O	O
opaques/ sulfides	T	T	T	T	T	T	T	T	T	T	T	T	T	O
talc	O	O	O	O	R	O	O	O	O	O	R	O	O	O
chlorite	R	O	R	O	R	O	O	O	R	R	R	O	O	O
serpentine	O	O	O	O	R	O	O	O	O	O	O	O	O	O
biotite	O	O	O	M	O	O	O	O	O	R	O	O	O	O
actinolite/ unidentified amphibole	O	O	O	M	T	O	O	O	O	R	O	O	O	TR
clinozoisite	O	O	O	O	O	O	O	R	O	O	O	O	O	O
sericite or white mica	O	O	R	O	O	O	O	O	R	O	O	O	O	O
leucoxene	O	O	O	O	R	O	O	O	O	O	O	O	O	O

X = Major constituent > 10 % estimated
X- = Important constituent > 5 % to 10 % estimated
X+ = Major constituent > 50 % estimated
M = Notable constituent 4-5 % estimated
S = Secondary mineral in cross-cutting veinlets
T = Trace amounts ≤ 3 %
R = Retrograde mineral
O = Not observed

tourmaline, sphene, rutile, and unidentified opaques. Compositional layering of these minerals and oriented hornblende laths define foliation in the metabasite. Table 4 lists the relative abundances of these minerals in twelve thin sections.

The metabasite is typically granoblastic. The mineral textures and assemblages indicate formation at upper-amphibolite to granulite grades of metamorphism (Spry, 1969; Turner, 1981; Best, 1982; Hyndman, 1985). The presence of orthopyroxene, clinopyroxene, and garnet in the assemblage provides evidence of high-pressure, granulite-facies conditions (Turner, 1981; Best, 1982; Hyndman, 1985). In addition, antiperthite denotes crystallization at high temperatures (Best, 1982).

Secondary carbonate veinlets cut the high-grade minerals in the metabasite. Alteration of primary grains is visible adjacent to these veinlets. Near the Red Pine vein, the veinlets contain microcrystalline quartz. Greenschist-facies minerals are also present locally due to retrograde metamorphism or hydrothermal alteration. These minerals are included in Table 4.

Quartz-Chlorite Rock

Quartz-chlorite rock is the most abundant of the two minor rock types along the Red Pine vein. The quartz-chlorite rock occurs in blocks, primarily in the hanging wall of the vein (Pl. 2). However, some blocks are also present below datum level in the footwall. The quartz-chlorite rock is extremely fine-grained with grain sizes ranging from <0.01 to 0.9 millimeter. It varies in color from medium

Table 4. Relative abundances of minerals in metabasite.

Thin Section Sample Sites Keyed to Plates 2 & 3, Appendix C, & Fig. 12

Sample Sites	T	U	V	W	X	Y	Z	AA	BB	CC	DD	UW-5
MINERALS												
plagioclase	X-	X	X	X	X	X	X	X	X	X	X	X
antiperthite	O	O	T	T	M	O	O	O	O	O	T	T
quartz	X-	X-	X	X-	T	M	M	X-	T	X-	M	X-
microcline perthite	O	O	O	O	O	O	O	O	O	O	T	O
biotite	O	O	O	O	R	X	RX-	O	T	O	O	O
hornblende	X	X	X	X	X	X	X	X	X	X	X	X
garnet	X	X	X	X	X	X	X	X	X	X	X	X
diopside	X	X	O	X	X	X	X	X	X	X	X	X
hypersthene enstatite	T	M	O	O	T	T	T	T	O	T?	T	T
opaques	T	M	M	M	M	M	T	M	M	T	T	M
apatite	T	T	T	T	T	T	T	T	T	T	T	T
zircon	T	T	T	T	T	T	T	T	T	T	T	T
tourmaline	O	T	O	O	T	T	O	O	O	O	O	O
sphene	O	T	O	O	O	O	O	O	O	O	O	O
sericite/ white mica	R	R	R	R	R	R	O	R	R	R	O	R
epidote	O	O	O	O	O	R	O	R	O	O	O	O
chlorite	O	R	R	O	O	O	R	R	R	O	O	O
carbonate	SR	O	R	SR	O	SR	O	O	O	O	O	O
actinolite/ blue-green hornblende	O	O	O	R	O	?	?R	?R	?R	O	O	?R

X = Major constituent > 10 % estimated
X- = Important contituent > 5% to 10 % estimated
X+ = Major constituent > 50 % estimated
M = Notable constituent 4-5 % estimated
T = Trace amounts </= 3 % ? = Identification uncertain
R = Retrograde mineral O = Not observed
S = Secondary mineral in cross-cutting veinlets

gray to forest green. Neither relict metamorphic textures nor relict minerals has been observed in the rock.

The rock is composed of quartz and unidentified opaques in a chlorite-rich matrix. The quartz grains possess nearly equant, slightly elongated, and irregular shapes. The grains show undulose extinction and evidence of slip bands. Quartz typically has curved boundaries. However, straight quartz-quartz boundaries exist and some slightly ragged boundaries occur against chlorite and carbonate.

Apatite, zircon, tourmaline, unidentified opaques, and vermicular feldspar occur as inclusions in the quartz. Along with sphene, these idioblastic to xenoblastic minerals are the common accessory minerals in the rock.

The unidentified opaque minerals are present as individual grains and as inclusions in chlorite mats. Irregular to ovoid in shape, they range in size from <0.01 to 0.6 millimeter. Under a hand lens, some of these opaques are identified as disseminated pyrite.

Chlorite is found in mats, veinlets, and as individual grains. It fills fractures in other mineral grains. Some chlorite is associated with very fine-grained dolomite, patchy calcite grains, and white mica or clay.

Numerous veinlets of carbonate and quartz cut the rock. Veinlets contain some combination of quartz, calcite and/or dolomite, pyrite, and acicular or irregular opaque minerals. Cross-cutting relations substantiate at least two generations of carbonate veinlets. Serrate textures indicate a reaction between quartz and carbonate in

some veinlets. These textures and the presence of carbonate in open-space fillings suggest that carbonate formed later than quartz.

Meta-Iron Formation

Blocks of meta-iron formation, 0.6 meter by 0.6 meter in maximum dimensions, are found in the hanging wall of the Red Pine vein (Pl. 2). These blocks are surrounded by coarse-grained marble. The iron formation contains folded, magnetite- and chlorite-rich layers in a quartz matrix.

Quartz, magnetite, biotite, garnet, zircon, and chlorite comprise the iron formation. Of these minerals, quartz is the most abundant. It occurs in ribbons with cuspate boundaries and as irregular and equant grains with curved boundaries. The quartz contains inclusions of subrounded zircon and ovoid to idioblastic apatite. Undulose extinction, subgrains, and slip bands are also present in the quartz.

Magnetite, the distinctive mineral of the iron formation, occurs as individual idioblastic to xenoblastic grains and as interconnected grains. In some cases, the grains rim quartz. The interconnected grains also define the cleavage and boundaries of amphiboles that have been incompletely replaced by secondary microcrystalline quartz.

Chlorite, primarily an alteration mineral, is found in mats and veinlets. Chlorite replaces ovoid garnet and blocky biotite in the iron formation. Where it has formed through alteration of biotite, chlorite contains inclusions of acicular rutile and rounded to hexagonal opaques.

Secondary veinlets of calcite and microcrystalline quartz are common features in the iron formation. These veinlets, some containing minute grains of pyrite, cut the layering of the iron formation. Microcrystalline quartz has replaced amphiboles and has encompassed other minerals in the rock. Angular growth bands in a quartz-filled veinlet may suggest that the microcrystalline quartz has replaced some carbonate. Moreover, microcrystalline quartz contains trace amounts of minute gold.

Zircon is found as discrete grains up to 1.2 millimeters in size. The grains are subrounded to irregular in shape, and some have pleochroic halos.

Graphite is present in the iron formation as fibers and subrounded grains. The largest sizes that have been observed are 0.2 millimeter for subrounded grains and 0.3 x 0.05 millimeter for fibers.

Pegmatite

Pegmatite bodies are emplaced in Archean quartzofeldspathic gneiss of the mine area. One body is also found along a contact of gneiss and marble. The pegmatites cut foliation in the Archean rocks (Fig. 4 and Pl. 2).

Minerals in the pegmatites include milky quartz, feldspar, and biotite. Quartz composes the pegmatite core in many cases, while microcline occurs in the marginal portions. Coarse-grained biotite may also be present near pegmatite boundaries.

Some quartz-rich pegmatites are found adjacent to the Red Pine vein (Pl. 2). Since cross-cutting relationships are not clear, an interpretation of the timing of these pegmatites is not possible.

Structure

The predominant structures related to country rocks at the mine site are folds, minor faults, and joints or fractures. The following discussion identifies significant characteristics of these structures.

Folding is evident on both regional and mesoscopic scales. On a large scale, the mine is located on the eastern flank of the Eclipse Gulch antiform, an upright isoclinal fold defined by impure Archean marble (Burger, 1966) (Pl. 1). On a smaller scale, isoclinal folds predominate in the country rocks at the mine site. Intrafolial folds are also present. Both types of folds are defined by foliation, compositional layering, and/or trains of silicate minerals.

The major foliations in marble and quartzofeldspathic gneiss are steeply dipping. The foliation strikes approximately N 8° E and dips 69° NW for marble (Fig. 6). The foliation in the gneiss is oriented N 8° E, 68° SE and N 10° E, 50° NW (Fig. 7).

Faults have been observed in the metamorphic country rocks only in the underground workings. Two minor faults are recognized in the adit of the lower level (Pls. 2 and 3) where metabasite in marble has been offset. Faulting along the vein is evident in the fractured and brecciated textures in both the vein and some adjacent wall rocks.

Joints are more prevalent than faults at the mine. They are common features in quartzofeldspathic gneiss and metabasite rather

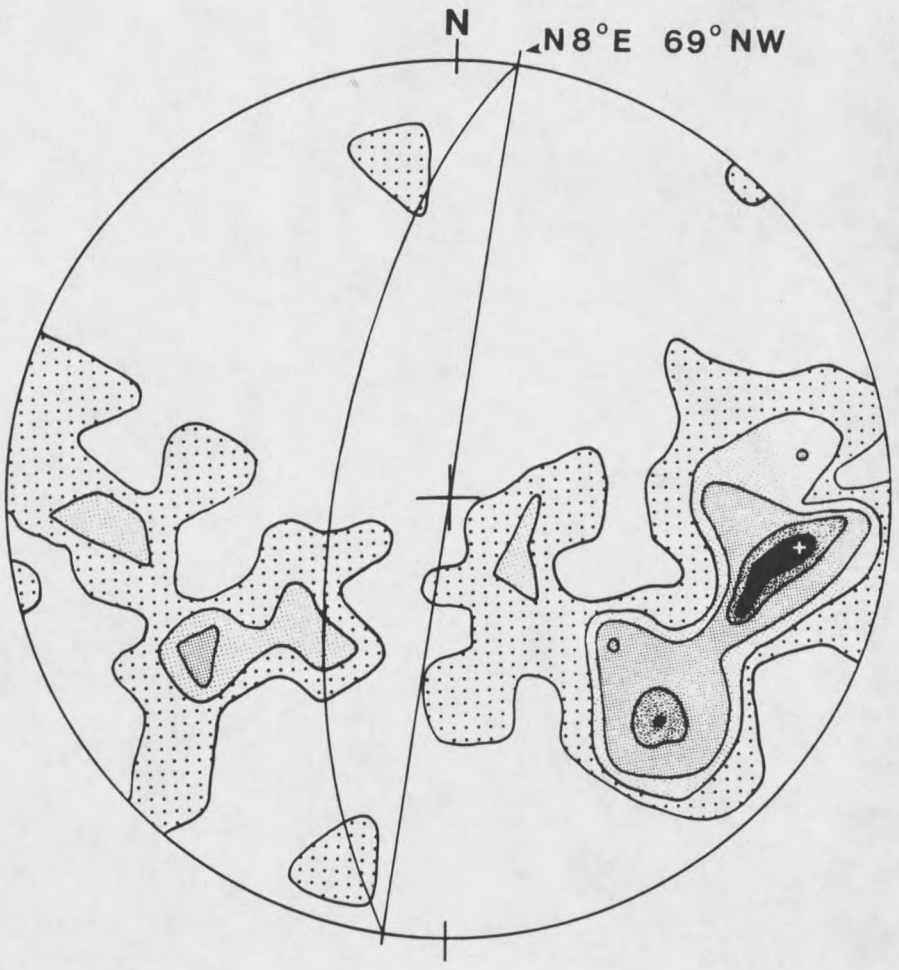

Figure 6. Lower hemisphere projection of poles to 64 foliation surfaces in marble which are plotted on a Schmidt equal-area net. Contours are at 1%, 3%, 5%, 8%, and 11% per 1% area with a maximum density at 13% (+). This diagram indicates steeply dipping foliation in marble that strikes N 8° E and dips 69° NW.

than in marble (Pls. 2 and 3 and Fig. 8). The major joint sets in the gneiss include planes oriented N 67° E, with a vertical dip; and EW, 83° S (Fig. 9). Of six metabasite joints measured, half strike N 5°-15° E and dip steeply to the northwest. Orientations of joints in marble are variable, but the major concentration of poles to these

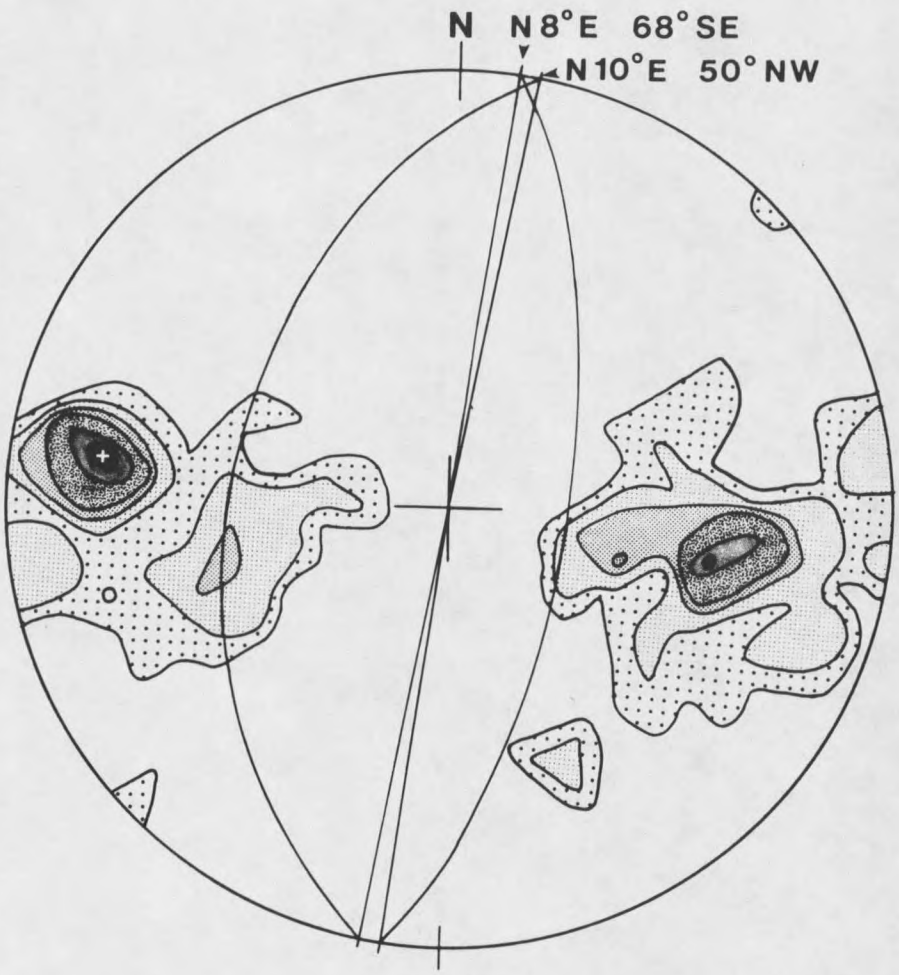

Figure 7. Lower hemisphere projection of 67 foliation surfaces in quartzofeldspathic gneiss which are plotted on a Schmidt equal-area net. Contours are at 1.5%, 3%, 6%, 7%, 10%, and 12% per 1% area with a maximum density at 15% (+). This diagram indicates steeply dipping foliation in the gneiss that has orientations of N 8° E, 68° SE and N 10° E, 50° NW.

joints indicates a significant joint set oriented N 26° E, 46° NW (Fig. 10). Another major joint set is oriented N 40° E, 37° NW.

The structure and lithology of the mine area described in this section provide the basis for describing the Red Pine vein. The vein is discussed in the following section.

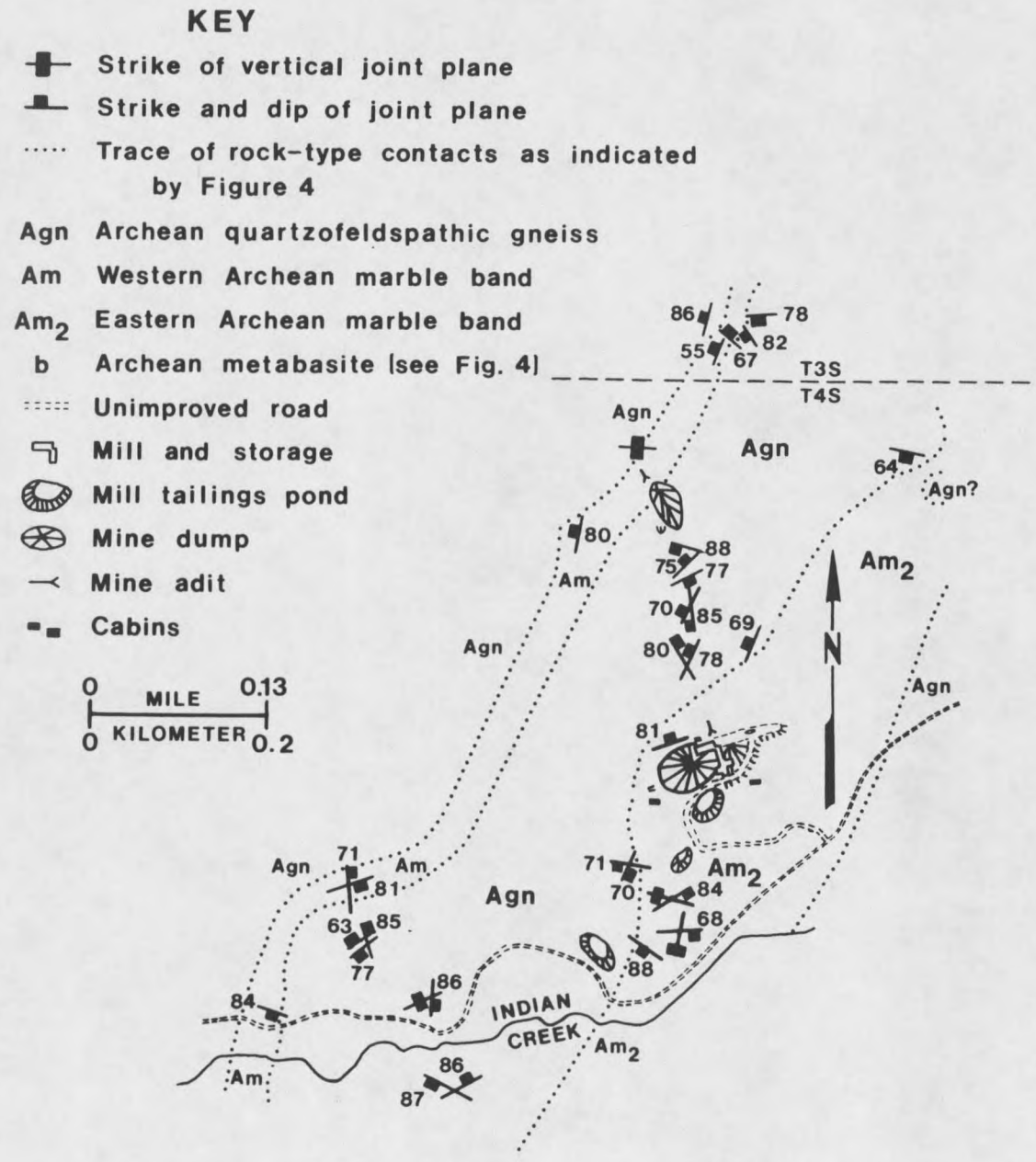

Figure 8. Orientations of joints in outcrops of metamorphic rocks at the Red Pine mine site.

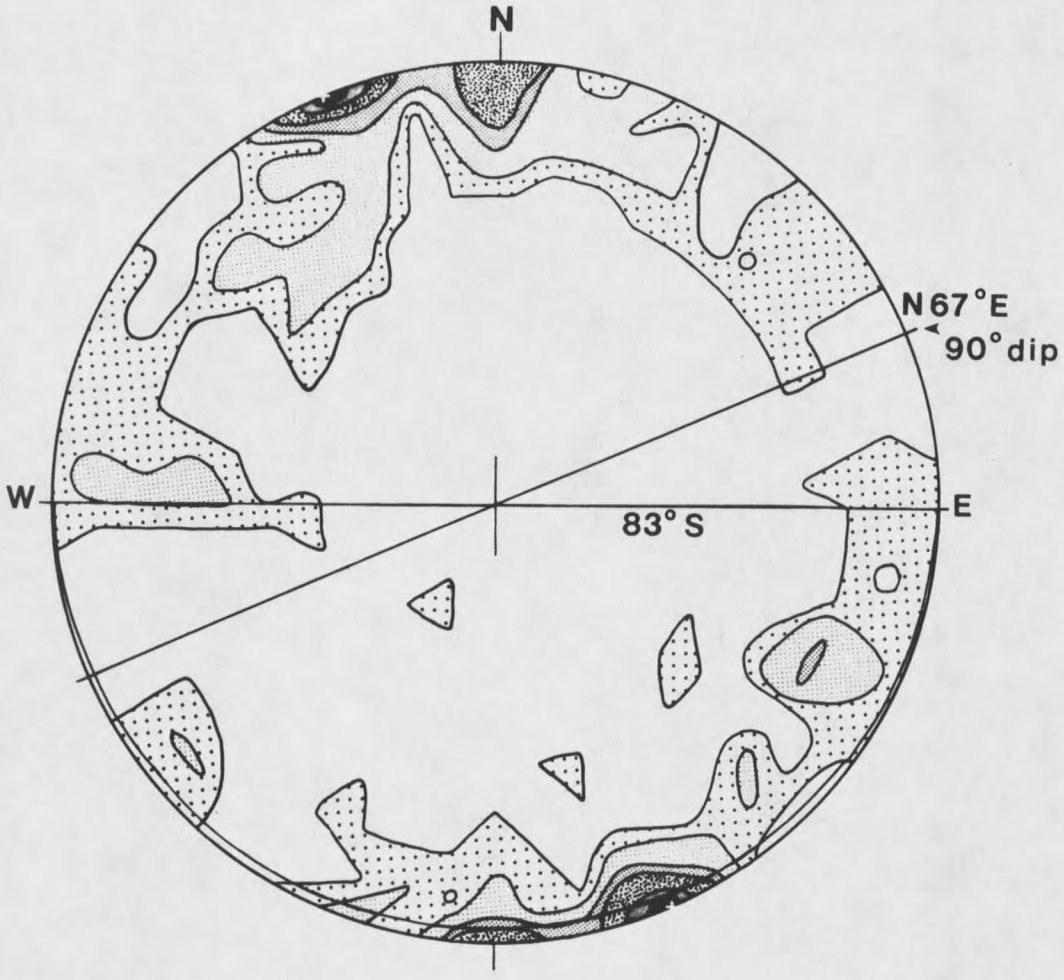

Figure 9. Lower hemisphere projection of poles to 79 joint surfaces in quartzofeldspathic gneiss which are plotted on a Schmidt equal-area net. Contours at 1%, 3%, 5%, 6%, 10%, and 13% per 1% area with a maximum density of 14% (+). The major orientation of joints strikes N 67° E and has a vertical dip. A second set of joint surfaces strikes E-W and dips 83° S.

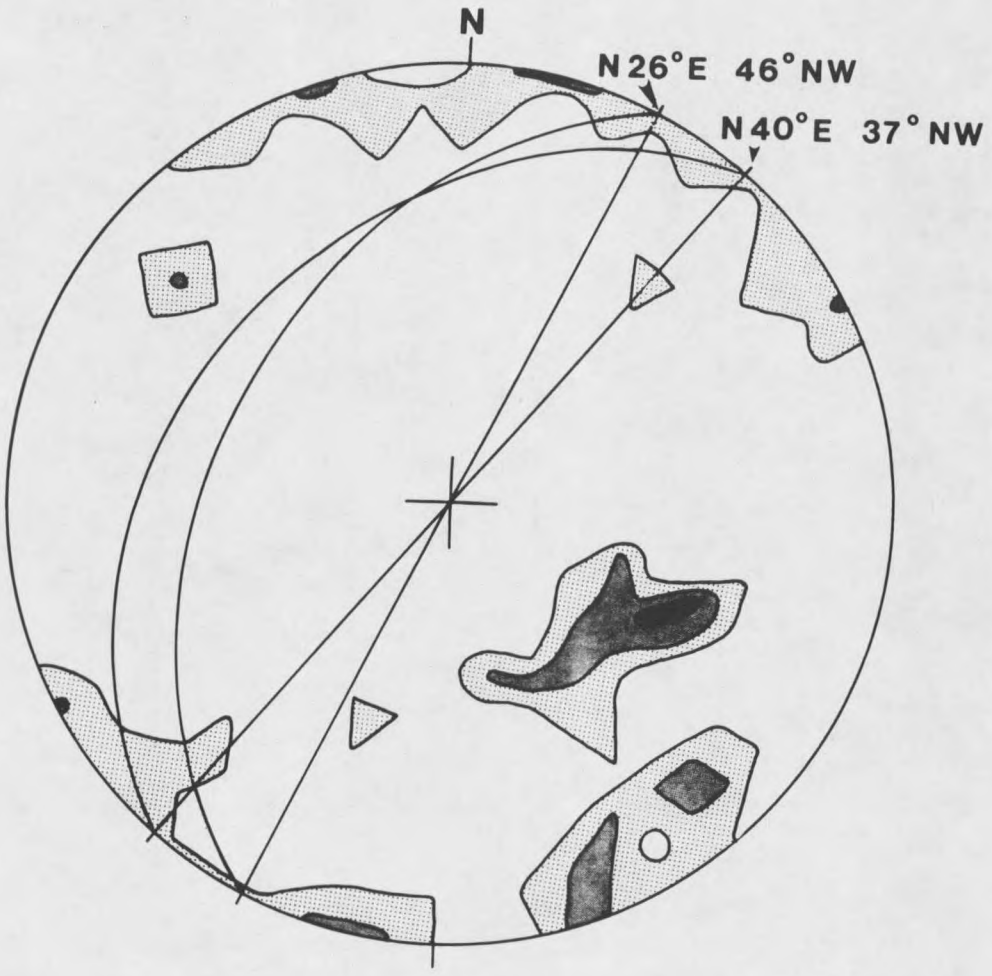

Figure 10. Lower hemisphere projection of poles to 33 joints and/or graphite-gouge fractures in marble which are plotted on a Schmidt equal-area net. Contours are at 3%, 6%, and 9% per 1% area. The concentration of poles indicates significant joint sets oriented N 26° E, 46° NW; and N 40° E, 37° NW.

RED PINE VEIN

Description

The Red Pine vein is a "complex", or multiply-injected vein system in a fissure (Jensen and Bateman, 1979; Guilbert and Park, 1986). The vein has some branching sections and some localized areas where replacement of the wall rock has taken place (Pl. 2). The vein occurs both in Archean marble and along the contact of marble with quartzofeldspathic gneiss (Pl. 2 and Fig. 11). It adjoins blocks of quartz-chlorite rock, iron formation, and quartzofeldspathic gneiss in marble (Pl. 2).

The orientation of the vein is variable. The vein cuts the foliation of the metamorphic host rocks. Yet, in some cases, the orientation of the vein is subparallel to this foliation (Pls. 2 and 3). The average strike and dip of the longest portion of the vein in the lower mine level is N 36° E, 50° NW (Pl. 2). However, the average orientation for the section in the southwestern portion of this level is N 45° E, 54° NW. Moreover, dip angles vary from 38 to 86 degrees in this level. In the upper level, the average orientation of the vein is N 32°-36° E, 44° NW (Figs. 11 and 12).

Dimensions of the vein are observable from underground workings. The longest portion of the vein is 213 meters in the lower (2298 m.) level (Fig. 11 and Pl. 2). The subparallel section of the vein in

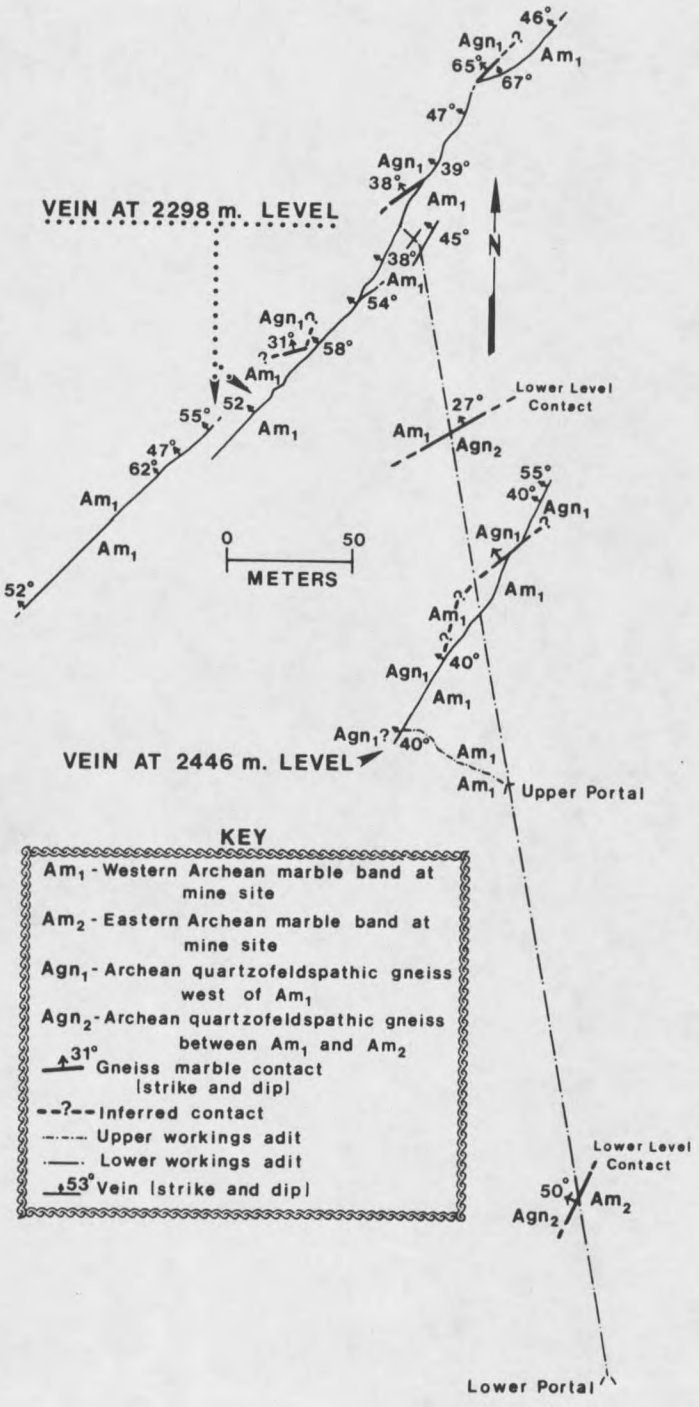

Figure 11. Line map in plan view showing relations of upper workings (2446 m. elevation) to lower workings [main level (2298 m. elevation)].

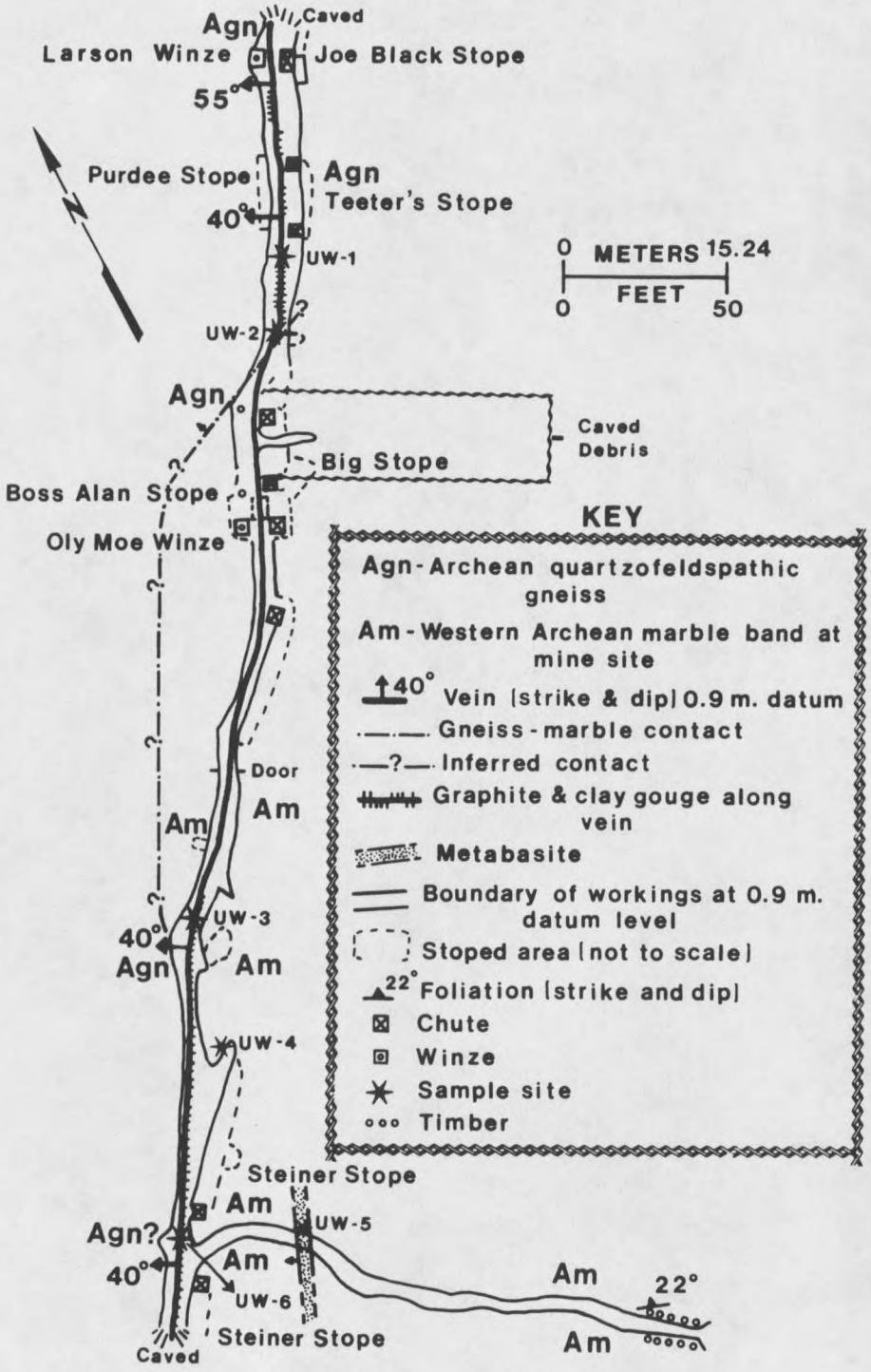

Figure 12. Plan map of Red Pine upper workings (2446 m. elevation). The geology is slightly modified from Ackerman (1957) base map provided by John Magnus.

the southwestern portion of this level is exposed for 103 meters (Fig. 11 and Pl. 2). The vein pinches and swells along strike and dip (Pl. 2). This produces variable widths ranging from 5 centimeters to 3 meters.

The enlargement of the vein along areas of flattened dip suggests reverse faulting along an irregular surface (Guilbert and Park, 1986). These enlarged areas serve as sites for concentrated ore deposition.

The principal components of the vein are milky quartz, gray to black microcrystalline quartz, pyrite, chalcopyrite, tetrahedrite, native gold, calcite, and graphite gouge (Fig. 13). Wall rock incorporated in the vein includes brecciated and altered metabasite or gneiss, and fractured, brecciated, and/or silicified marble. Massive milky quartz, milky quartz lenses, microcrystalline quartz, graphite-gouge stringers, and, less commonly, sulfides in marble or in quartz-chlorite rock define the borders of the vein. These components have been mapped separately where possible (Pl. 2).

The widest sections of the vein include areas where graphite-gouge stringers diverge from the main quartz vein. In these wide areas, blocks of marble are incorporated in the vein zone (Pl. 2). These blocks are unaltered or silicified in varying degrees. Other wide areas include sections where milky quartz is accompanied by microcrystalline quartz that heals breccia fragments of milky quartz.

The vein may branch, as indicated by quartz-filled fissures that connect to the main portion of the vein. Branching could also be interpreted from the divergent and horsetail characteristics of

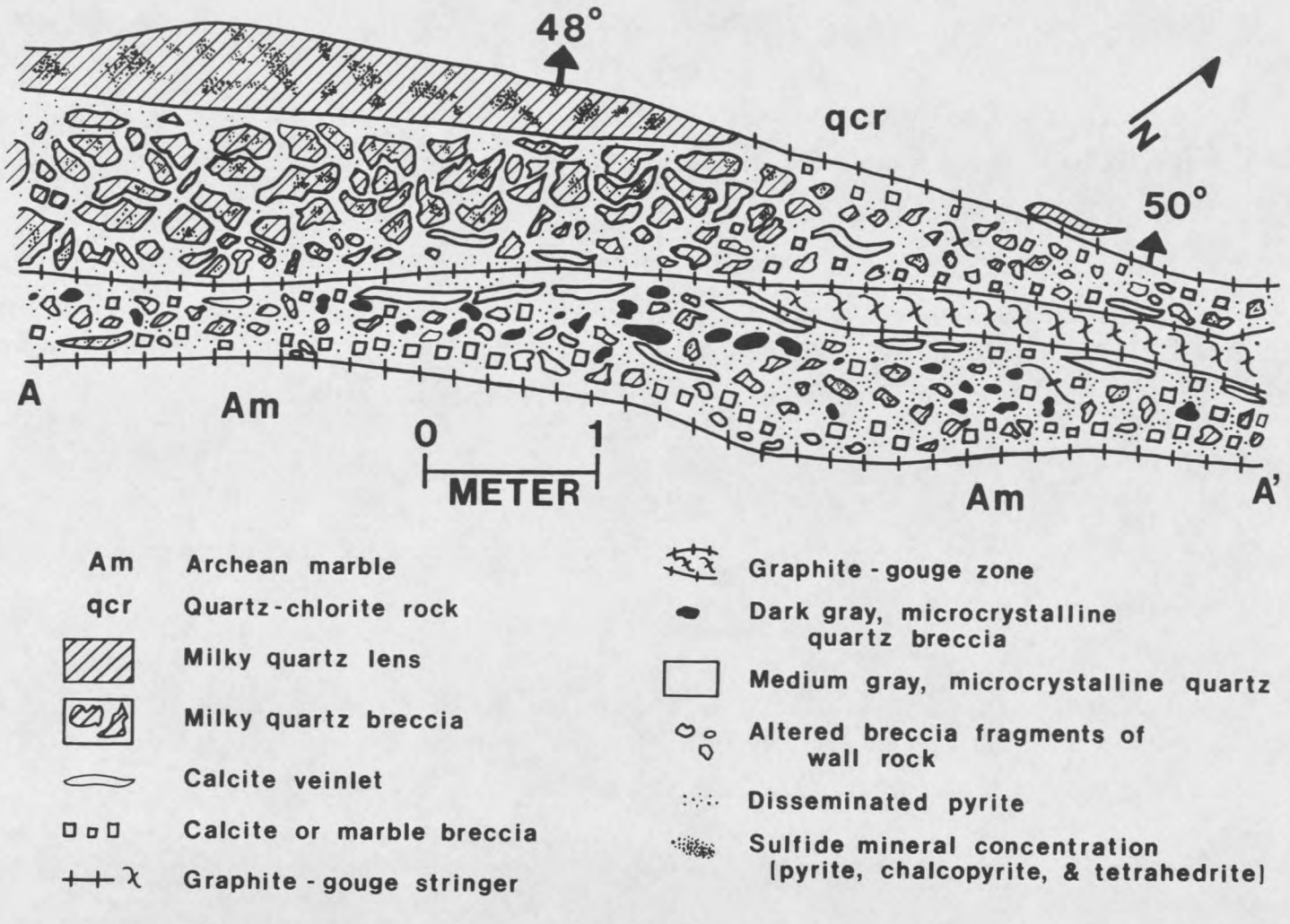

Figure 13. Detailed plan view of vein and its components along section A to A' on Plate 2.

graphite-gouge stringers along the vein. The subparallel section of the vein in the southwestern portion of the lower level could be a large branch of the main vein. Alternatively, the southwestern portion could be an offset segment of the vein. This interpretation is made from the presence of two major fractures where the vein pinches down to a graphite-gouge stringer prior to the southwestern fork of the drift (Pl. 2). However, a definite interpretation is not possible because slickensides were not observed along these fractures.

Two major periods of mineralization are recognized in the vein through petrographic observations. An episode of intensive brecciation separates these two periods. Episodes of brecciation and fracturing also occur during the two periods of mineralization and are localized features in some cases. Moreover, a minor period of secondary alteration follows the major periods of mineralization. The periods of mineralization and the characteristics of the accompanying minerals will be discussed in detail in the section on paragenesis. The two principal episodes of mineralization are designated Period 1 and Period 2 in the following discussions.

The mineralogy of the vein is generally simple. The primary ore minerals, in decreasing order of abundance, are pyrite, chalcopyrite, tetrahedrite, gold, and silver. Bismuthinite, pyrrhotite, and sphalerite are also present in minor amounts. Quartz, calcite, dolomite, muscovite or white mica, and graphite, in decreasing order of abundance, are the nonsulfide minerals in the vein. Trace amounts of a rare earth phosphate have been observed in milky quartz

(Fig. 14). Djurleite ($Cu_{1.96}S$), covellite, iron oxide, and malachite comprise the secondary alteration minerals of the primary sulfides.

The ore and gangue show both massive and brecciated textures in varying degrees. Massive textures are characteristic of quartz lenses and stringers and of coarse-grained calcite. Brecciated textures are shown by some pyrite, marble, calcite, microcrystalline quartz, and by milky quartz that contains sulfides and gold. Some fracturing and brecciation of pyrite is contemporaneous with formation of ore in the deposit because gold and other sulfides fill fractures in the pyrite. The healing of milky quartz breccia fragments by gangue minerals (calcite and microcrystalline quartz) suggests faulting prior to the deposition of the gangue minerals. Faulting is also evident in the

Figure 14. Rare earth phosphate (REP) in milky quartz (black) with pyrite (white), chalcopyrite (cp), djurleite (dots), covellite (vertical lines), and goethite (cross-hatched). Chalcopyrite is altering to djurleite and covellite. Sample S-25-6.5 B. Diameter of field of view is 0.47 mm.

local offset of a mineralized quartz lens along a graphite-gouge stringer (Fig. 15). Brecciation has not been observed to affect late-stage calcite. These observations suggest that much of the deformation associated with the vein took place prior to and during the emplacement of the deposit.

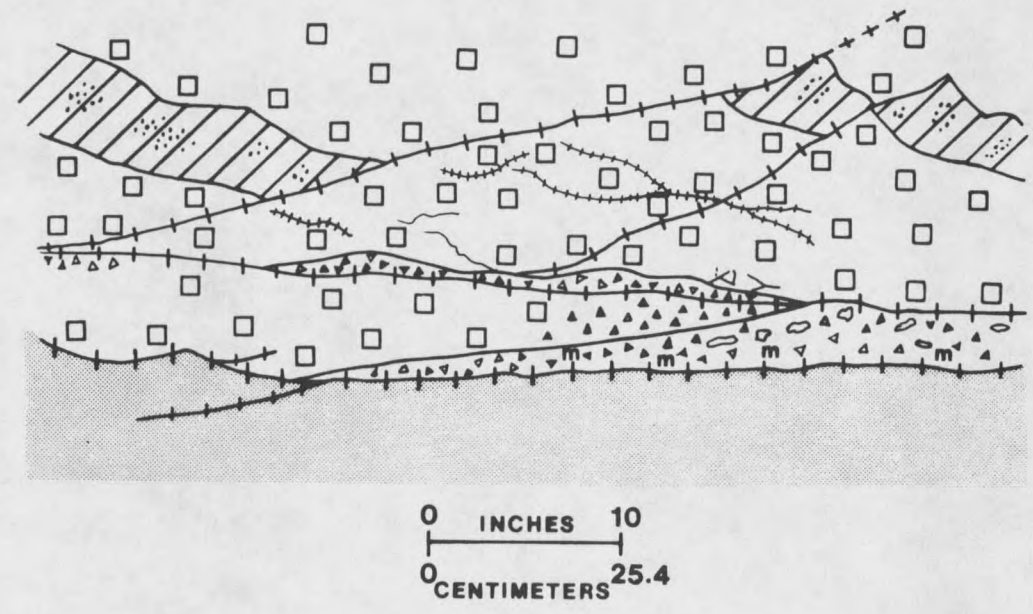

Figure 15. Offset of pyrite-bearing lens of milky quartz along a graphite-gouge stringer in the Red Pine vein on Plate 2. View is looking up dip.

Mineral Paragenesis

The paragenesis of vein mineralization can be determined through the correlation of ore and gangue textures and periods of brecciation (Fig. 16). The textures and occurrences of minerals in the periods of mineralization and secondary alteration are described below. The minerals are discussed in their general sequence of deposition, as interpreted from their occurrences and textural relations, to clarify their age relationships. The sample sketches that accompany this discussion are keyed to Plates 2 and 3 for samples taken in the southwestern portion (S) and in the northeastern portion (N) of the lower workings. Samples taken in the upper workings (UW) are keyed to Figure 12. DP is the designation for samples taken from a stockpile of ore at the mine.

Period 1

Milky quartz is the first major mineral emplaced in the vein during Period 1 mineralization. The milky quartz occurs in lenses and as a massive vein that contacts the adjacent wall rock or is separated from the wall rock by gouge. Several episodes of crystallization of milky quartz are evident in the milky quartz that heals fractures in later pyrite. The episodes are also evident in the veinlets of milky quartz that cut pyrite and other sulfides later in Period 1. Examination of thin sections shows that milky quartz and pyrite were fractured and/or brecciated during Period 1 and healed by medium- to fine-grained milky quartz. Milky quartz containing pyrite and other sulfides has also been brecciated in some sections of the vein and

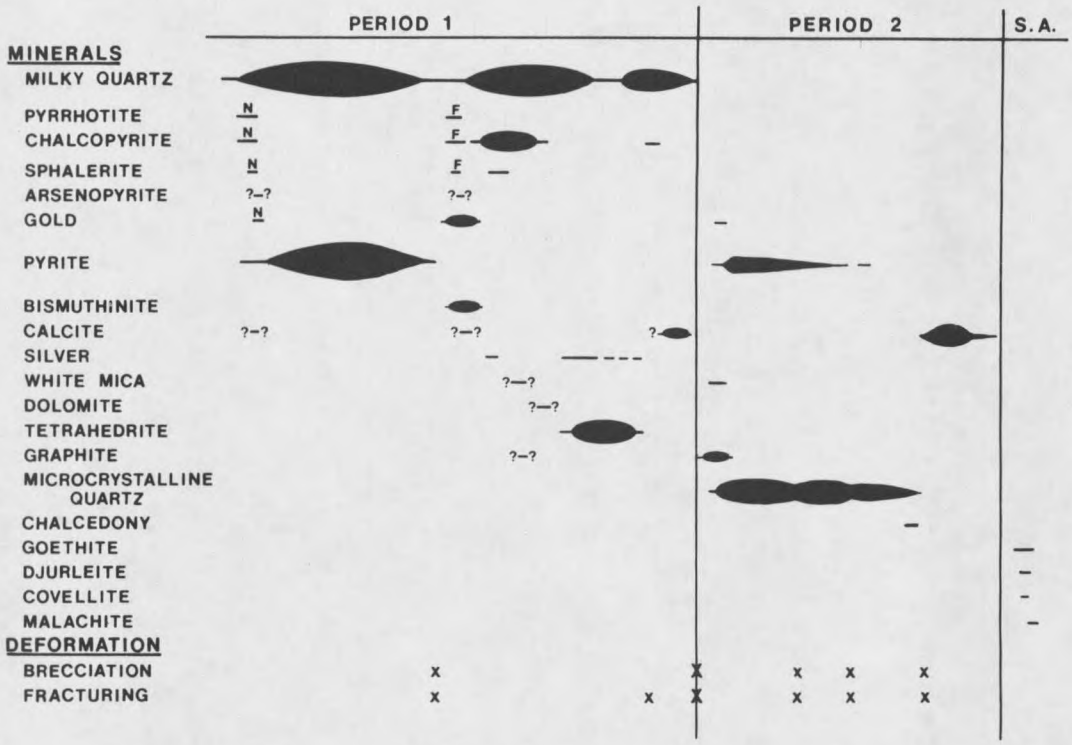

Figure 16. Paragenetic sequence for mineralization at the Red Pine mine.

S.A. Secondary alteration.

---- Indicates uncertainty of duration of mineral precipitation.

F General paragenetic position if mineral grains are in or along a fracture or open-space filling.

N General paragenetic position if mineral grains are inclusions or are exsolved from pyrite.

Bulbs Indicate a major pulse of mineral emplacement.

? Position in the paragenetic sequence is uncertain.

X Major system event

x Possibly local features in the system.

healed by Period 2 mineralization (Fig. 13 and P1.2). Other sections of milky quartz in the vein appear undisturbed by brecciation. However, strain is indicated in thin sections of this milky quartz by undulose extinction and by fractures in quartz and pyrite. Milky to clear quartz is also found as crystals lining vugs both in the vein and in brecciated or fractured wall rock.

Milky quartz is rich in fluid inclusions. It also contains subhedral to anhedral apatite inclusions in trace amounts. The sizes and shapes of milky quartz are listed in Appendix D, along with sizes and shapes of other vein minerals.

Deposition of pyrite precedes, overlaps, and follows emplacement of milky quartz. Pyrite is present in milky quartz as euhedral to subhedral grains (Fig. 17), many of which have been fractured, and as anhedral grains and breccia fragments (Fig. 18). These brecciated and fractured grains are healed by combinations of milky quartz, calcite, gold, chalcopyrite, bismuthinite, and tetrahedrite.

Less commonly, pyrite occurs as equant grains which have grown together in a circular pattern and have subhedral outer boundaries (Fig. 19). It also is present as individual grains that have grown in an ellipsoidal pattern. The circular pyrite grains have quartz or other gangue at the center of the crystal ring. The ellipsoidal arrangement of euhedral pyrite crystals encompasses some quartz and tetrahedrite. The ellipsoidal occurrence suggests that the pyrite lined a vug that later filled with other minerals. The pyrite in the circular pattern probably grew from a nucleus projecting into a vug.

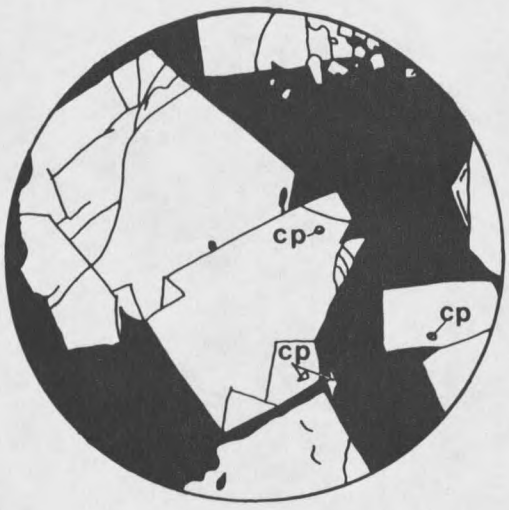

Figure 17. Fractured, subhedral to euhedral pyrite (white) in milky quartz matrix (black). Chalcopyrite (cp) inclusions are present in pyrite. Sample S-25-6.5B. Diameter of field of view is 2.9 mm.

Figure 18. Pyrite breccia (white) in milky quartz matrix (black). Sample N-1-RA. Diameter of field of view is 0.23 mm.

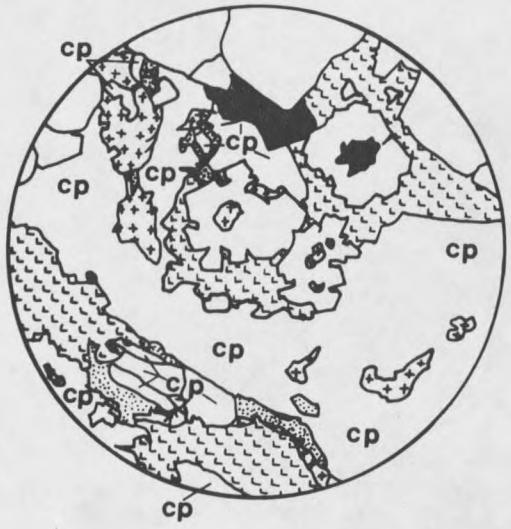

Figure 19. Subhedral pyrite grains (white) grown in circular patterns. Some pyrite contains quartz (black) or pitted (+) centers. Larger anhedral and subhedral pyrite grains are also present with anhedral chalcopyrite (cp) in later calcite (L pattern). Some alteration of chalcopyrite to djurleite (dots) is present. Sample S-25-6.5C. Diameter of field of view is 2.9 mm.

Minor amounts of pyrrhotite, chalcopyrite, sphalerite, gold, quartz, carbonate, and bismuthinite occur as irregular, or ovoid to elongated, minute grains in pyrite. These grains have curved to straight boundaries against pyrite. Neither a preferred orientation nor evidence of exsolution has been observed for these grains.

Cross-cutting relations are inconclusive in determining the exact placement of these grains in the paragenetic sequence for Period 1. However, their common occurrence within pyrite indicates early crystallization in the paragenetic sequence. Pyrrhotite and

chalcopyrite occur either as separate or combined grains (Figs. 20, 21, 22, and 23). In rare cases pyrrhotite exhibits subhedral hexagonal boundaries as in Figure 23. Sphalerite is observed within pyrite only in rare instances where it occurs primarily as individual grains (Fig. 24). Gold is present as separate grains (Fig. 25), but it can also occur with bismuthinite (Fig. 22) and with pyrrhotite and chalcopyrite in combined grains (Fig. 21). Bismuthinite is generally found as grains within pyrite in samples that contain a noticeable concentration of bismuthinite that fills fractures in pyrite (Figs. 22, 23, and 25). Quartz and carbonate also occur as separate grains.

Several possible interpretations of these individual or combined grains exist. They could be inclusions and thus be older than pyrite, or they could be partially contemporaneous with pyrite deposition. Moreover, they could be exsolved grains and thus be the same age as pyrite. Alternatively, apparent inclusions may actually be related to fractures or open-space fillings not evident in the two dimensions of a polished surface. The grains that fill fractures or open spaces must be younger than pyrite.

It is unlikely that these minute grains in pyrite are exsolution features. Evidence for expected crystallographic control of exsolved grains is lacking. Moreover, Ramdohr (1969) mentions that exsolved grains that could be expected due to the immiscibility of pyrite with other elements are nearly unknown. He proposes that minute grains in pyrite are inclusions, later infiltrations, or remnants resulting from replacement (Ramdohr, 1969).

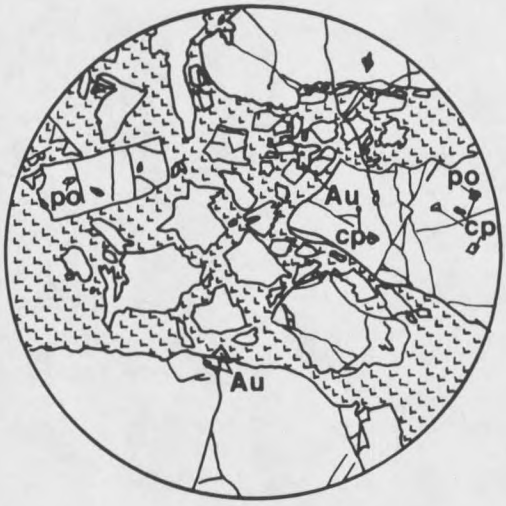

Figure 20. Fractured and brecciated pyrite (white) in calcite (L) matrix. Grains of gold (Au) border pyrite or occur in fractures. Pyrrhotite (po) and chalcopyrite (cp) are also present in pyrite. Sample S-30-1. Diameter of field of view is 2.9 mm.

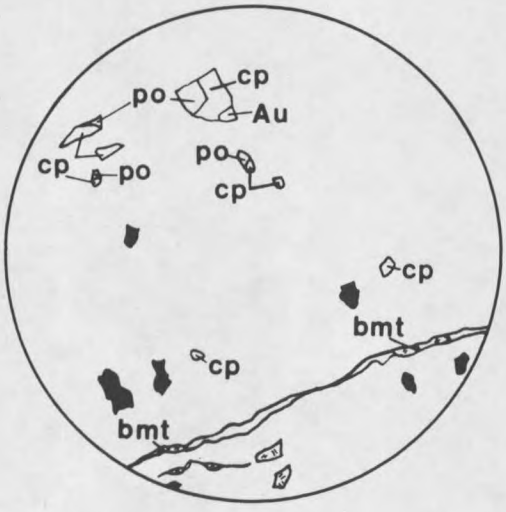

Figure 21 Minute grains of pyrrhotite (po), chalcopyrite (cp), quartz (black), gold (Au), and bismuthinite (bmt or =) in pyrite (white). Bismuthinite is also present in fractures. Sample S-23-8. Diameter of field of view is 0.2 mm.

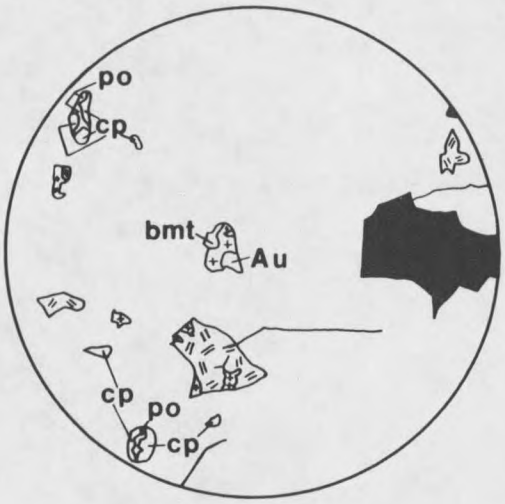

Figure 22. Combined grains of pyrrhotite (po) and chalcopyrite (cp) and individual grains of chalcopyrite, bismuthinite (bmt, =), and quartz (black) in pyrite (white). One gold grain is separated by a pit (+) from bismuthinite. Note connection of quartz and bismuthinite to fractures. Sample S-23-8. Diameter of field of view is 0.23 mm.

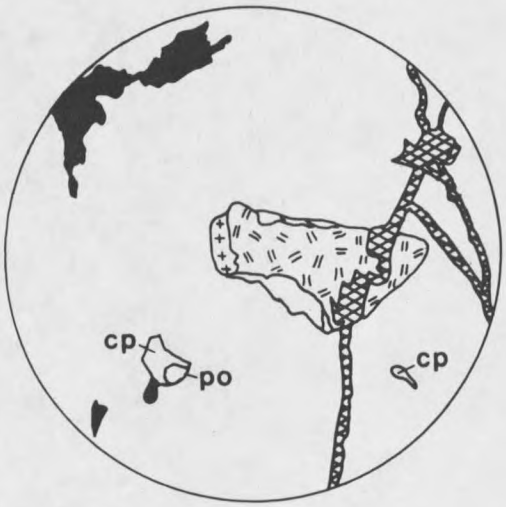

Figure 23. Chalcopyrite (cp) and pyrrhotite (po) in an open-space filling in pyrite (white). Quartz (black) and bismuthinite (=) grains are likely fracture fillings. Goethite (cross-hatched) veinlets cut pyrite and bismuthinite. (+) is a pit. Sample S-23-8. Diameter of field of view is 0.23 mm.

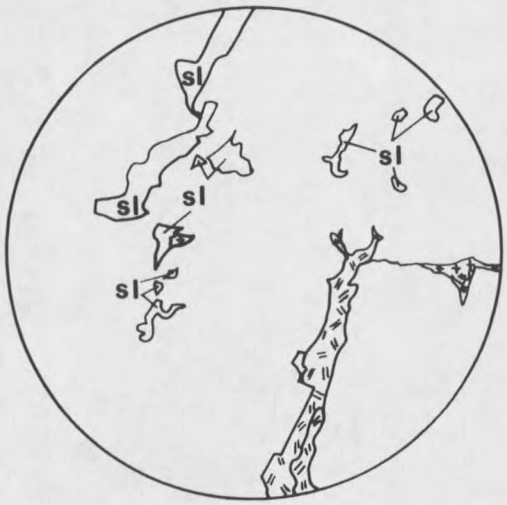

Figure 24. Sphalerite (sl) grains in pyrite (white) near bismuthinite (=) that is filling an open space. Sphalerite grains with straight boundaries may indicate open-space filling, while grains with curved boundaries could be inclusions. (+) patterns are pits in sample. Sample DP-1. Diameter of field of view is 0.23 mm.

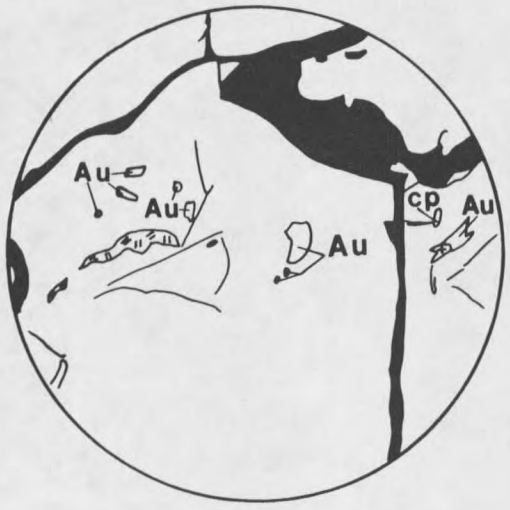

Figure 25. Inclusions of gold (Au), bismuthinite (=), and chalcopyrite (cp) in brecciated pyrite (white) that is healed by milky quartz (black). (+) is a pit in sample. Sample DP-6. Diameter of field of view is 0.47 mm.

Interpretation of the minute grains in pyrite as inclusions, possibly as contemporaneous diablastic intergrowths, and as fracture or open-space fillings is appropriate. This interpretation is supported by the shapes and boundaries of the grains. Irregular borders and shapes may denote grains that fill fractures or grains that have grown contemporaneously with pyrite. Grains enclosed by subhedral to euhedral boundaries of pyrite are interpreted as open-space fillings. Ovoid to ellipsoidal grains may be interpreted as inclusions. Moreover, combined grains and grains that have subhedral to euhedral boundaries against pyrite are probably inclusions. Each of these relationships is indicated by some of the minute grains in the pyrite from the Red Pine mine.

Pyrite also contains minute grains localized in or connected to fractures and grains that fill open spaces between grains of pyrite or a negative-crystal cavity in pyrite. These grains include chalcopyrite, gold, bismuthinite, quartz, carbonate, and sphalerite, and, very rarely, tetrahedrite and pyrrhotite. Gold (Fig. 26), chalcopyrite, bismuthinite (Figs. 21, 22, and 24), quartz, and carbonate are present as individual fillings. Moreover, several minerals may occur in a single filling. Observed associations include gold and bismuthinite; gold and quartz; chalcopyrite, sphalerite and/or carbonate or quartz; and chalcopyrite, pyrrhotite, and sphalerite. In these cases the grains are younger than the pyrite.

Pyrrhotite is present in rare instances as discrete grains in a milky quartz matrix (Fig. 27). Pyrrhotite also occurs as individual grains in marble where it is associated with pyrite, chalcopyrite,

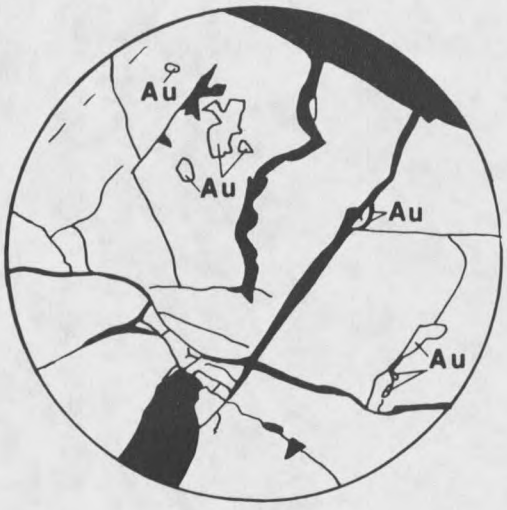

Figure 26. Grains of gold (Au) within pyrite (white) and connected to fractures in pyrite. Grains within pyrite may be inclusions or fracture fillings that are perpendicular to the plane of the polished section. Quartz (black) also fills fractures in pyrite. Sample N-1-RB. Diameter of field of view is 0.47 mm.

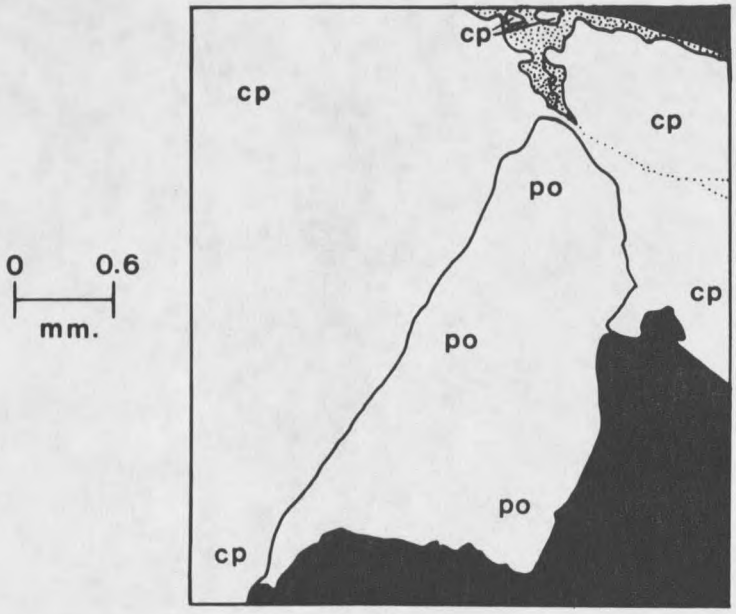

Figure 27. Discrete pyrrhotite grain (po) in milky quartz (black) with chalcopyrite (cp). Chalcopyrite is altering to djurleite (dots) along some grain margins. Sample S-23-27.6A.

arsenopyrite (Fig. 28), gold, and trace amounts of quartz. The pyrrhotite does not contain any observable exsolution features in either case. These occurrences do not definitely identify the position of pyrrhotite in the paragenetic sequence.

Arsenopyrite is noted only in marble wall rock, in trace amounts, where it penetrates some pyrrhotite (Fig. 28). This may indicate that the arsenopyrite is younger than or the same age as the pyrrhotite. However, due to the trace amounts involved, cross-cutting relationships do not clearly indicate the position of arsenopyrite in the paragenetic sequence.

Gold has a number of occurrences in Period 1 mineralization. It is present as inclusions and as grains that fill open spaces within pyrite (Figs. 25 and 26). However, gold is more abundant as

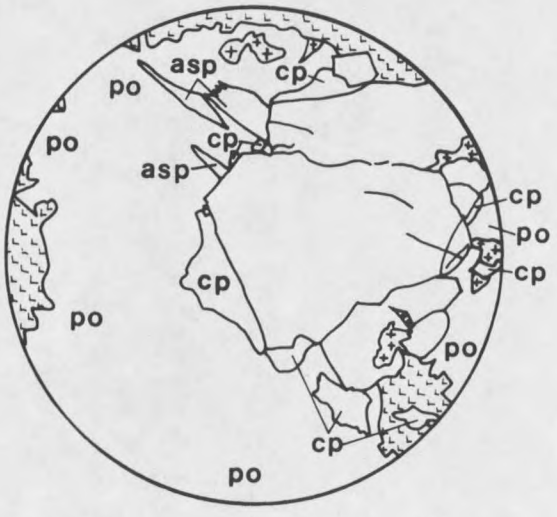

Figure 28. Pyrrhotite (po) and pyrite (white) grains with associated chalcopyrite (cp) and arsenopyrite (asp) in marble. Carbonate matrix is (L). (+) is a pit in sample. Sample S-23-8WB. Diameter of field of view is 0.47 mm.

discrete grains in fractures in pyrite (Figs. 26, 29, and 30). It is also found between and along the edges of pyrite fragments in a calcite matrix (Fig. 20). Some gold is found between milky quartz grains in the gangue matrix of the vein (Fig. 31). Gold in this occurrence can have bismuthinite inclusions (Fig. 31) or be in contact with larger bismuthinite and/or tetrahedrite grains (Figs. 32, 33, and 34). This gold may be later than the bismuthinite or contemporaneous with it. A few small grains of gold have also been noted in chalcopyrite (Fig. 33) and calcite grains. The uncommon occurrence of gold and chalcopyrite in the ore may indicate that the gold was emplaced prior to the major stage of chalcopyrite growth. Minor occurrences of gold with chalcopyrite, tetrahedrite, and carbonate could indicate either crystallization during the waning stages of gold deposition or minor remobilization of gold after fracturing and brecciation of pyrite.

Gold is also present in trace amounts in the wall rock. It occurs with pyrrhotite in marble and in microcrystalline quartz that replaces minerals in iron formation. In the marble, single grains of gold abut pyrrhotite along curved boundaries. In the iron formation, the gold occurs as subrounded to irregular grains in the secondary microcrystalline quartz and possibly as an open-space filling with this quartz in magnetite.

Crystallization of most bismuthinite (Bi_2S_3) follows deposition and deformation of pyrite in Period 1 mineralization. Bismuthinite is present as anhedral grains in fractures (Figs. 21 and 35) and as open-space fillings (Figs. 24 and 36) in pyrite. It also is found between

Figure 29. Gold (Au) localized along a fracture in pyrite (white). Additional fracture filling includes milky quartz (black), goethite (cross-hatched), and djurleite (dots). (+) is a pit in sample. Sample S-21-17.7. Diameter of field of view is 0.23 mm.

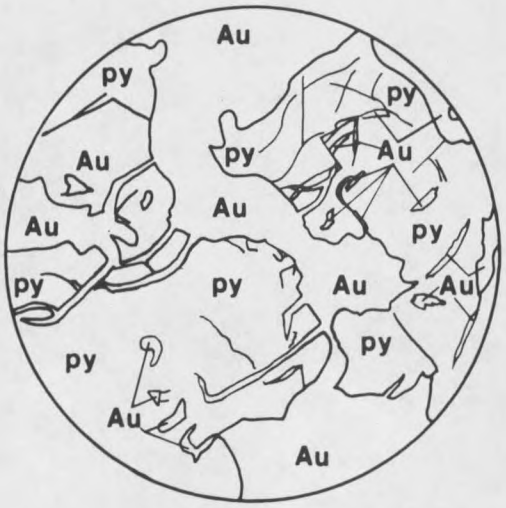

Figure 30. Abundant gold (Au) in and between grains of pyrite (py). Textures suggest possible minor replacement of pyrite by gold. Sample S-41-24. Diameter of field of view is 0.47 mm.

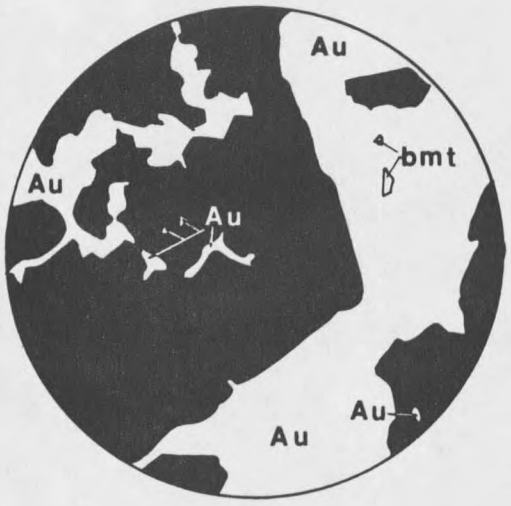

Figure 31. Gold (Au) containing inclusions of bismuthinite (bmt). Gold grains are present between milky quartz grains (black). Sample S-41-24B. Diameter of field of view is 0.52 mm.

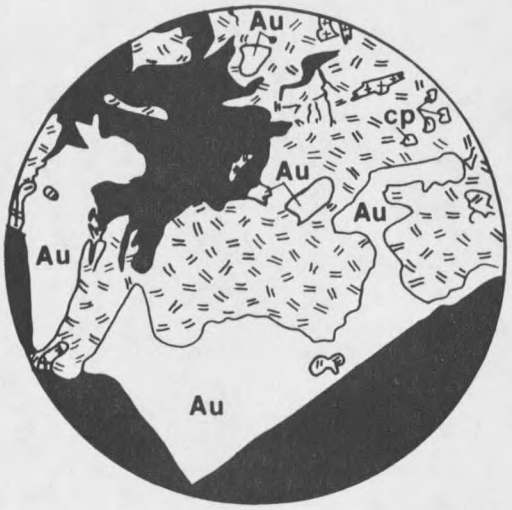

Figure 32. Gold (Au) with bismuthinite (=) in a matrix of milky quartz (black). Textures possibly indicate replacement of gold by bismuthinite. Bismuthinite also contains minute inclusions of chalcopyrite. Sample S-41-24. Diameter of field of view is 0.47 mm.

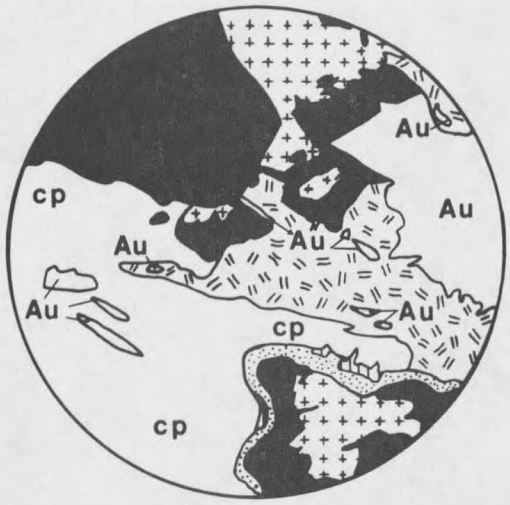

Figure 33. Grains of gold (Au) in chalcopyrite (cp) and bismuthinite (=). Chalcopyrite is altering to djurleite (dots) and covellite (vertical lines) along one grain margin. Sulfides and gold are in a matrix of milky quartz (black). (+) shows pits in the sample. Textures may indicate a reaction between bismuthinite and large grain of gold. Sample DP-6. Diameter of field of view is 0.47 mm.

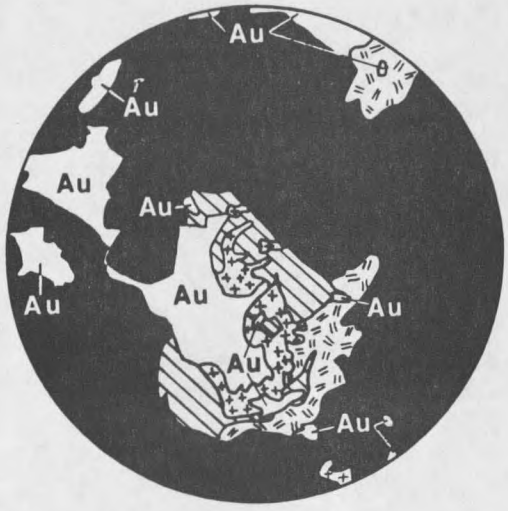

Figure 34. Gold (Au) associated with bismuthinite (=) and tetrahedrite (diagonal lines) in a matrix of milky quartz (black). (+) indicates pits in sample. Sample S-41-24B. Diameter of field of view is 0.47 mm.

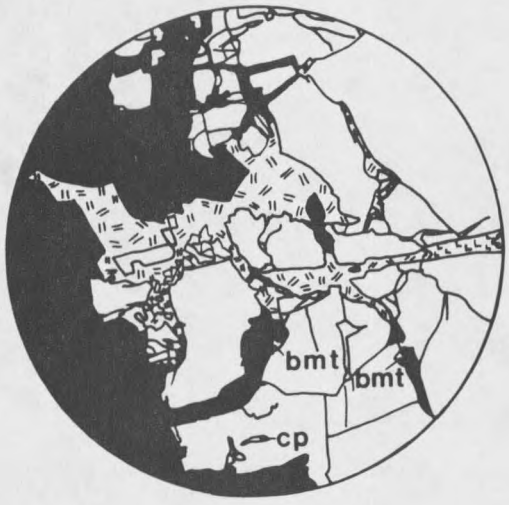

Figure 35. Bismuthinite (=) and milky quartz (black) in fractures in pyrite (white). One grain of chalcopyrite (cp) is present in pyrite. Sample S-25-22B. Diameter of field of view is 2.9 mm.

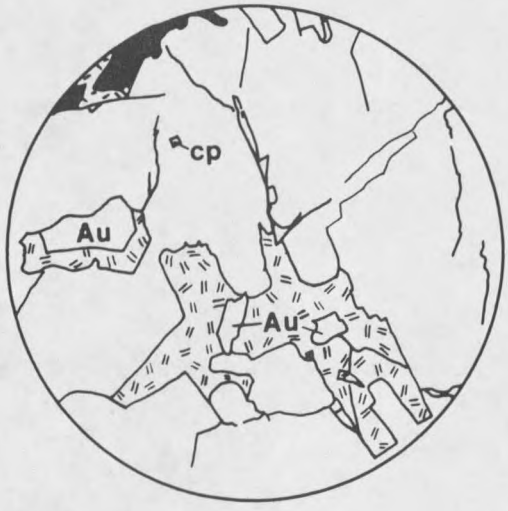

Figure 36. Bismuthinite (=) and gold (Au) in an open-space filling in pyrite. Mica (-) and milky quartz (black) bound pyrite. (cp) is a chalcopyrite grain in pyrite. Sample S-23-8. Diameter of field of view is 0.23 mm.

quartz grains (Fig. 37). Minor bismuthinite grains in pyrite suggest overlap of deposition near the end of crystallization of pyrite. Alternatively, these grains could be bismuthinite that occurs in fractures that are perpendicular to the plane of the polished surface, in which case they would be younger than pyrite. Relict grains of bismuthinite are found in tetrahedrite (Fig. 38), indicating that bismuthinite is older than tetrahedrite. Bismuthinite is cut by veinlets containing chalcopyrite (Fig. 39) and native silver (Fig. 40). Bismuthinite contains irregular grains of chalcopyrite and tetrahedrite (Fig. 41) along probable cleavage planes and in open-space fillings. These grains also occur along bismuthinite grain boundaries. These grains of chalcopyrite and tetrahedrite appear to be younger than or contemporaneous with bismuthinite.

Silver is associated with bismuthinite and tetrahedrite in the Red Pine ore, in addition to its typical association with gold in solid solution (Ramdohr, 1969). The occurrence of native silver with bismuthinite is uncommon in the ore. The native silver is present as elongated and nearly equant blebs in bismuthinite and in veinlets that cut the bismuthinite (Figs. 39 and 40).

Silver occurs more commonly with tetrahedrite than with bismuthinite, possibly because the tetrahedrite is the more abundant of the two minerals. Even though the silver is not readily recognized in reflected-light analysis of tetrahedrite, the association of silver with tetrahedrite is substantiated by preliminary compositional analyses by Wilson (1985) (Appendix E) and by assay data (Appendix F).

Figure 37. Bismuthinite (=) in milky quartz (black). Sample S-41-24. Diameter of field of view is 0.47 mm.

Figure 38. Relict grains of bismuthinite (=) in tetrahedrite (diagonal lines). Additional components in this sketch include milky quartz (black), chalcopyrite (cp) and pits in the sample (+). Sample S-23-27.6D. Diameter of field of view is 0.23 mm.

Figure 39. Veinlets of chalcopyrite (cp) cut bismuthinite (=) contained in a matrix of milky quartz (black). Some veinlets contain silver (Ag). A patch of mica (-) borders bismuthinite. Sample S-41-24C. Diameter of field of view is 2.9 mm.

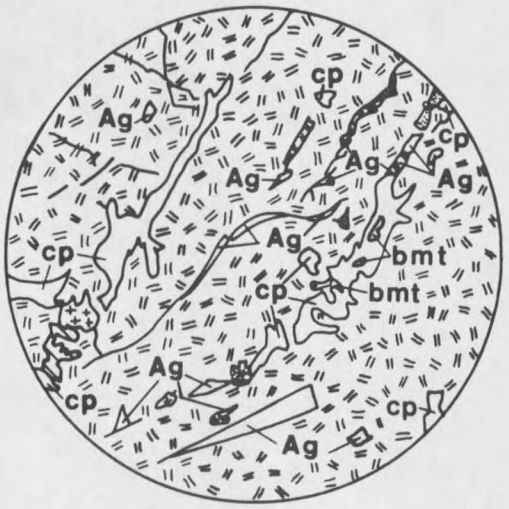

Figure 40. Veinlets and grains of silver (Ag) and chalcopyrite (cp) in bismuthinite (=). Minor alteration of chalcopyrite to djurleite (dots) is present along one veinlet. Also present are tetrahedrite (diagonal lines) and pits in the sample (+). Sample S-41-24C. Diameter of field of view is 0.47 mm.

Figure 41. Grains of chalcopyrite (cp), tetrahedrite (diagonal lines), and silver (Ag) in bismuthinite (=). These grains suggest open-space or fracture filling perpendicular to the plane of the polished section. (+) is a pit in the sample. Sample S-41-24C. Diameter of field of view is 0.47 mm.

Silver assays of ore from the Red Pine are higher when tetrahedrite is present (Appendix F).

The assay values for silver suggest that it is part of the tetrahedrite structure. However, the position of native silver in the paragenetic sequence is not entirely clear from its occurrences with bismuthinite and tetrahedrite. It is both later than bismuthinite and contemporaneous with tetrahedrite; it may also be contemporaneous with deposition of chalcopyrite.

Chalcopyrite is present in milky quartz as anhedral grains (Fig. 42). It also fills portions of fractures in pyrite (Fig. 43) and surrounds anhedral to euhedral pyrite, indicating that the major

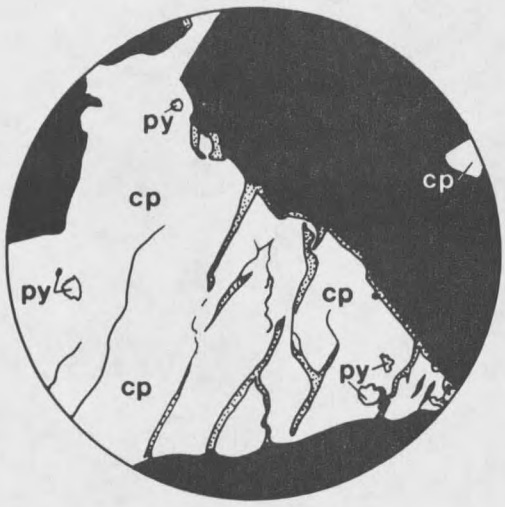

Figure 42. Chalcopyrite (cp) in a matrix of milky quartz (black). Chalcopyrite apparently replaces some minute pyrite grains (py). Chalcopyrite is altering to djurleite (dots) along grain boundaries and fractures. Sample UW-2. Diameter of field of view is 1.1 mm.

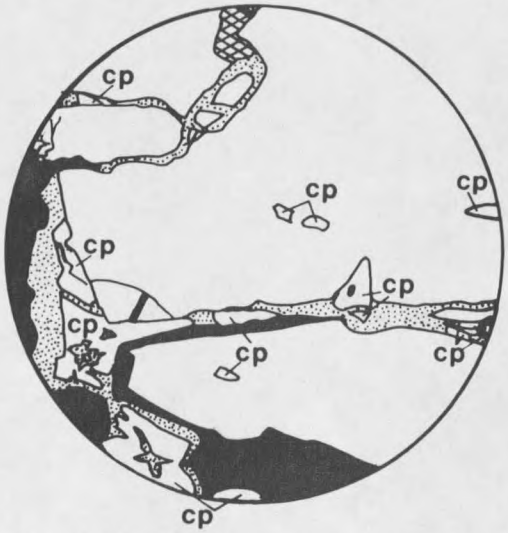

Figure 43. Chalcopyrite (cp) filling fractures in pyrite (white). Minute chalcopyrite grains in pyrite could be inclusions or fracture fillings that are perpendicular to the plane of the polished surface. Chalcopyrite is altering to djurleite (dots). Milky quartz (black) and goethite (cross-hatched) also fill fractures in pyrite. Sample S-23-27.6. Diameter of field of view is 0.52 mm.

episode of chalcopyrite is younger than pyrite. Although boundaries between chalcopyrite and pyrite are generally curved to straight, some irregular textures between these two minerals suggest that chalcopyrite has replaced some pyrite (Fig 42).

Anhedral sphalerite is present predominantly as relict grains in tetrahedrite and as minute blebs in pyrite. The relict grains contact chalcopyrite (Fig. 44) or occur as individual grains. The absolute timing of sphalerite in Period 1 mineralization is indeterminate, but the major episode of crystallization may be contemporaneous with chalcopyrite that was deposited earlier than tetrahedrite.

Tetrahedrite is the major sulfide mineral that crystallizes late in Period 1. The irregular textures of relict grains of bismuthinite (Fig. 38), chalcopyrite, sphalerite (Fig. 44), and pyrite (Fig. 45) in tetrahedrite are evidence of the replacement of these minerals by tetrahedrite. Veinlets of tetrahedrite cut pyrite and chalcopyrite and extend into the marble wall rock for as much as 10 to 15 centimeters. Anhedral tetrahedrite also fills fractures in pyrite and surrounds some subhedral and brecciated pyrite grains. Where this texture is common, tetrahedrite is found, in rare instances, as minute grains in pyrite. These grains suggest that the tetrahedrite fills fractures that are perpendicular to the plane of the polished surface. Tetrahedrite also surrounds dolomite rhombohedrons and euhedral quartz grains (Fig. 46), indicating that the tetrahedrite has filled a vug. Tetrahedrite is cut by some chalcopyrite and milky quartz veinlets (Fig. 47). These veinlets denote a minor episode of chalcopyrite and quartz emplacement that is younger than the tetrahedrite.

Figure 44. Relict grains of chalcopyrite (cp) and sphalerite (sl) in tetrahedrite (diagonal lines). Other components in the sketch are milky quartz (black), pyrite (py), and pits (+) in the sample. Sample S-23-27.6A. Diameter of field of view is 0.23 mm.

Figure 45. Relict grains of pyrite (white) in tetrahedrite (diagonal lines). Other minerals in the sketch include djurleite (dots), milky quartz (black), goethite (cross-hatched), and chalcopyrite (cp). Sample S-23-27.6B. Diameter of field of view is 0.47 mm.

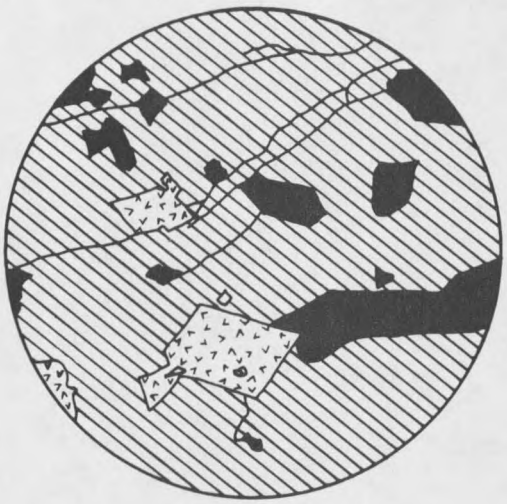

Figure 46. Dolomite rhombohedrons (v v) and euhedral to subhedral milky quartz (black) in tetrahedrite (diagonal lines). Sample S-23-27.6D. Diameter of field of view is 0.47 mm.

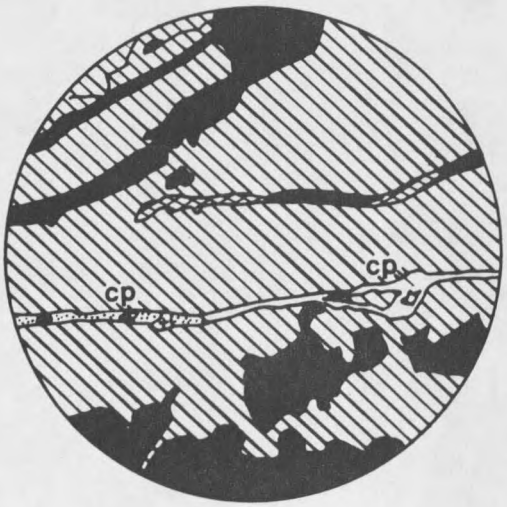

Figure 47. Veinlets containing milky quartz (black), goethite (cross-hatched), and chalcopyrite (cp) cut tetrahedrite (diagonal lines). Some chalcopyrite is altering to djurleite (dots). (+) is a pit. Sample S-23-27.6D. Diameter of field of view is 0.47 mm.

The remaining gangue minerals in Period 1 mineralization cannot be clearly placed in the paragenetic sequence. These minerals include calcite, dolomite, white mica (sericite and/or muscovite), and graphite. However, the paragenetic position of these minerals has been inferred in Figure 16 using the following observations. Calcite commonly occurs as an open-space filling between pyrite and quartz crystals. In other instances, calcite and dolomite envelop euhedral and brecciated pyrite, denoting that these carbonates are later than pyrite. Dolomite also fills open spaces around quartz crystals projecting into a vug. Moreover, dolomite rhombohedrons are surrounded by tetrahedrite, indicating that they are probably earlier than this mineral. White mica (muscovite) is present in milky quartz as blocky grains and mats. A few large grains of mica are cut or partially encompassed by chalcopyrite, suggesting that the mica was deposited during the main phase of crystallization of chalcopyrite. In rare instances, graphite fibers are found in the milky quartz.

Period 2

A major period of fracturing and/or brecciation created additional sites of deposition for Period 2 mineralization. This deformation is evident in the brecciation of Period 1 mineralization and in the presence of graphite veinlets and graphite-gouge stringers which cut the vein and adjacent wall rock.

Graphite begins the emplacement of minerals in Period 2. It occurs as veinlets, fibers, stringers, and irregular masses. The graphite cuts milky quartz, calcite, and dolomite and surrounds some

pyrite and chalcopyrite. Some graphite fibers are bent or folded in milky quartz fractures (Fig. 48). Graphite in these fractures is associated with white mica. Wilson (1985) observed several types of graphite grains in Red Pine samples provided by the author and described these as "laths, cellular masses, and globular grains". The sizes for these grains are listed in Appendix D.

Some gold is found along grains of milky quartz that contact areas filled with graphite veinlets and white mica (Fig. 49). It is also attached to graphite grains (Fig. 50). This occurrence of gold may indicate a remobilization of gold from Period 1 by deformation and a subsequent localization of the gold near the graphite veinlets. This remobilization may be supported by the lower values of gold for assay samples containing Period 2 mineralization (Appendix F).

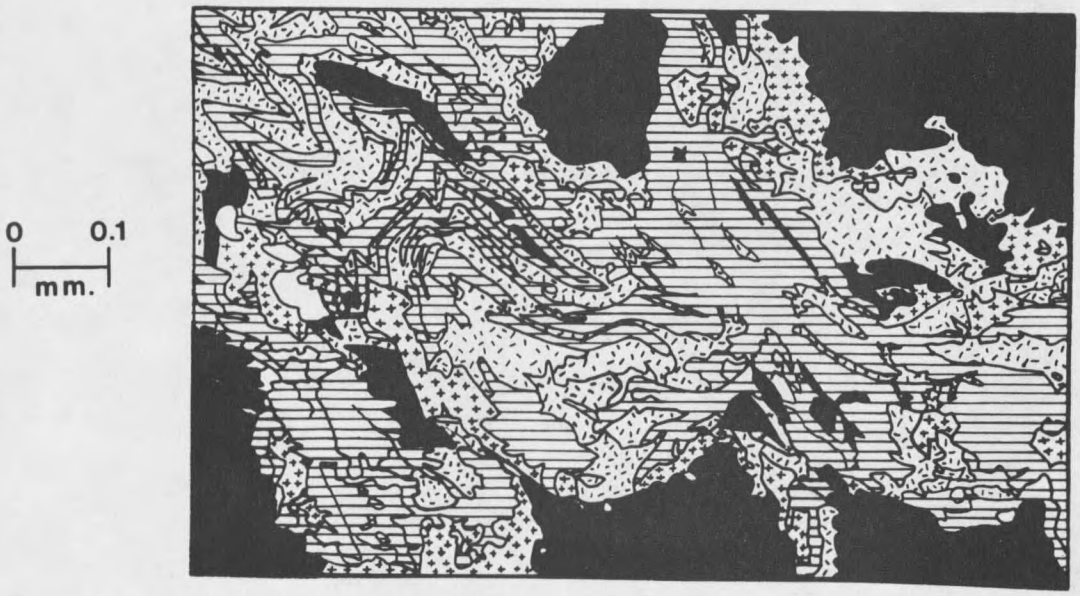

Figure 48. Bent graphite fibers (horizontal line pattern) and white mica(-) in a fracture in milky quartz (black). (+) is a pit in sample. Sample DP-6.

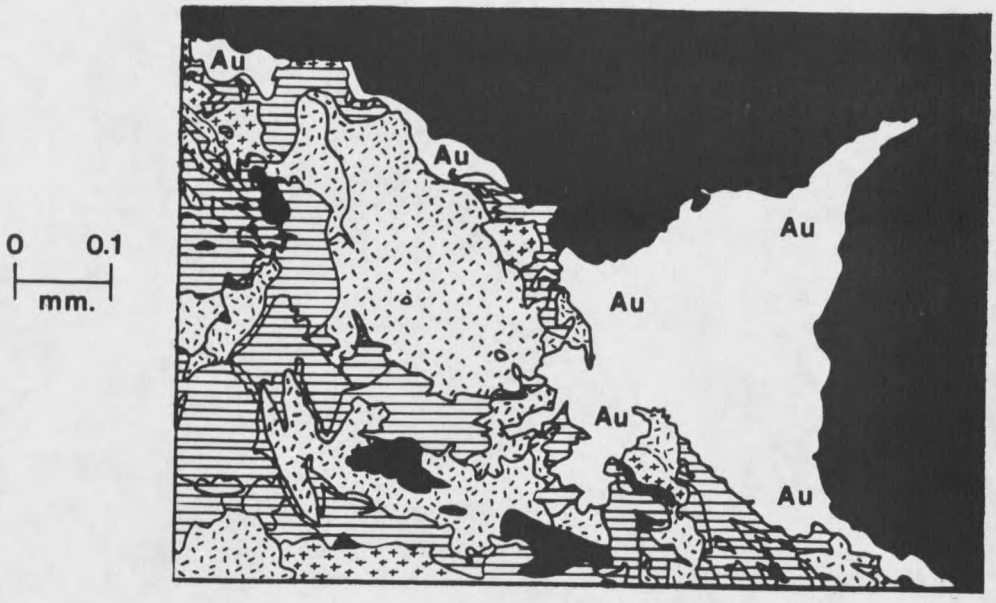

Figure 49. Gold (Au) along milky quartz (black) adjacent to a fracture filled with graphite and white mica. Graphite is shown by horizontal lines, mica by (-), and pits in sample by (+). Sample DP-6.

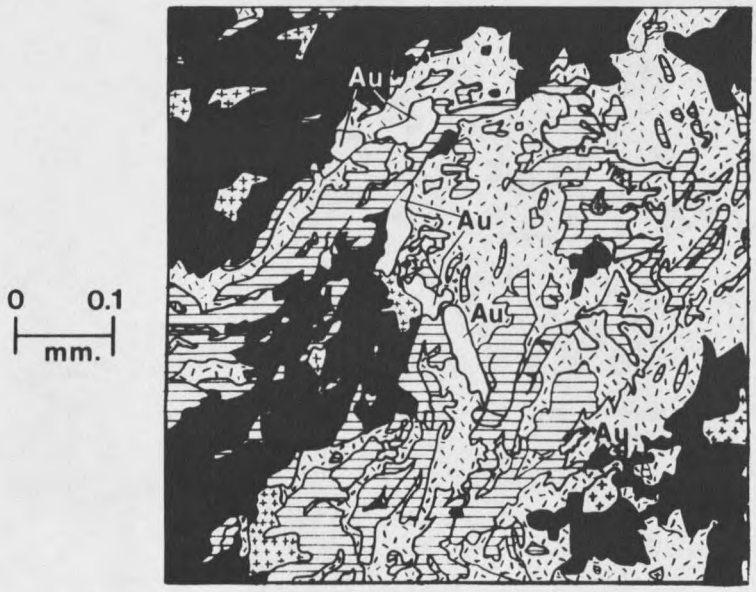

Figure 50. Gold (Au) attached to and possibly cutting graphite fibers (horizontal lines) in a fracture in milky quartz (black). White mica (-) is also present in the fracture. (+) pattern indicates pits in the sample. Sample DP-6.

At least three episodes of formation of microcrystalline quartz follow emplacement of graphite. In these episodes the microcrystalline quartz incorporates minute opaques (possibly graphite and/or sulfides) to produce a black to gray quartz. A dusting of minute carbonate particles also contributes to the darker appearance of the quartz. Cross-cutting relationships show that the darkest quartz is the oldest, followed by the medium gray quartz and the lighter gray quartz, indicating that the amount of opaque material decreases with each episode. Some textures of the microcrystalline quartz are comparable to textures of jasperoid described by Lovering (1972).

The microcrystalline quartz contains breccia fragments of material from the vein and the wall rock. These fragments include pyrite, calcite, dolomite, untwinned feldspar, marble, gneiss or metabasite, barren and pyrite-bearing milky quartz, dark microcrystalline quartz, and grains composed of graphite, serpentine, and sericite. These fragments are generally angular, but some grains show slightly curved corners. Fragments of the dark microcrystalline quartz in the light microcrystalline quartz are ovoid and nearly equant.

In some cases, microcrystalline quartz is associated with trace amounts of chalcedony that exhibits radial extinction. Both the microcrystalline quartz and the chalcedony replace coarse- and fine-grained carbonate that surrounds pyrite from Period 1 mineralization.

Pyrite, the only sulfide recognized in Period 2, is contemporaneous with microcrystalline quartz. It is found as euhedral, subhedral, and minor anhedral grains ranging in size from

0.01 to 1.5 millimeters. Some pyrite in the microcrystalline quartz has numerous, small crystal faces that produce a rough texture along the boundaries of the grains. Grains of other sulfides have not been observed within pyrite deposited in Period 2. The pyrite of Period 2 can be distinguished from the pyrite of Period 1 by its association with microcrystalline quartz, its euhedral to subhedral shape, its minute size, and its lack of inclusions or associated sulfide grains.

Breccia fragments of coarse calcite in dark microcrystalline quartz indicate that some calcite of Period 1 was emplaced prior to the microcrystalline quartz in Period 2. Moreover, a major period of deposition of coarse-grained calcite follows the emplacement of the microcrystalline quartz late in the paragenetic sequence. Evidence for this deposition is observed in cross-cutting relationships where calcite veinlets cut both milky quartz and microcrystalline quartz. Coarse-grained calcite also encompasses breccia fragments of milky quartz that have been cut by graphite veinlets.

Summary of Periods 1 and 2

Specific features identify major events in the paragenetic sequence (Fig. 16). Period 1 mineralization is characterized by milky quartz, most of the sulfide and precious-metal mineralization, and at least one period of brecciation (possibly local). The break between mineralization in Period 1 and Period 2 is defined by offset of lenses of milky quartz, by graphite-gouge stringers, and brecciation of milky quartz. Period 2 mineralization is represented by graphite-gouge stringers, gray to black microcrystalline quartz that heals brecciated

milky quartz, and calcite that cuts milky quartz and microcrystalline quartz.

Mineralization in Period 1 begins with deposition of milky quartz and is followed by deposition of pyrite. Some minor deposition of pyrrhotite, chalcopyrite, gold, and sphalerite may precede or overlap deposition of pyrite. The main stage of crystallization of bismuthinite follows brecciation of pyrite. The primary period of gold emplacement precedes, overlaps, and follows bismuthinite. Chalcopyrite is younger than pyrite, as seen in its filling of fractures in pyrite. Some chalcopyrite is younger than bismuthinite and could be associated with native silver in bismuthinite. Chalcopyrite is associated with sphalerite as relict grains in silver-bearing tetrahedrite. Pyrite and bismuthinite also occur as relict grains in tetrahedrite. Therefore, tetrahedrite is younger than all four sulfides. Minor chalcopyrite veinlets that cut tetrahedrite are the final sulfide mineralization deposited in Period 1. Additional minerals that have not been unequivocally positioned in the paragenetic sequence for Period 1 are calcite, dolomite, white mica, graphite, and arsenopyrite. The graphite and arsenopyrite occur only in trace amounts.

A major episode of brecciation separates Period 1 mineralization from mineralization in Period 2. Graphite and white mica are the first of the gangue minerals that dominate Period 2. Some gold is found with graphite in fractures that cut milky quartz. This gold may have been remobilized from Period 1 as a result of deformation. At least three episodes of crystallization of microcrystalline quartz

overlap and follow the emplacement of graphite. Each episode is successively lighter gray in color. Pyrite, the only sulfide of Period 2, is contemporaneous with deposition of microcrystalline quartz. A trace amount of chalcedony occurs late in the sequence. Calcite is the last major gangue mineral of Period 2. Fracturing and some local brecciation took place subsequent to emplacement of dark and medium gray microcrystalline quartz.

Secondary Alteration

Late-stage alteration consists of oxidation and supergene alteration of the ore. Each of these changes is evident in both levels of the mine. However, oxidation is more pronounced in the upper level, while supergene alteration is more prevalent in the lower level. Leaching of sulfides has accompanied oxidation in the upper level, as indicated by the voids present in some of the vein quartz. The primary minerals affected by oxidation and supergene alteration are pyrite and chalcopyrite, respectively.

Pyrite oxidizes to goethite in varying degrees and leaves behind the grains of gold that it contained. The goethite is present as red-brown (gray in polished section) pseudomorphic grains after pyrite. Some of these grains contain colloidal textures. Goethite also selectively replaces pyrite along grain boundaries and fractures (Fig. 51). Some goethite, along with quartz, fills fractures in pyrite (Figs. 23 and 29). This goethite and veinlets of goethite that cut tetrahedrite are possibly by-products of the replacement of

Figure 51. Replacement of pyrite (white) by goethite (cross-hatched). Milky quartz (black) is the matrix. Sample UW-1. Diameter of field of view is 0.47 mm.

chalcopyrite by djurleite. Minute orange-red, acicular grains and globules and mats of the iron oxide envelop pyrite and some quartz. Minute goethite grains also outline carbonate rhombohedrons that have been replaced by quartz. Moreover, some goethite outlines carbonate veinlets from Period 2 that cut microcrystalline quartz.

Djurleite ($Cu_{1.96}S$) replaces chalcopyrite along grain boundaries (Figs. 42 and 43). This replacement also takes place along fractures in chalcopyrite. Some djurleite is intergrown with covellite (Fig. 14) which occurs in trace amounts. In rare instances, djurleite replaces tetrahedrite.

Botryoidal malachite, some grains consisting of radiating acicular crystals, occurs in open-space fillings in goethite, on milky quartz, and in irregular patches against iron oxide and/or muscovite.

Malachite has also been deposited as a coating and/or as botryoidal grains on graphite, chalcopyrite, and tetrahedrite. Some botryoidal grains are present in quartz vugs.

Acicular gypsum crystals are found on exposed surfaces of graphite-gouge stringers along the vein. These crystals apparently form after mining operations have been conducted along the vein.

Hydrothermal Alteration

Hydrothermal alteration is evident in the country rocks around the vein. The major processes which have brought about this alteration are denoted by the minerals produced. These processes include carbonatization, silicification, chloritization, and sericitization. The minerals produced by these processes are listed in Tables 2, 3, and 4 for the major rock types. Alteration minerals are also discussed briefly in the text in the descriptions of the minor rock types.

Moreover, retrograde or hydrothermal alteration is observed at some distance from the vein in samples taken in the adit. This alteration may have resulted from either meteoric water or ascending hydrothermal fluids that gained access to the system along the many joints in the metamorphic rocks.

Quartz flooding is evident in the vein structures and in the local healing of brecciated or fractured marble by quartz. This latter process produced some small vugs lined with quartz crystals. In thin sections, quartz flooding is evident in some replacement textures involving quartz and carbonate. In some instances in Period

2, microcrystalline quartz and trace amounts of chalcedony replace carbonate.

Flooding of coarse-grained calcite also occurred late in the paragenetic sequence. Concentrations of calcite heal some brecciated portions of the vein as well as some fractured and brecciated sections of the wall rock (Pl. 2).

Disseminated sulfides are found in the wall rock and are probably related to vein emplacement. These include pyrite, pyrrhotite, chalcopyrite, trace amounts of arsenopyrite, and unidentified opaques. Pyrite is present in many veinlets of carbonate and quartz which penetrate the wall rock. According to John Magnus, owner-operator, assay values for gold are highest when the sulfides are in quartz rather than in marble, a relationship that is also indicated in the assays presented in Appendix F. Because of the higher values of gold in quartz, emphasis in this study has been placed on the vein mineralization rather than mineralization in the wall rocks.

DISCUSSION AND INTERPRETATION

The following sections interpret gold mineralization at the Red Pine deposit with respect to general deposit type, generalized paragenetic sequences, mineral associations of gold and silver, conditions of ore mineralization, generalized structural controls of mineralization, timing of mineralization, and sources of ore fluids and metals.

General Deposit Type

The Red Pine deposit has characteristics suggestive of either a syngenetic deposit related to the host Archean rocks or an epigenetic deposit which has been emplaced after the development of the host rocks. Evidence at the mine suggests that the deposit is epigenetic rather than syngenetic. The metamorphic rocks of the mine area are of upper-amphibolite- to granulite-facies grade. Rocks of this metamorphic grade are generally poorly mineralized (Groves and Batt, 1984; Guilbert and Park, 1986). If gold had been emplaced prior to metamorphism, it is reasonable to expect that these metamorphic conditions would have remobilized the gold (Boyle, 1979). Moreover, greenschist-facies alteration minerals associated with the deposit are not compatible with upper-amphibolite- to granulite-facies metamorphism which originally affected the host rocks. In addition, folding of the ore that could be expected with metamorphism

is not present. Instead, brittle deformation is found in the vein and in some country rocks adjacent to the vein. Locally, the Red Pine vein cuts the metamorphic foliation of the country rocks, particularly when the vein is in the marble. These factors do not indicate a syngenetic origin for the deposit, but rather an epigenetic origin which postdates high-grade regional metamorphism.

Significance of the Red Pine Paragenetic Sequence

Comparison of the Red Pine paragenetic sequence to the generalized sequences of Boyle (1979) (Fig. 52), and Jensen and Bateman (1979) (Fig. 53) serves two purposes here. Firstly, it provides a connection with typical mineral occurrences and relative timing of mineral emplacement for epigenetic gold deposits from the sequence by Boyle (1979). Secondly, a comparison with the sequence from Jensen and Bateman (1979) permits the characterization of the Red Pine deposit with respect to general temperature of emplacement. This interpretation is possible due to the categories of low to high temperature for hydrothermal ore deposits delineated in the sequence by Jensen and Bateman (1979).

The Red Pine paragenetic sequence, summarized in Figure 16, follows part of the generalized paragenetic sequence for epigenetic gold deposits (Fig. 52) described by Boyle (1979). This correlation is evident in the early emplacement of quartz and pyrite, the intermediate deposition of chalcopyrite and possibly sphalerite, and the late crystallization of tetrahedrite in Period 1 mineralization. The early occurrence of bismuthinite and gold in the sequence is also

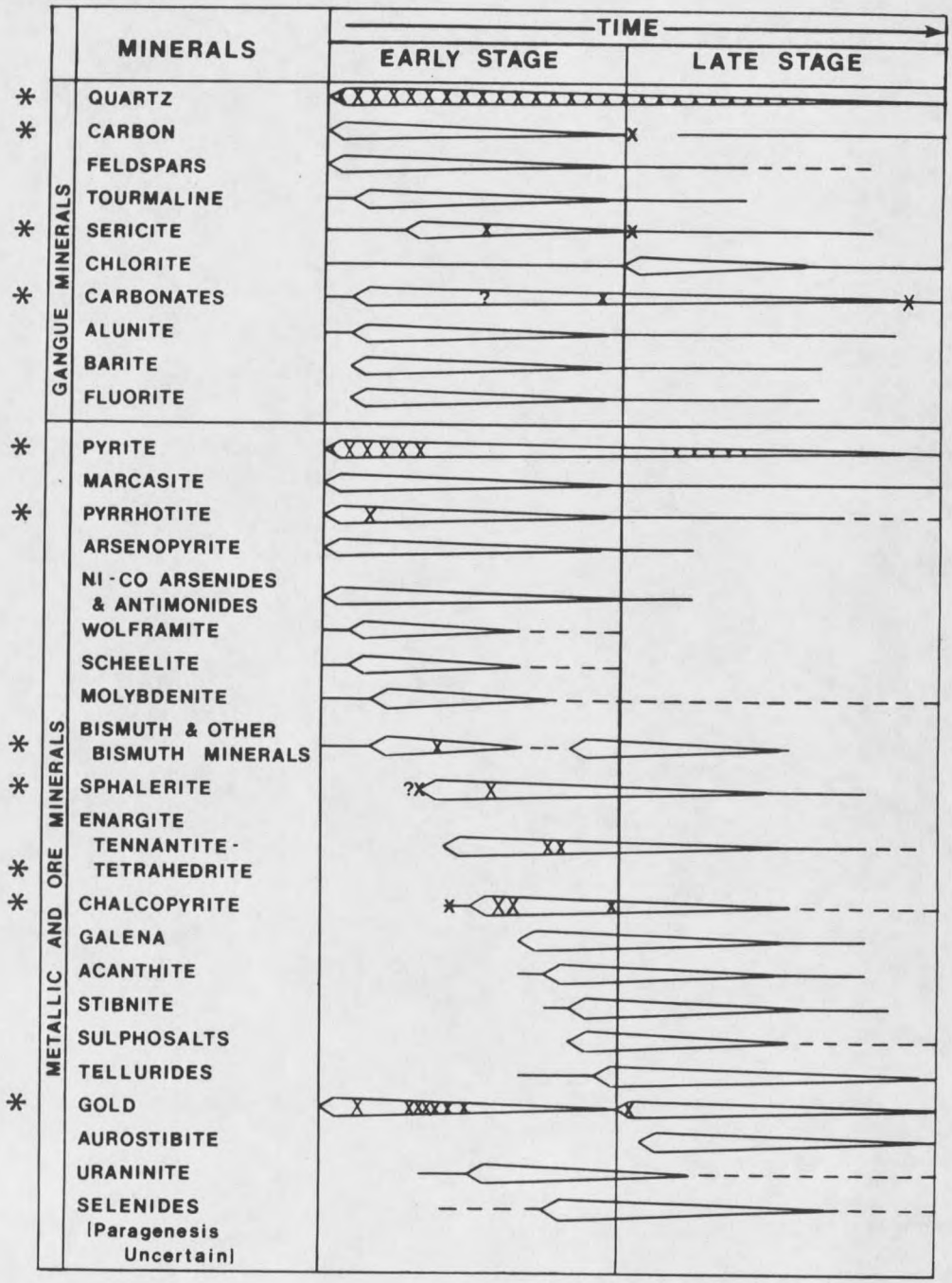

Figure 52. Generalized paragenetic sequence of principal minerals in epigenetic gold deposits (modified from Boyle, 1979). Comparative occurrences of Red Pine mineralization are noted by the cross-hatched pattern. Asterisks indicate minerals unique to the Red Pine. Question marks indicate position is uncertain. Minerals from wall-rock alteration zones are excluded from this diagram (Boyle, 1979).

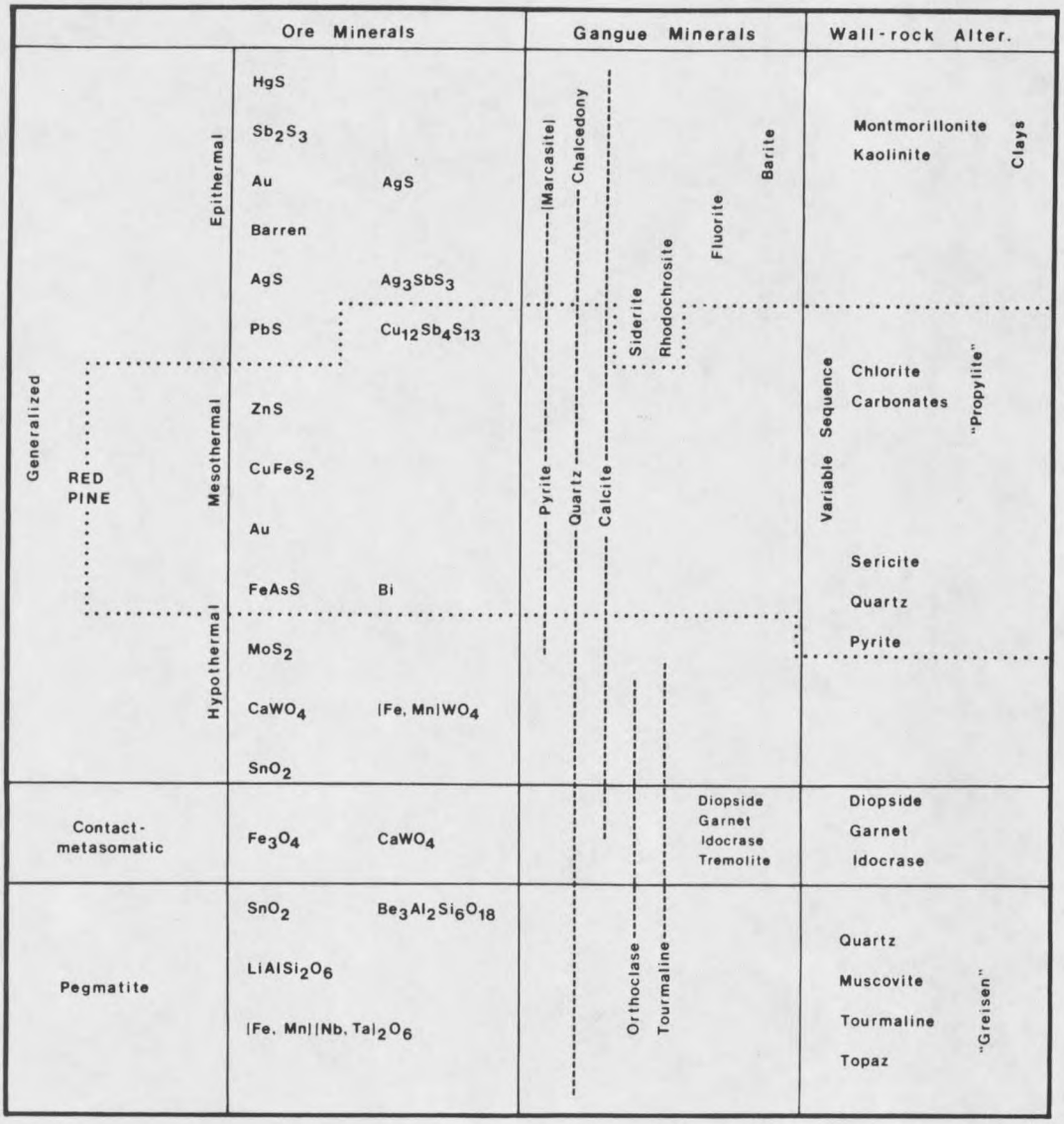

Figure 53. Generalized chemical and mineralogical associations with epi-meso-hypothermal zones of ore minerals, gangue minerals, and the wall rock alteration (modified from Jensen and Bateman, 1979). Red Pine minerals fall between the dotted lines in the hypothermal to mesothermal categories of formation. Jensen and Bateman (1979) delineate the temperature ranges for these categories as follows: epithermal (50° to 200° C), mesothermal (200° to 500° C), hypothermal (500° to 600° C), pegmatite (575° $\pm$ C), and contact metasomatic (not given).

consistent with the pattern presented by Boyle (1979). This evidence is significant, for it establishes that the Red Pine sequence of mineralization is consistent with that of other epigenetic gold deposits.

Differences between the sequence described by Boyle (1979) and the Red Pine sequence involve sphalerite and carbon (graphite). Sphalerite grains associated with pyrite may be either a local variation or an overlap of these minerals occurring during the late stages of the emplacement of pyrite in Period 1. Graphite in the Red Pine sequence occurs later than is noted in the paragenetic sequence by Boyle (1979). However, Boyle (1979) notes in his discussion that carbon (graphite) can be introduced later in the sequence.

The Red Pine sequence also contains minerals comparable to those outlined in Jensen and Bateman (1979) that occur in the mesothermal to hypothermal categories of formation (Fig. 53). The minerals are bracketed from the low-temperature range of hypothermal deposition to the low-temperature range of mesothermal deposition. The alteration minerals in the wall rocks and the ore and gangue minerals of the vein fit this pattern. This correlation is supported by the occurrence of gold and bismuthinite early in the paragenetic sequence, intermediate chalcopyrite and sphalerite, and late-stage tetrahedrite. Moreover, the presence of the gangue minerals (quartz, pyrite, and calcite) and alteration minerals (pyrite, quartz, white mica, calcite, dolomite, and chlorite) is consistent with the pattern listed by Jensen and Bateman (1979).

Interpretations of Mineral Associations of Gold

Gold is associated with pyrite, bismuthinite, and graphite in the Red Pine ore. These associations are significant because they place limits on conditions of mineralization and on timing of ore emplacement as discussed below.

Gold and Pyrite

Determination of the Red Pine paragenetic sequence and study of mineral associations and textures show that gold occurs relatively early in the first of two main stages of mineralization. This occurrence is supported by the association of gold with pyrite, quartz, and bismuthinite in Period 1. It is important because gold occurs later in the sequence in many epithermal deposits (Buchanan, 1981).

Gold associated with pyrite is a common occurrence in some gold deposits (Ramdohr, 1969; Boyle, 1979). However, as noted by Schwartz (1944), the association is not always consistent. In some deposits pyrite carries gold values; in others pyrite is barren and different minerals carry the gold values (Schwartz, 1944). Schwartz (1944) and Crocket (1978) propose that the association of gold with pyrite or other sulfides is a product of timing and environment rather than a result of any precipitating properties that the sulfides may have. Boyle (1979) supports the alternative that in many cases submicroscopic gold occurs in chemical combination in pyrite rather than as discrete grains (<0.1 micron in size).

Boyle (1979) states that gold can be present in pyrite in three forms:

1. "submicroscopic, perhaps in the lattice of the mineral";
2. "as native gold in small blebs, droplets, and as ramifying masses, generally at random, and";
3. "as irregular masses, plates, and grains along fractures, slips and seams, or coating the faces of crystals".

According to Boyle, (1979) the second category strongly indicates exsolution of the gold. The third category could also indicate exsolution, but points toward introduction of gold from outside the pyrite crystal or mass (Boyle, 1979). In addition to the interpretation of exsolution proposed by Boyle (1979), the second category may have additional interpretations. Gold could have formed in pyrite by contemporaneous growth along boundaries of a crystallizing grain of pyrite, as early porphyroblasts incorporated in the pyrite, in negative-crystal or open-space fillings (Ramdohr, 1969), or in a fracture perpendicular to the plane of a polished surface. Gold in the Red Pine deposit is consistent with both the second and third categories.

Gold in the submicroscopic category has not been found in the Red Pine deposit. Short scans using a scanning electron microscope-energy dispersive system (SEM-EDS) on several pyrite grains were conducted with the help of Dr. Vernon Griffiths of Butte, MT. These spot, line, and area scans did not indicate conclusively whether or not gold is present as a submicroscopic lattice constituent or as discrete submicroscopic grains in the pyrite. Spot and line scans, when placed directly on or across the gold, did detect visible and

microscopically visible gold particles. The SEM-EDS equipment has a limited sensitivity for minute amounts of elements (0.05 weight-percent detectability) (Goldstein and others, 1981). A longer counting period than the few minutes utilized in this case may provide better results in detecting the submicroscopic gold. However, even if it is present, the submicroscopic gold may not be detectable, for Boyle (1979) notes that more intensive microprobe studies have rarely discerned the position of submicroscopic gold in pyrite. More compositional analyses by SEM-EDS may better define the answer to this question, but submicroscopic gold does not appear to be present in the pyrite at the Red Pine mine.

Gold and Bismuthinite

The association of gold with bismuthinite occurs early in the paragenetic sequence and aids in the interpretation of some conditions of mineral emplacement for the deposit. Many bismuth minerals have a close relationship with gold (Schwartz, 1944; Boyle, 1979), which leads both these authors to propose that bismuth minerals could be important in localizing gold. The mere presence of bismuthinite is also significant because it has not been previously noted in the literature on ore deposits in the Sheridan district.

The position of bismuthinite in the paragenetic sequence of the Red Pine deposit is consistent with the early formation of this mineral in the general paragenetic sequence developed by Boyle (1979) (Fig. 52). Boyle (1979) finds that most bismuth minerals are earlier than or contemporaneous with native gold.

The presence of bismuthinite suggests that the Red Pine deposit was formed by hydrothermal fluids in the low-temperature range of hypothermal deposition or in the high-temperature range of mesothermal deposition. This interpretation is further supported by the occurrence of bismuthinite in other ore deposits. Bismuthinite is present primarily in deposits formed at high temperatures (including some gold veins, tin and wolframite veins, and contact metasomatic deposits) (Ramdohr, 1969). Boyle (1979) mentions that bismuthinite is one of the common bismuth minerals noted in many gold deposits, but on the whole, bismuth minerals are recorded mainly in skarn, gold-quartz, and polymetallic deposits. Arhens and Erlank (1978) also note that bismuth minerals typically occur in granite pegmatites and hydrothermal ore deposits. These occurrences imply an igneous association for the hydrothermal fluids that resulted in the Red Pine deposit.

Gold and Graphite

The association of gold and graphite does not indicate a strong influence of graphite on gold emplacement in Period 1, due to the position of graphite in the paragenetic sequence, (primarily at the beginning of Period 2 mineralization). This apparent lack of strong influence is significant because gold has precipitated through the influence of carbonaceous matter in some deposits (Boyle, 1979). In the Red Pine deposit, a minor amount of gold could have been introduced into graphite-filled fractures from adjacent quartz and/or pyrite grains during Period 2 mineralization. Remobilization of the

early gold into these areas may have been accomplished through deformation or later influx of hydrothermal fluids. The presence of gold along quartz grains adjacent to graphite veinlets and the presence of gold that cuts or is attached to small graphite veinlets supports this explanation. The crystallization of a minor amount of gold with graphite early in Period 2 mineralization may be an alternative interpretation. Further work is needed to determine the exact role of the graphite in localization of gold and to determine the source of the graphite.

Discussion of Mineral Associations of Silver

According to Boyle (1979), native silver in the hypogene ore of gold deposits is an uncommon occurrence. Therefore, its apparent association with bismuthinite in the Red Pine ore is interesting. However, it is possible that the silver is electrum, since the composition of the silver has not been determined and the association of silver and bismuthinite is rare in the ore. Another possibility is that the native silver exsolved from bismuthinite along cleavage or grain boundaries. Some silver is also found with chalcopyrite in minute veinlets that cut the bismuthinite, indicating that it is younger than bismuthinite. A better picture of the association of silver and bismuthinite may be provided by electron microprobe studies.

Silver is also associated with gold and tetrahedrite in the Red Pine ore, as is evident from assay (Appendix F) and SEM-EDS data (Appendix E). Ramdohr (1969) notes that silver is found in solid

solution in gold in other deposits. Silver also can extensively replace copper in tetrahedrite, as observed from analyses of tetrahedrite from other deposits (Ramdohr, 1969).

Conditions of Mineralization

Many physicochemical factors control deposition or emplacement of an ore deposit. Among these are temperature, pressure, oxidation potential, pH, "the activities of various complexing ligands" (Seward, 1984), the bulk chemical composition of the hydrothermal fluids, and the composition of the enclosing country rocks (Phillips and others, 1983). In the present study, only general temperatures and pressures of ore emplacement are considered. These conditions have been inferred from the physical surroundings and/or from the mineralogy of the deposit.

The temperatures of formation for most gold deposits range from 175° to 450° C (Seward, 1984). The Red Pine deposit probably formed in this temperature range and possibly at a slightly higher temperature. This interpretation is supported by the presence and position of bismuthinite and pyrrhotite in the paragenetic sequence. Moreover, the Red Pine deposit fits into the hypothermal- to mesothermal-temperature range (500° to 200° C or slightly lower) outlined by Jensen and Bateman (1979) (Fig. 53).

In addition, pyrite and pyrrhotite appear to be in textural equilibrium in the ore, so this would constrain the temperature in the system and the composition of iron and sulfur to the pyrite-pyrrhotite field below 743° C, the upper stability limit for pyrite (Arnold,

1962). The rare occurrence of hexagonally-shaped pyrrhotite grains in pyrite also suggests a high temperature of ore deposition. However, a definite temperature of formation cannot be determined from pyrrhotite because of its tendency to lose its high-temperature composition and structure in low-temperature environments (Craig and Scott, 1974).

High temperature of formation is also indicated by the "frozen" appearance of vein boundaries at wall rock contacts (Ramdohr, 1969). This appearance results when strong silicification is present that does not allow the vein to separate readily from the wall rock when broken (Ramdohr, 1969). This feature is a useful indicator of high temperatures of formation because at these temperatures there are no clay minerals (which denote low temperatures) formed along vein boundaries (Ramdohr, 1969). Some "frozen" features are evident along the Red Pine vein, so a high temperature of formation is indicated.

The formation of alteration minerals, such as sericite, carbonate, chlorite, quartz, pyrite, serpentine, talc, and clinozoisite, near the vein, reflects the influence of hydrothermal fluids on the high-grade metamorphic country rocks. The presence of these minerals suggests thermal alteration at greenschist-facies conditions. The temperature of formation for greenschist minerals ranges from 250° to 450° C (Ehlers and Blatt, 1982). Alteration that produces pyrite, quartz, and sericite is characteristic of upper-mesothermal to lower-hypothermal temperatures, while alteration producing chlorite and carbonate occurs at middle- to lower-mesothermal temperatures (Fig. 53). Guilbert and Park (1986) note sericitic or "phyllic" alteration in the temperature range 425° to

300° C with a pressure of 1 kilobar. Alteration that produces chlorite, Mg-Fe-Ca carbonate, and epidote occurs below 400° C at 1 kilobar (Guilbert and Park, 1986).

The Red Pine paragenetic sequence also denotes a progressive decrease in temperature. Lower temperatures of formation are indicated by the precipitation of microcrystalline quartz and trace amounts of chalcedony in Period 2. Graphite-gouge stringers also suggest lower temperatures of formation during Period 2 mineralization based on the probable existence of clay in the gouge (Ramdohr, 1969; Guilbert and Park, 1986).

Decreasing temperatures are also indicated by the presence of djurleite as a secondary alteration mineral. The upper stability limit for djurleite is 93° C (Uytenbogaardt and Burke, 1985), but the presence of djurleite alone does not indicate that secondary alteration of sulfides specifically was restricted to temperatures below 93° C. Alteration could have started at a higher temperature, in which case hexagonal chalcocite and high digenite would have formed until temperatures fell below 93° C (Uytenbogaardt and Burke, 1985). Then djurleite would have formed through reversible reaction processes (Uytenbogaardt and Burke, 1985).

Depending on the depth of a hydrothermal system, pressures could be hydrostatic, lithostatic, or a combination of the two (Seward, 1984). Pressures are approximately hydrostatic for hydrothermal systems that are relatively shallow (4-5 kilometers) and sufficiently permeable (Seward, 1984). Lithostatic pressures may result at depths greater than 4-5 kilometers (Seward, 1984). In addition, Butler

(1942) interprets brecciated textures as evidence for shallow emplacement of ore deposits. Therefore, brecciated textures of the Red Pine deposit indicate shallow emplacement and possibly hydrostatic pressures.

Since the properties of the fluids and the physical conditions of the wall rocks are interrelated in their role in ore deposition, it is unlikely that any one factor would be entirely responsible for ore deposition (Guilbert and Park, 1986). Further work is needed to quantify better the conditions of ore deposition at the Red Pine mine. Possible avenues of research include studies of geochemistry, mineral compositions, and fluid inclusions.

General Structural Controls on Mineralization

Structural features also have had a role in ore deposition. The mineralization is restricted to a fissure vein system, indicating that the presence of this structure has facilitated ore deposition. Dilational zones along the fissure, in areas having flattened dip, serve as centers for concentrated mineralization.

Episodes of brittle fracturing and brecciation during and after Period 1 mineralization provided additional access of fluids to sites of deposition. These sites were utilized by Period 2 mineralization. Local fracturing and brecciation during Period 2 mineralization provided continued access to the system for hydrothermal fluids, resulting in deposition of microcrystalline quartz and calcite and in secondary alteration.

Moreover, on a regional scale, the N 36° E, 50° NW orientation of the Red Pine vein approximates the orientation of the N 30°-35° E regional fracture system suggested by Burger (1966) to be related to the Tobacco Root batholith. Structural control of mineralization by this system is supported by the occurrence of other veins in the Sheridan district, for they are oriented approximately parallel to it (Burger, 1966). Furthermore, a portion of the Red Pine vein has an average orientation of N 45° E, 54° NW. This orientation approximates the N 50° E orientation of a fracture system within the Tobacco Root batholith (Burger, 1967).

An exact relation of faulting in the Red Pine deposit to the emplacement of the Tobacco Root batholith is not clear. However, Reid (1957) suggests that continued movement on northwest-trending faults after the intrusion of the Tobacco Root batholith permitted formation of ore deposits in the northwestern portion of the range. This may be true of northeast-trending faults in the range, for they also offset the batholith as shown by Vitaliano and others (1979). Moreover, Levandowski (1956) notes that some northeast-trending veins in the Sheridan and Alder districts occur in faults that cut satellitic stocks. Thus, the northeast-trending fault system may also have provided a locus for deposition in the Red Pine system after the intrusion of the batholith. Wilton and Strong (1986) mention the possibility of deformation occurring in an intrusive system where boiling of late-stage fluids raised enough pressure to cause fracturing of the surrounding country rocks. This pressure-induced fracturing could be a mechanism for faulting. Alternatively, faulting

may result from readjustment of the rocks after the intrusion of the batholith.

Interpretations of Timing of Ore Emplacement

Several possibilities exist for the timing of deposition of the Red Pine deposit. Archean, Proterozoic, Cambrian, Cretaceous, and Tertiary time periods are considered in this paper. These possibilities will be examined to determine which is the most feasible for the deposit. The mineralogy, textures, other observed features at the mine, and information from previous literature on the area and on gold deposits in general will be used in interpreting the timing of ore emplacement.

Archean

The Archean is a plausible time for emplacement of the deposit because the Red Pine vein was deposited in Archean metamorphic rocks. However, evidence at the mine does not support this hypothesis, primarily because brittle textures are associated with the deposit and because the metamorphic grade of the country rocks differs from that of the vein material. This evidence is discussed in more detail in the preceding section on general deposit type (see pages 78-79).

Additional support for a post-Archean age of mineralization is found in the presence of bismuthinite in the ore. Although there are exceptions, bismuth minerals are generally found in ores younger than Precambrian (Boyle, 1979).

Proterozoic

The timing of mineralization of the Red Pine deposit may be linked to Proterozoic thermal events that include emplacement of pegmatites and diabase dikes in the Tobacco Root Mountains (Gilletti, 1966; Wooden and others, 1978). However, formation of the deposit during this time period is unlikely because mines in the region do not appear to be associated with the pegmatites or diabase dikes. The lack of outcrops of diabase dikes and the lack of sulfide or precious-metal mineralization in the pegmatites of the mine area support this interpretation. The lack of mineralization in the pegmatites is consistent with the observations by Vitaliano and others (1979) of Proterozoic pegmatites throughout the Tobacco Root Mountains.

Cambrian

A interpretation of the timing of ore emplacement as Paleozoic can be inferred from a hypothesis presented by Ruppel (1985) for a Middle Cambrian sedimentary origin of gold deposits in the Tidal Wave district, northwest of the Red Pine area. The Paleozoic timing and sedimentary origin of the mineralization do not appear to fit the Red Pine scenario for three reasons. Firstly, there is presently no evidence of Paleozoic rocks in the mine area. This absence may result from any of three factors:

1. the Paleozoic rocks were eroded since their deposition;
2. the Red Pine area was a highland during Paleozoic sedimentation and the Paleozoic units were not deposited;

3. only part of the Paleozoic package was deposited and it has since been eroded away.

Secondly, the development of a gold deposit from descending solutions from the dewatering of the Park Shale proposed by Ruppel (1985) seems improbable, even under highly permeable conditions. Ramdohr (1969) notes that gold-bearing descending solutions deposit gold readily within limited depths below the surface. Therefore, the probable presence of overlying sections of rock that had to be penetrated for descending solutions to reach the Archean metamorphic rocks suggests that development of gold mineralization by these solutions is unlikely. Thirdly, the mineralogy and paragenetic sequence for the Red Pine deposit denote a higher temperature of formation than would be plausible for descending solutions.

Cretaceous

There are four major lines of evidence indicating that the Red Pine deposit is of Cretaceous age. Firstly, the minerals in the deposit point to a hydrothermal origin of ore emplacement at temperatures in the hypothermal to mesothermal range and to a probable igneous source. This source could well be the Late Cretaceous Tobacco Root batholith or a related satellitic intrusive body. Secondly, the presence of igneous bodies at some distance from the main outcrop of the batholith suggests the occurrence of an igneous body at depth in the mine area. The closest satellitic intrusive outcrop is located approximately 1.8 kilometers southeast of the mine (Vitaliano and others, 1979) (Pl. 1). The closest margin of the batholith crops out

4.4 kilometers northeast of the mine site (Pl. 1). Moreover, the proximity of the batholith is still within a reasonable range to provide a heat source to circulate hydrothermal fluids. Under the proper conditions, hydrothermal fluids can move tens of kilometers (Skinner, 1979). The presence of numerous joints, fractures, and lithologic contacts in the metamorphic rocks surrounding the batholith represents possible channelways for fluid migration in the rocks. Thirdly, the relation of the deposit to the batholith is suggested from the strike and dip of the vein. The N 36° E, 50° NW and N 45° E, 45° NW orientations of the vein approximate the regional N 30°-35° E and N 50° E fracture systems associated with the batholith (Burger, 1966). Fourthly, the brecciated textures of the vein suggest shallow emplacement (Butler, 1942) which could be related to a shallow portion of the batholith or a related body. This interpretation is plausible, for the batholith was emplaced at depths of 3 to 8 kilometers (Smith, 1970).

Furthermore, sulfide mineralization is present in pegmatites associated with the Tobacco Root batholith (Vitaliano and others, 1979). This characteristic distinguishes them from the Proterozoic pegmatites (Vitaliano, and others, 1979). The development of some mines near or in some of these Cretaceous pegmatites and/or Cretaceous intrusive bodies also supports the hypothesis that the Red Pine deposit was emplaced during the Late Cretaceous.

Tertiary

Timing of ore emplacement may also be related to the early Tertiary. Some late-stage pegmatites associated with the Tobacco Root batholith are Tertiary in age and probably represent a continuation of pegmatite emplacement from the Late Cretaceous discussed above.

An additional interpretation for Tertiary timing of ore emplacement is related to volcanism during this time. The Tertiary volcanic rocks closest to the mine are located approximately 2.7 kilometers to the northwest (Pl. 1), so a Tertiary age of deposition could be possible. However, this interpretation does not seem feasible for the Red Pine deposit. There are no outcrops of volcanic rocks in the mine area, possibly due to erosion or lack of emplacement. Moreover, the banded and crustified ore textures typically found in volcanic-associated ("epithermal") deposits (Boyle, 1979; Buchanan, 1981) are not present in the Red Pine ore. Based on this absence, it is unlikely that Red Pine mineralization would be associated with volcanism during the early Tertiary.

Source of Metals and Fluids

Even though a Late Cretaceous to early Tertiary timing of emplacement is indicated for the deposit by the preceding discussion, the source of the gold, other metals, and ore fluids is less clear. This interpretation is consistent with the observations of Guilbert and Park (1986) who mention the ongoing controversy over this question of source of metals and fluids for ore deposits in general.

Researchers have examined the possibility of the granitic system as a source for metals and hydrothermal fluids. Wilton and Strong (1986) support the idea that granitic rock systems contribute to the origin of ore through aqueous phase separation from the magma. This phase separation is thought to contain selectively partitioned Au, Ag, Cl, S, and base metals (Wilton and Strong, 1986). The opposing view is based on the information that rocks of mafic and intermediate composition are found by Tilling and others (1973) to have larger amounts of gold associated with them than felsic rocks. This view leads Boyle (1979) to suggest that the granitic system is not a source of metals, but just a heat pump.

Metals may have originated from the country rocks or an aqueous phase separation from a granitic intrusive. These sources could have some significance for the Red Pine area and the Tobacco Root Mountains. Based on the typical igneous association of bismuthinite, some of the metals in the Red Pine deposit probably have an igneous source. The Tobacco Root batholith, and/or other Late Cretaceous to early Tertiary intrusives could have been the catalyzing influence for the system. These intrusives probably provided a heat source and hydrothermal fluids needed to carry metals in the aqueous phase separation or to remobilize various metals from the country rocks. When physicochemical conditions were appropriate, the metals were concentrated and deposited in fracture systems and along contacts of the various country rocks.

Another explanation for the source of metals could be the surrounding country rocks. However, this is unlikely because of

the high metamorphic grade of the Archean rocks. The same reasons for discounting a Paleozoic timing of ore deposition may also eliminate sedimentary country rocks as a source of metals.

Aqueous phase separation from the batholith could also account for some fluids in the system. Some mixing of juvenile and surface water is possible since the deposit has apparently been emplaced at shallow depths. A fluid source from surrounding country rocks is improbable due to the absence of sedimentary rocks and the high metamorphic grade of the Archean rocks in the area. Future studies of fluid inclusions and oxygen isotopes could provide information needed to better define the source of ore fluids.

Model Scenario

Guilbert and Park (1986) and Groves and Batt (1984) note the unlikeliness of mineral deposits occurring in high-grade metamorphic environments, so in this respect the Red Pine and other deposits in the Tobacco Root Mountains are unique. However, the possibilities are greater for formation of ore deposits in such an environment due to other factors. These factors are the proper conditions for deposition, the presence of the nearby Tobacco Root batholith, and the ability of hydrothermal fluids to move tens of kilometers when the system is sufficiently permeable (Skinner, 1979).

The hydrothermal features discussed above have implications for a petrogenetic model for the Red Pine mine and deposits occurring in similar geologic settings. Most likely the Tobacco Root batholith dips steeply beneath the Archean rocks of the area (Burfeind, 1967).

There may also be a cupola at depth in the mine area providing the heat source to move the hydrothermal fluids. The cupola could be related to the Tobacco Root batholith and/or an associated satellitic intrusive body.

Smith (1970) estimates that pressure conditions for the batholith range from 0.9 to 2.1 kilobars. Using the figures of Guilbert and Park (1986) for pressure at depth (1 kilobar per 4 kilometers of depth), pressures for the batholith range from 0.75 to 2 kilobars, so the measurements are consistent. Low pressures are also suggested for the batholith by the hornfels-facies mineralization produced by contact metamorphism when the batholith was intruded (Hess, 1967). As a result of the emplacement of the batholith at 3 to 8 kilometers (Smith, 1970), pressures would possibly be lithostatic for the deeper portions of the system and hydrostatic for the shallower portions of the system (Seward, 1984) (see pages 90-91 in this report). Hydrostatic pressures at shallow depths of emplacement are probable because of the greater possibility of a surface connection for the system.

Smaller intrusive bodies and hydrothermal fluids probably took advantage of zones of weakness (faults, joints, fractures, intraformational faults, and bedding planes) as conduits for emplacement and/or movement. When the appropriate changes in the various physicochemical factors occurred, the deposit formed in the conduit fissure system as hydrothermal fluids approached the surface of the earth. Brecciated textures in the deposit suggest shallow emplacement. Previous reverse movement along the irregular surface of

the fissure produced some dilation where the dip of the surface flattened. This dilational area then became a center for concentrated mineralization in the fissure. Cooler surface water may have mixed with the high- to medium-temperature hydrothermal fluids to produce a sequence of decreasing temperatures. Brittle fracturing and brecciation provided fluids with continued access to deposition sites in the system.

CONCLUSIONS

Hydrothermal fluids in the hypothermal to mesothermal range of temperatures formed the Red Pine gold deposit in a fissure vein. These fluids were most likely late-stage, associated with Late Cretaceous to early Tertiary igneous activity related to the Tobacco Root batholith or an associated igneous body at depth in the mine area. Brittle fracturing and brecciation accompanied ore emplacement and provided additional fluid access to deposition sites.

Two periods of mineralization are evident in the Red Pine deposit along with late-stage secondary alteration. The major deposition of gold and sulfides occurs with milky quartz in the first period. Pyrite is the first principal sulfide present in the paragenetic sequence, followed by chalcopyrite and tetrahedrite. Bismuthinite, a minor but significant sulfide, is precipitated between the deposition of pyrite and chalcopyrite. Gangue mineralization that takes place in the second period involves deposition of graphite, white mica, microcrystalline quartz, a minor amount of pyrite, and carbonate.

Gold is primarily found early in the paragenetic sequence. It is associated with pyrite, milky quartz, and some bismuthinite in Period 1 mineralization. In rare instances, it occurs with chalcopyrite, tetrahedrite, and carbonate in Period 1 and with graphite in Period 2.

Additional work is needed to quantify and characterize conditions of ore deposition and sources of metals and fluids in more detail.

Avenues of research could involve microprobe analyses and studies of geochemistry, oxygen isotopes, fluid inclusions, and alteration of the wall rock.

REFERENCES CITED

REFERENCES CITED

Ackerman, W., 1957, Red Pine mine - upper adit (transit survey): Proprietary report from the files of Shermont Mining Company, Sheridan, Montana, 1:50 scale.

Ahrens, L.H., and Erlank, A.J., 1978, Bismuth: Abundance in sulfides and in rock-forming minerals; Bismuth minerals in Wedepohl, K.H., ed., Handbook of geochemistry, Vol. II/5 Elements La(57) to U(92): Berlin, Springer-Verlag, p. 83-D-(1-7).

Arnold, R.G., 1962, Equilibrium relations between pyrrhotite and pyrite from 325° to 743° C: Economic Geology, v. 57, p. 72-90.

Best, Myron G., 1982, Igneous and metamorphic petrology: New York, W.H. Freeman and Company, 630 p.

Boyle, Robert W., 1979, The geochemistry of gold and its deposits: Geological Society of Canada Bulletin 280, 584 p.

Buchanan, L.J., 1981, Precious-metal deposits associated with volcanic environments in the southwest in Dickinson, W.R. and Payne, W.D., eds., Relations of tectonics to ore deposits in the southern Cordillera: Arizona Geological Society Digest, v. 14, p. 237-262.

Burfeind, Walter John, 1967, A gravity investigation of the Tobacco Root Mountains, Jefferson Basin, Boulder batholith and adjacent areas of southwestern Montana [abs.]: Dissertation Abstracts International, v. 28b, p. 2489-B.

Burger, H. Robert, III, 1966, Structure, petrology, and economic geology of the Sheridan district, Madison County, Montana [Ph.D. thesis]: Bloomington, Indiana University, 156 p.

_____. 1967, Bedrock geology of the Sheridan district, Madison County, Montana: Montana Bureau of Mines and Geology Memoir 41, 22 p.

_____. 1969, Structural evolution of the southwestern Tobacco Root Mountains, Montana: Geological Society of America Bulletin, v. 80, p. 1329-1341.

Butler, B.S., 1942, Some inter-relations of structure, mineralogy, and association with intrusive bodies in ore deposits in Newhouse, W.H., ed., Ore deposits as related to structural features: Princeton, New Jersey, Princeton University Press, p. 3-5.

Cole, Marshall Morris, 1983, Nature, age, and genesis of quartz-sulfide-precious-metal vein systems in the Virginia City mining district, Madison County, Montana [M.S. thesis]: Bozeman, Montana, Montana State University, 76 p.

Cordua, W.S., 1973, Precambrian geology of the southern Tobacco Root Mountains, Madison County, Montana [Ph.D. thesis]: Bloomington, Indiana University, 247 p.

Craig, J.R., and Scott, S.D., 1974, Sulfide phase equilibria in Ribbe, Paul H., ed., Mineralogical Society of America Reviews in Mineralogy Volume 1: Sulfide mineralogy: Chelsea, Michigan, Bookcrafters, Inc., p. CS-1-CS-110.

Crocket, J.H., 1978, Gold: Behavior in magmatogenic processes in Wedepohl, K.H., ed., Handbook of geochemistry Vol. II/5 Elements La(57) to U(92): Berlin, Springer-Verlag, p. 79-F-(1-5).

Ehlers, Ernest G., and Blatt, Harvey, 1982, Petrology: Igneous, sedimentary, and metamorphic: San Francisco, W.H. Freeman and Company, p. 546.

Giletti, Bruno J., 1966, Isotopic ages from southwestern Montana: Journal of Geophysical Research, v. 71, no. 16, p. 4029-4036.

Goldstein, Joseph I., Newbury, Dale E., Echlin, Patrick, Joy, David, Fiori, Charles, and Lifshin, Eric, 1981, Scanning electron microscopy and x-ray microanalysis: A text for biologists, materials scientists, and geologists: New York, Plenum Press, 673 p.

Groves, D.I., and Batt, W.D., 1984, Spatial and temporal variations of Archean metallogenic associations in terms of evolution of granitoid-greenstone terrains with particular emphasis on the western Australian shield in Kroner, A., Hanson, G.N., and Goodwin, A.M., eds., Archean geochemistry: Springer-Verlag, New York, p. 73-98.

Guilbert, John M., and Park, Charles F., Jr., 1986, The geology of ore deposits: New York, W.H. Freeman and Company, 985 p.

Hess, David F., 1967, Geology of pre-Beltian rocks in the central and southern Tobacco Root Mountains, with reference to superposed effects of the Laramide-age Tobacco Root batholith [abs.]: Dissertation Abstracts International, v. 28b, p. 2480-2481-B.

Hyndman, Donald W., 1985, Petrology of igneous and metamorphic rocks (2nd edition): New York, McGraw-Hill, 786 p.

James, Harold L., 1981, Bedded Precambrian iron deposits of the Tobacco Root Mountains, southwestern Montana: U.S. Geological Survey Professional Paper 1187, 16 p.

James, H.L., and Hedge, C.E., 1980, Age of basement rocks of southwest Montana: Geological Society of America Bulletin, v. 91, p. 11-15.

Jensen, Mead L., and Bateman, Alan M., 1979, Economic mineral deposits (3rd edition): New York, John Wiley and Sons, 593 p.

Johns, Willis M., 1961, Geology and ore deposits of the southern Tidal Wave mining district, Madison County, Montana: Montana Bureau of Mines and Geology Bulletin 24, 53 p.

Krohn, Douglas H., and Weist, Margaret Mlynarczyk, 1977, Principal information on Montana mines: Montana Bureau of Mines and Geology Special Publication 75, p. 98.

Levandowski, D.W., 1956, Geology and mineral deposits of the Sheridan-Alder area, Madison County, Montana [Ph.D. thesis]: Ann Arbor, Michigan, University of Michigan, 318 p.

Lorain, S.H., 1937, Gold lode mining in the Tobacco Root Mountains, Madison County, Montana: U.S. Bureau of Mines Information Circular 6972, 74 p.

Lovering, T.G., 1972, Jasperoid in the United States--Its characteristics, origin, and economic significance: U.S. Geological Survey Professional Paper 710, 164 p.

Marvin, R.F., and Dobson, S.W., 1979, Radiometric ages: Compilation B, United States Geological Survey: Isochron/West, no. 26, p. 3-32.

Mueller, Paul A., and Cordua, W.S., 1976, Rb-Sr whole rock age of gneisses from the Horse Creek area, Tobacco Root Mountains, Montana: Isochron/West, no. 16, p. 33-36.

Phillips, G.N., Groves, D.I., and Clark, M.E., 1983, The importance of host-rock mineralogy in the location of Archean epigenetic gold deposits in De Villiers, J.P.R., and Cawthorn, P.A., eds., ICAM 81: Proceedings of the first international congress on applied mineralogy: The Geological Society of South Africa Special Publication No. 7, p. 79-86.

Ramdohr, Paul, 1969, The ore minerals and their intergrowths: Braunschweig, West Germany, Pergamon Press, 1174 p.

Reid, Rolland R., 1957, Bedrock geology of the northern end of the Tobacco Root Mountains, Madison County, Montana: Montana Bureau of Mines and Geology Memoir 36, 25 p.

Ruppel, Edward T., 1982, Cenozoic block uplifts in east-central Idaho and southwest Montana: U.S. Geological Survey Professional Paper 1224, 24 p.

_____. 1985, The association of Middle Cambrian rocks and gold deposits in southwest Montana: U.S. Geological Survey Open-File Report 85-207, 26 p.

Samuelson, Kiff J., and Schmidt, Christopher J., 1981, Structural geology of the western Tobacco Root Mountains, southwestern Montana: Southwest Montana, Montana Geological Society Field Conference and Symposium, p. 191-199.

Schmidt, Christopher J., and Hendrix, Thomas E., 1981, Tectonic controls for thrust belt and Rocky Mountain foreland structures in the northern Tobacco Root Mountains - Jefferson Canyon area, southwestern Montana: Southwest Montana, Montana Geological Society Field Conference and Symposium, p. 167-180.

Schmidt, Christopher J., and Garihan, John M., 1983, Laramide tectonic development of the Rocky Mountain foreland of southwestern Montana, in Lowell, James D., and Gries, Robbie, eds., Rocky Mountain foreland basins and uplifts: Denver, Rocky Mountain Association of Geologists, p. 271-294.

Schwartz, George M., 1944, The host minerals of native gold: Economic Geology, v. 39, p. 371-411.

Seward, T.M., 1984, The transport and deposition of gold in hydrothermal systems in Foster, R.P., ed., Gold '82: The geology, geochemistry and genesis of gold deposits: Geological Society of Zimbabwe Special Publication No. 1, Rotterdam, Netherlands, A.A. Balkema Publishers, p. 165-181.

Skinner, Brian J. 1979, The many origins of hydrothermal mineral deposits in Barnes, Hubert L., ed., Geochemistry of hydrothermal ore deposits (2nd edition): New York, Wiley-Interscience, p. 1-21.

Smith, John L., 1970, Petrology, mineralogy, and chemistry of the Tobacco Root batholith, Madison County, Montana [abs.]: Dissertation Abstracts International, v. 31b, p. 5429-B.

Spry, Alan, 1969, Metamorphic textures: Oxford, England, Pergamon Press, 350 p.

Tansley, Wilfred, Schafer, P.A., and Hart, L.H., 1933, A geological reconnaissance of the Tobacco Root Mountains, Madison County, Montana: Montana Bureau of Mines and Geology Memoir 9, 57 p.

Tilling, Robert I., Gottfried, David, and Rowe, Jack J., 1973, Gold abundance in igneous rocks: Bearing on gold mineralization: Economic Geology, v. 68, p. 168-186.

Turner, Francis J., 1981, Metamorphic petrology--Mineralogical, field, and tectonic aspects (2nd edition): New York, McGraw-Hill, 524 p.

Uytenbogaardt, W., and Burke, E.A.J., 1985, Tables for microscopic identification of ore minerals: New York, Dover Publications, 430 p.

Vitaliano, Charles J., Cordua, W.S., Burger, H.R., III, Hanley, T.B., Hess, D.F., and Root, F.K., 1979, Geologic map of southern Tobacco Root Mountains, Madison County, Montana: Geological Society of America Map and Chart Series, MC-31, 1:62,500 scale.

Vitaliano, Charles J., Kish, Stephen, and Towell, David G., 1980, Potassium-argon dates and strontium isotopic values for rocks of the Tobacco Root batholith, southwestern Montana: Isochron/West, no. 28, p. 13-15.

Wilson, Graham, 1985, Preliminary electron microprobe analyses of gold, tetrahedrite, pyrite, and ankerite, and petrographic analysis of graphite from the Red Pine mine, southwestern Montana (unpublished report): Isotrace Laboratory, University of Toronto, Toronto, Canada.

Wilton, D.H.C., and Strong, D.F., 1986, Granite-related gold mineralization in the Cape Ray fault zone of southwestern Newfoundland: Economic Geology, v. 81, no.2, p. 281-295.

Winchell, A.N., 1914, Mining districts of the Dillon quadrangle, Montana and adjacent areas: U.S. Geological Survey Bulletin 574, 191 p.

Wooden, Joseph L., Vitaliano, Charles J., Koehler, Steven J., and Ragland, Paul C., 1978, The late Precambrian mafic dikes of the southern Tobacco Root Mountains, Montana: Geochemistry, Rb-Sr geochronology, and relationship to Belt tectonics: Canadian Journal of Earth Science, v. 15, no.4, p. 467-479.

APPENDICES

APPENDIX A

METHODS OF STUDY

APPENDIX A

Methods of Study

Mapping

Tape and brunton mapping of the lower (2298 m.) level of the Red Pine mine was conducted during the summer field season in 1982. Samples were collected from the vein and country rocks for analysis. Surface mapping of outcrops and related structural features was also conducted. Additional mapping and description of the vein continued during the summer field season in 1983. In the fall of 1983 and spring of 1984, some weekends were utilized to collect additional data.

Adit and drift boundaries were mapped at a 0.9-meter datum by measuring distances to the walls at this level from the tape stretched from station to station. Mapping of the strike of the adit was begun by taking foresight and backsight orientations with the brunton. However, a mechanical method for turning angles was improvised after the iron ventilation pipe in the adit was suspected of disrupting brunton readings. This method involves four steps as presented below:

1. Sight the strike of the longest expanse of adit with the brunton in an area without pipe where the outside light is still visible.

2. Record the strike in a field notebook and as a line on a preliminary map.

3. Turn angles from this strike by the following method:
   a. place map on flat surface (the seat of a chair, the top of a stool, or the top of a small stepladder) over the marked station in the center of the drift;

b. realign the strike line on the map by placing the edge of the brunton on the strike line and use the brunton's mirror to sight on the original or backsight station;

c. maintain alignment of map and clipboard on flat surface;

d. rearrange brunton in the opposite direction with the north-south edge parallel to the strike of the line (take care not to disturb anything);

e. turn brunton from this orientation to align sight line in the mirror with the next station marked by an assistant's light;

f. mark along north-south edge of brunton to record angle turned from the original orientation of the strike.

4. Continue the process for backsight and foresight stations until mapping is completed. Strike of the adit or drift can be calculated by adding or subtracting the angle turned from the original strike measured.

The vein was mapped at a 2.1-meter datum level. Vein boundaries were measured with respect to the tape stretched along the strike of the drift. A drill steel, 2.1 meters in length, was used to determine datum level. Projections behind the wall for contacts of the vein that fell below the datum level were determined geometrically from several measurements. These were width of the vein perpendicular to dip, projected dip of the vein, and length of each contact below the datum.

Surface mapping consisted of a tape and brunton survey and mapping on aerial photographs. A tape and brunton survey on the surface along a N 10° W strike between the adits of the lower and upper workings provided information on how the two levels are related in space. Surface outcrops were mapped on an enlarged portion of an aerial photograph with a scale of 1 inch equals 0.13 mile or 0.2 kilometer.

Mineral Identification

Minerals related to the vein and the surrounding country rocks were identified in several ways. The use of reflected-light and transmitted-light petrography resulted in the identification of ore and gangue minerals in the country rock. A total of 24 polished surfaces, 17 polished thin sections, and 10 regular thin sections of vein-related mineralization were studied. Fifty thin sections were also studied for identification of mineral associations in the country rock.

In an effort to determine if submicroscopic gold was present in the Red Pine sulfides, a scanning electron microscope was used. After preliminary area scans of sulfide minerals were conducted by Mike Jolley in the physics laboratory at Montana State University, a comparison of data was sought. Dr. Vernon Griffiths at Montana Tech., Butte, MT, conducted area, spot, and line scans on various sulfides, primarily pyrite, using a computer-assisted scanning electron microscope-energy dispersive system (SEM-EDS). In addition to detecting gold and silver in spot scans of grains of gold within pyrite, the SEM-EDS analyses gave the first indication of a bismuth-bearing mineral and a mineral containing phosphorous, cerium, neodymium, and lanthanum in the ore (Fig. 14).

The identification of bismuthinite, tetrahedrite, djurleite, and graphite with mica was confirmed by Lester Zeihen, at Montana Tech., Butte, MT, using x-ray diffraction (powder camera techniques).

Preliminary compositional analyses of tetrahedrite, gold, pyrite, and ankerite have been conducted by Dr. Graham Wilson at Isotrace

Laboratory in Toronto, Canada. He used an electron microprobe-energy dispersive system with a finely collimated beam on samples supplied by this author. His estimate of carbon content in some samples was an approximated volume percent from petrographic observations using reflected and transmitted light. The preliminary findings provided by Wilson (1985) are given in Appendix E.

Assays were provided by Dr. Henry McClernan at the Montana Bureau of Mines and Geology, Butte, MT, to show which materials contained the gold and silver. This assay data is listed in Appendix F.

APPENDIX B

SYNOPSIS OF MINING HISTORY

APPENDIX B

Synopsis of Mining History

The history of the Red Pine mine is not well documented. The deposit was discovered in the early 1900s by William (Bill) Steiner (John Magnus, personal communication). Since the discovery of the deposit, ownership of the mine has changed several times. Early development was in the oxidized ore of the upper level. Development of the lower level began in the mid-1920s. (John Magnus, personal communication). At the time of reports by Tansley and others (1933) and Lorain (1937), the adit of the lower workings had reached the vein area and some mining had been done along it. The mine was operated until World War II when a government directive stopped all mining of nonessential metals. The estimated cumulative production of gold for the period 1900 to 1936 was 5000 ounces of gold and the ore grade averaged 0.3 oz./ton (Krohn and Weist, 1977). Mining resumed after the war only in the lower level. Electric lines, which supplied power to the mill at the site, were stolen during the war and were not reestablished. Shermont Mining Company originally leased the property in 1960 and now owns the Red Pine claims (John Magnus, personal communication).

APPENDIX C

LOCATION MAP FOR THIN SECTION SAMPLES FROM SURFACE OUTCROPS AT THE RED PINE MINE

APPENDIX C

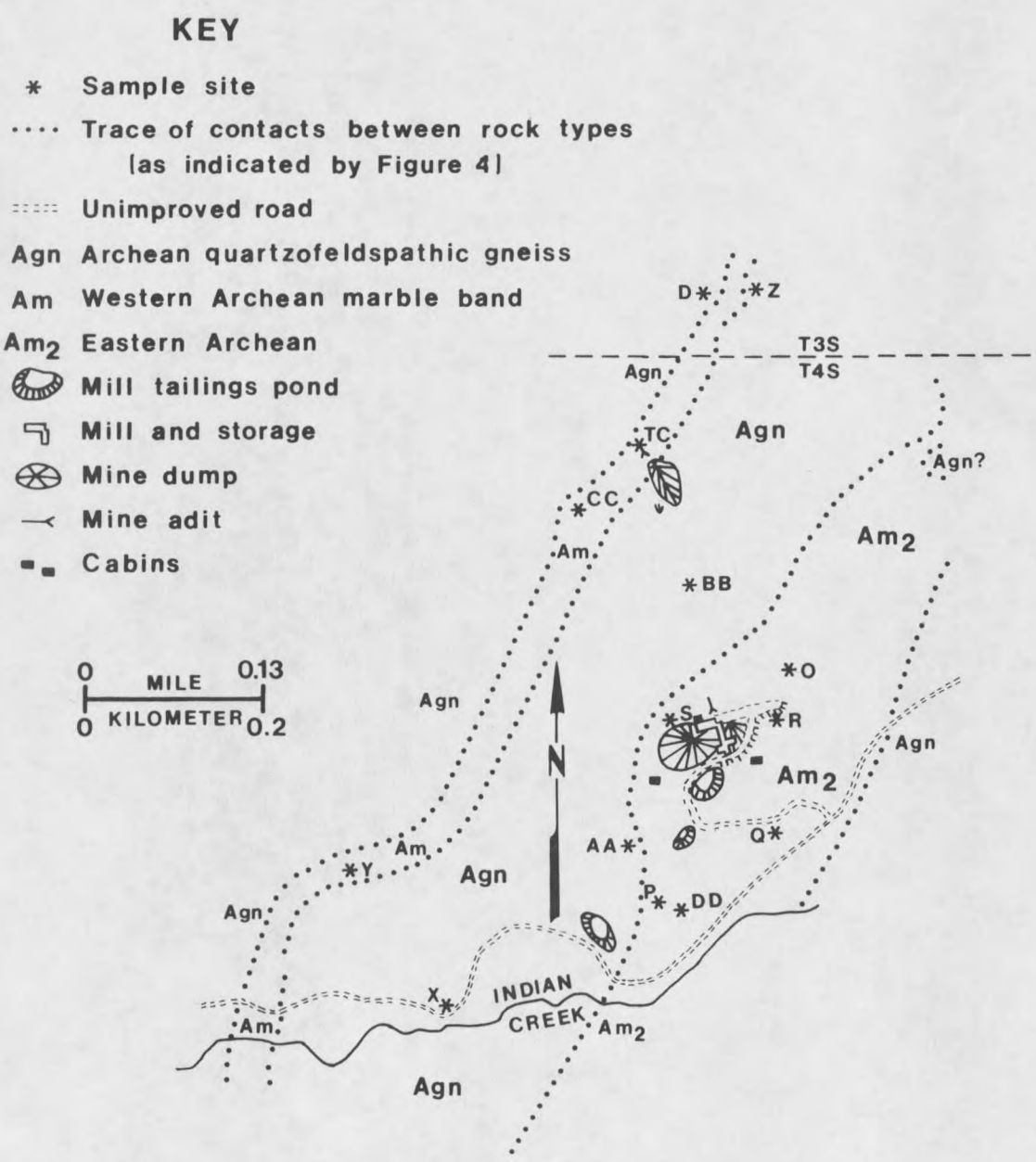

Figure 54. Location map for thin section samples from surface outcrops at the Red Pine mine.

APPENDIX D

SHAPES AND SIZES OF VEIN MINERALS AND SPECIAL METHODS OF IDENTIFICATION

APPENDIX D

Table 5. Shapes and sizes of vein minerals and special methods of identification. Methods of identification are listed only for each main mineral.

Minerals	Shapes	Observed Size Range	Method of Identification
Pyrite in milky quartz	euhedral to anhedral	≤0.01 to 8 mm.	Reflected light
Crushed rectangular patches of pyrite	anhedral	up to 3.5 cm.	
Pyrite with carbonate		≤0.01 to 5 mm.	
Pyrite rings-elongated vug lining	subhedral	0.27 to 0.58 mm. 1 x 7 mm.	
Pyrite in dark quartz	euhedral to subhedral	≤0.01 to 1.5 mm.	
Pyrrhotite in pyrite	anhedral	≤0.01 to 0.06 mm.	Reflected light
single grain	anhedral	≤0.01 to 0.85 mm.	
Chalcopyrite in pyrite	anhedral	≤0.01 to 0.06 mm.	Reflected light
single grains	anhedral	0.01 to 11 mm.	
Sphalerite in pyrite	anhedral	≤0.01 to 0.05 mm.	Reflected light
in tet.	anhedral	0.01 to 0.09 mm.	
Bismuthinite in quartz	anhedral	0.01 to 3 mm.	Reflected light SEM-EDS X-ray diffraction
in pyrite	anhedral	<0.01 to 0.03 mm.	
in tet.	anhedral	0.04 to 0.22 mm.	

Table 5--Continued

Minerals	Shapes	Observed Size Ranges	Method of Identification
Silver in bmt.	anhedral	≤0.01 to 0.12 mm.	Reflected light SEM-EDS
Tetrahedrite	anhedral	≤0.01 to 11 mm.	Reflected light SEM-EDS X-ray diffraction
Gold	anhedral		Reflected light
in pyrite		≤0.01 to 0.5 mm.	SEM-EDS Electron probe
in quartz	anhedral	<0.01 to 1.7 mm.	
with bmt.	anhedral	≤ 0.01 to 0.3 mm.	
in cp.	anhedral	≤0.01 to 0.03 mm.	
with pyrrhotite	anhedral	0.03 to 0.04 mm.	
with graphite	anhedral	≤0.01 to 0.1 mm.	
in carbonate	anhedral	≤0.01 to 0.03 mm.	
with goethite	anhedral	0.01 to 0.07 mm.	
in quartz with magnetite	anhedral	≤ 0.01 mm.	
Covellite	anhedral	0.01 to 0.02 mm.	Reflected light
Djurleite	anhedral	≤0.01 to 3 mm.	X-ray diffraction
Arsenopyrite	anhedral	0.01 to 0.08 mm.	Reflected light
Graphite			Reflected light
	fibers	0.01 to 0.24 mm.	X-ray diffraction
	* globules	up to 15 microns	Reflected light Transmitted light
	* mass	700 x 300 microns	
	* laths	up to 50 x 6 microns	

Table 5--Continued

Minerals	Shapes	Observed Size Ranges	Method of Identification
Dolomite	anhedral to euhedral	0.02 to 7 mm. & microcrystalline powder	Alizarin red - not stained Weak reaction to dilute HCl
Calcite	anhedral	≤0.01 to 4 mm.	Alizarin red - stained Vigorous reaction to dilute HCl
Quartz			Transmitted light
milky	euhedral to anhedral	≤0.01 to 8 mm.	
dark	micro-crystalline	≤0.01 mm.	Transmitted light
Mica	blades	0.06 x 0.5 mm. 0.1 x 1.2 mm. ≤0.01 mm.	Transmitted light
	mats	0.15 x 0.4 mm.	
Rare earth phosphate?	anhedral	0.10 to 0.73 mm.	SEM-EDS

* indicates description from Wilson (1985)
bmt. = bismuthinite
cp. = chalcopyrite
tet. = tetrahedrite
? = exact name unknown

APPENDIX E

PRELIMINARY COMPOSITIONAL ANALYSES

APPENDIX E

Preliminary Compositional Analyses

Wilson (1985) analyzed the composition of Red Pine mineral species including gold, tetrahedrite, dolomite (ankerite), and pyrite in samples provided by the author. An electron microprobe-energy dispersive system was used in these analyses.

An average of six electron probe analyses of one grain of gold within pyrite indicated the composition of gold to be 86 weight percent Au and 14 weight percent Ag, with silver varying from 13.0 to 15.6 weight percent. The analyses also detected a minor (<0.6%) Fe impurity. However, they did not discover any Sb, Te, Cu, Zn, As, or S impurities in the gold bleb that was studied (Wilson, 1985).

Using the average of six analyses for one large tetrahedrite grain, Wilson (1985) noted that the tetrahedrite composition varies. However, the percentage relationships of the elements almost always indicated Cu > S > Sb >> Zn > As >> Fe > Ag, with one exception where Sb > S. Minor (<1%) Ag was detected in three analyses; Pb, Bi, Hg, and Te were not found in the tetrahedrite. These preliminary analyses indicated a zoning from a Sb-rich core to a relatively As-rich margin (Wilson, 1985). Table 6 lists the average data for these analyses.

Five preliminary analyses of pyrite failed to detect any Au, Ag, As, or Cu, however, one analysis detected 0.5 percent Zn. Wilson (1985) also noted that the pyrite "coexists with chalcopyrite, in which no Sb, Ag, As, or Zn were detected in a single analysis".

Wilson (1985) also observed two types of carbonate in Red Pine samples; calcite and ankerite. The calcite was identified in hand samples and the ankerite was classified by four electron probe analyses. Table 6 shows the average data for the ankerite analyses. Ankerite is the "dolomite" referred to in this paper.

Wilson (1985) estimated the carbon content of a graphite sample to be <10 percent C, despite its black and sooty characteristics in hand specimen that imply a larger amount of carbon than is present. This estimate was a volume percent determined from transmitted-light and reflected-light petrography. This percentage of carbon is consistent "with findings from gold-related material elsewhere" (Wilson, 1985).

Table 6. Average elemental analyses of tetrahedrite and ankerite, Red Pine mine (from Wilson, 1985).

Tetrahedrite

Element	1A-center	1B-rim	IC-mean	Range
Fe	1.08+/-0.71	1.20+/-0.33	1.14	0.57- 1.89
Cu	38.74+/-0.82	40.43+/-0.65	39.59	37.85-40.80
Sb	24.47+/-3.58	18.74+/-1.68	21.60	17.74-28.27
S	25.12+/-0.41	25.74+/-0.21	25.43	24.65-25.94
Zn	6.05+/-0.83	5.98+/-0.09	6.02	5.10- 6.63
As	1.57+/-1.61	4.74+/-0.94	3.16	nd- 5.29
Ag			0.42	nd- 0.76

Data based on 6 analyses (3 near-center, 3 near-rim), except for Ag (3 analyses). Greater variation in the 3 central analyses underscores the point that the sparse data do not define the absolute variation in this mineral.

Ankerite

Element	Element wt. %	Cations	Oxide wt. %	Carbonate wt. %
Mg	8.21	7.99+/-0.64	13.62+/-1.31	28.49
Ca	21.15	12.48+/-0.41	29.58+/-0.77	52.80
Fe	8.34	3.53+/-0.33	10.73+/-0.85	17.30
C			44.66	
Total	37.70	24.00	98.59	98.59

Cation sum with respect to 24(O), excluding O in CO_2. CO_2 calculated assuming perfect stoichiometry. Partial ($-CO_2$) oxide total 53.93%. Mg/(Mg+Fe) ratios; molecular 0.622, ionic 0.693.

APPENDIX F

FIRE ASSAY DATA FROM VARIOUS GRAB SAMPLES ALONG THE VEIN

APPENDIX F

Table 7. Fire assay data from various grab samples along the vein. Sample numbers are keyed to sites on Plate 2 except for UW-2 (on Fig. 12) and DP-1 which was collected from an ore stockpile.

Sample Number	Assays oz/ton		Estimated % mineral in sample				Matrix		Condition of pyrite		Period
	Au	Ag	py	cp	tet	dj	qtz	mbl	brecc.	euhd.	
AS-23-27.6	8.17	27.7	41	2	40.5		x		x--------x		1
AS-25-6.5	2.68	3.92	40	10		1	x		x--------x		1
AN-1-RB	8.49	3.41	60				x		x		1*
AS-30-1	8.74	1.46	88				x		x		1
AS-25-10	5.50	4.6	69			2	x	cc	x--------x		1
UW-2	0.88	0.92	26				x		x		1
DP-1	1.08	7.92	95	3			unknown			x	1
AS-23-0	0.13	<0.1	36					x		x	?
AS-42-1	1.49	0.63	42				x		x		1*
AS-25-6.5C	3.98	5.46	17	10	1		x		x		1
AN-21-8	0.03	<0.05	4				graphite				2
AS-25-7A	0.204	0.44	24				mx			x	2**
AS-25-7B	0.176	0.46	6				mx		x		2**
AS-23-7R	0.636	0.06	61				x & cc		x		1
AS-23-27.6T	0.330	98.93	5		50		x				1
AS-41-23.5P	0.551	3.53	3	25			x				1
AS-41-23.5C	0.632	1.23	3	?			x				1

* = some mineralization from Period 2 is associated with this sample
** = some mineralization from Period 1 is associated with this sample

cc = coarse calcite
m = microcrystalline
brecc. = brecciated
euhed. = euhedral
py = pyrite
mbl = marble
? = unknown
cp = chalcopyrite
tet = tetrahedrite
dj = djurleite

AN-1-RB is cut by graphite in fractures
AS-42-1 has a minor amount of microcrystalline quartz that heals brecciated grains
AS-25-7A & B contain a few small breccia fragments of sulfide-bearing milky quartz

PLATE 1. GEOLOGIC MAP OF THE SHERIDAN MINING DISTRICT AND ADJACENT AREAS IN THE WESTERN TOBACCO ROOT MOUNTAINS, SOUTHWESTERN MONTANA

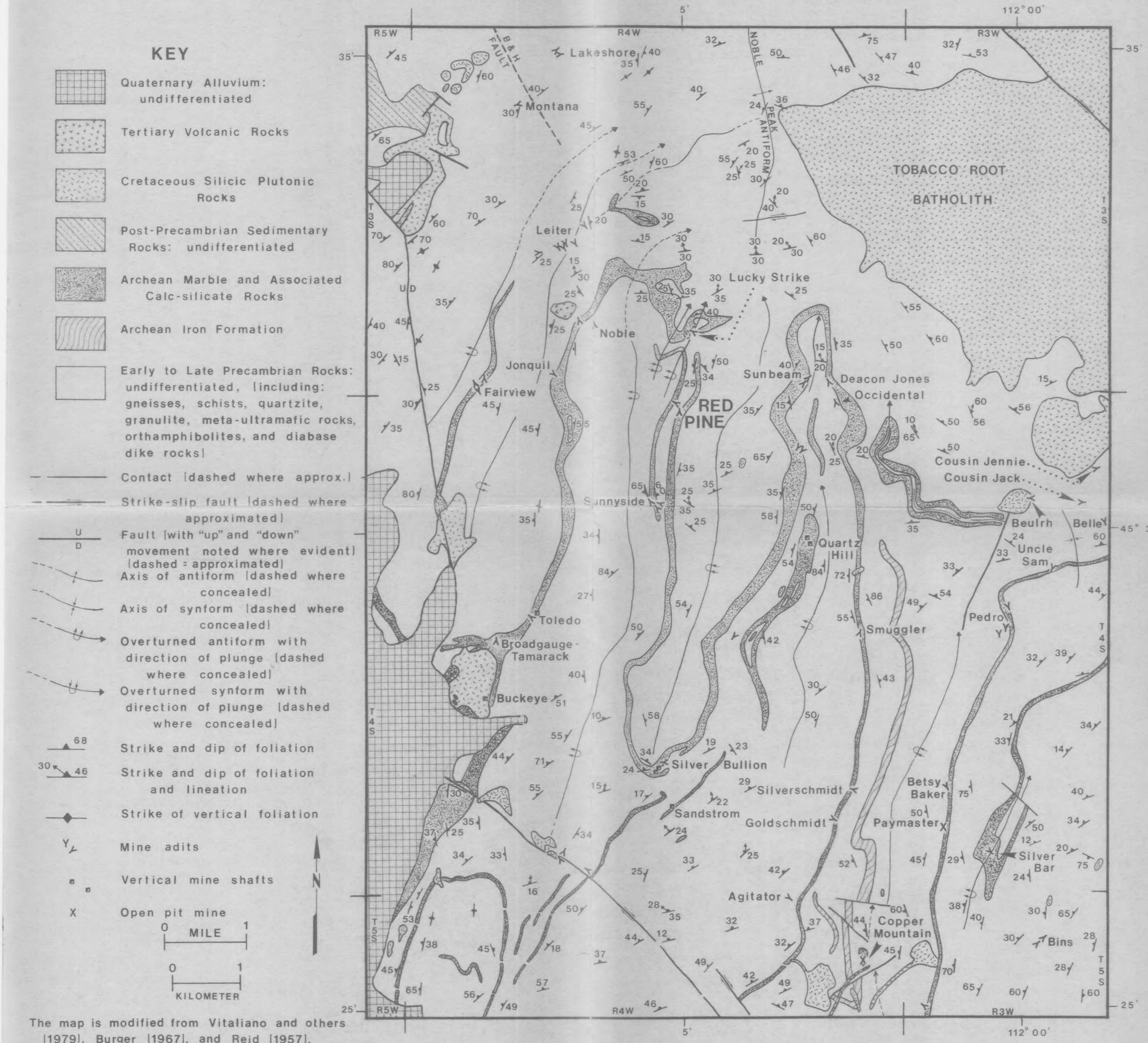

The map is modified from Vitaliano and others [1979], Burger [1967], and Reid [1957].

Additional information on names and locations of mines compiled from Winchell [1914], Lorain [1937], Tansley and others [1933], Levandowski [1956], Burger [1967], John Magnus [personal communication], and USGS topography maps [Waterloo & Virginia City 15' quadrangles and Sheridan & Copper Mountain 7.5' quadrangles].

GEOLOGY OF THE RED PINE GOLD MINE

WESTERN TOBACCO ROOT MOUNTAINS, SOUTHWESTERN MONTANA

Plan Map of Lower Level (Elev. ~2298 m.) Drift with Portion of Connecting Adit

PLATE 2

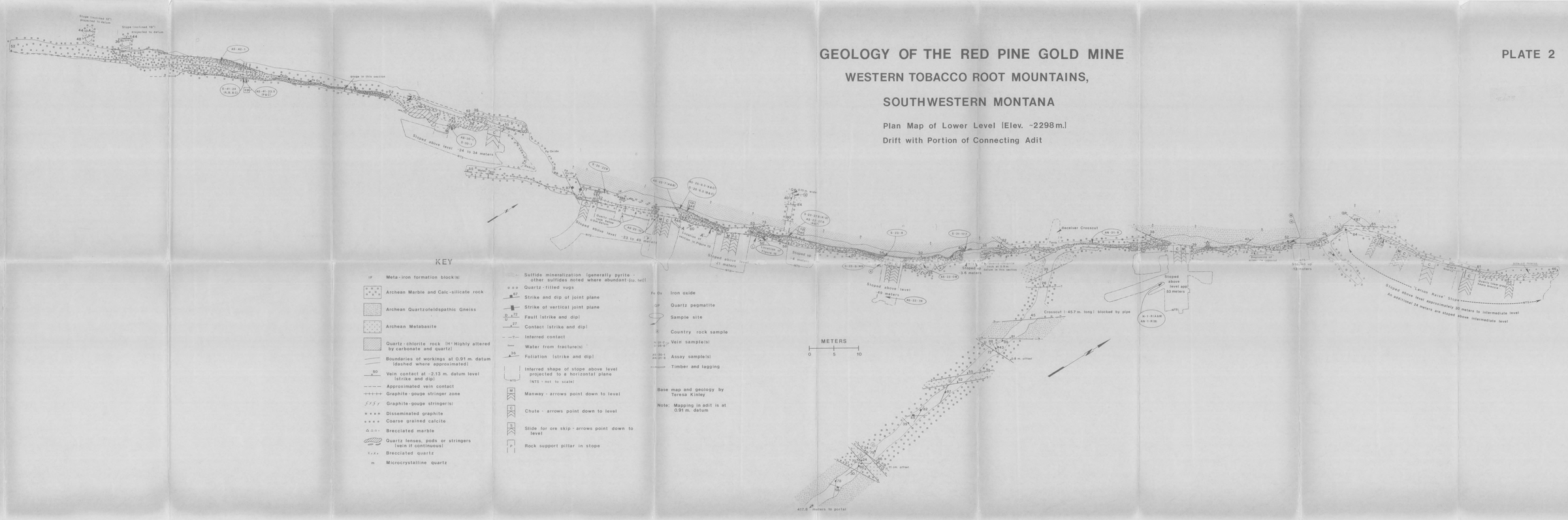

KEY

- IF — Meta-iron formation block(s)
- Archean Marble and Calc-silicate rock
- Archean Quartzofeldspathic Gneiss
- Archean Metabasite
- Quartz-chlorite rock (H = Highly altered by carbonate and quartz)
- Boundaries of workings at 0.91 m. datum (dashed where approximated)
- 50 — Vein contact at ~2.13 m. datum level (strike and dip)
- Approximated vein contact
- Graphite-gouge stringer zone
- Graphite-gouge stringer(s)
- Disseminated graphite
- Coarse grained calcite
- Brecciated marble
- Quartz lenses, pods or stringers (vein if continuous)
- Brecciated quartz
- m — Microcrystalline quartz
- Sulfide mineralization (generally pyrite - other sulfides noted where abundant (py, tet))
- Quartz-filled vugs
- 67 — Strike and dip of joint plane
- Strike of vertical joint plane
- D 72 / U — Fault (strike and dip)
- 27 — Contact (strike and dip)
- Inferred contact
- Water from fracture(s)
- 36 — Foliation (strike and dip)
- Inferred shape of stope above level projected to a horizontal plane (NTS - not to scale)
- M — Manway - arrows point down to level
- C — Chute - arrows point down to level
- S — Slide for ore skip - arrows point down to level
- P — Rock support pillar in stope
- Fe Ox — Iron oxide
- QP — Quartz pegmatite
- Sample site
- Country rock sample
- Vein sample(s)
- Assay sample(s)
- Timber and lagging

Base map and geology by Teresa Kinley

Note: Mapping in adit is at 0.91 m. datum

PLATE 3. PLAN MAP OF THE RED PINE MINE ADIT — LOWER LEVEL (~2298 m. Elevation)

SHERIDAN MINING DISTRICT, WESTERN TOBACCO ROOT MOUNTAINS, SOUTHWESTERN MONTANA

KEY

- Archean metabasite
- Am_1 - Western Archean marble band
- Am_2 - Eastern Archean marble band
- Archean quartzofeldspathic gneiss
- Vein at ~2.13 m. datum level
- Boundary of workings at 0.91 m. datum
- 38 Foliation (strike and dip)
- Strike of vertical foliation
- 76 Strike and dip of joint plane
- Strike of vertical joint plane
- Graphite-clay gouge stringer
- Quartz pod 0.5 m. wide in back
- 49 Contact (strike and dip)
- Inferred contact
- 85 D U Fault
- Water from fracture(s)
- (A) Sample site
- Timber and lagging
- ★ Major clay-gouge zone 0.25 m. wide in back

Base map and geology
by
Teresa Kinley